

THESIS ON MECHANICAL ENGINEERING E88

**RANS Numerical Modelling of  
Turbulent Polydispersed Flows in  
CFB Freeboard**

ALEXANDER SHABLINSKY

**TUT**  
**PRESS**

TALLINN UNIVERSITY OF TECHNOLOGY  
Faculty of Mechanical Engineering  
Department of Thermal Engineering

Dissertation was accepted for the defence of the degree of Doctor of Philosophy in Engineering on December 2, 2014

Supervisors:

Prof. Ph D Andres Siirde, Faculty of Mechanical Engineering  
D Sc Alexander Kartushinsky, Faculty of Science

Opponents:

Prof. Gangolf Kohlen  
Baden-Wuerttemberg Cooperative State University

Ph D Aleksandr Schmidt, Head of the Computational Physics Laboratory, Ioffe Physical Technical Institute, Russian Academy of Sciences

Defence of the thesis: January 16, 2014

Declaration

Hereby I declare that this doctoral thesis, my original investigation and achievement, submitted for the doctoral degree at Tallinn University of Technology has not been submitted for any degree or examination.

Copyright: Alexander Shablinsky, 2014

ISSN 1406-4758

ISBN 978-9949-23-711-1 (publication)

ISBN 978-9949-23-712-8 (PDF)

MEHCHANOTEHNIKA E88

**Turbulentsete voolude matemaatiline  
RANS modelleerimine tsirkuleeriva  
keevkihi tingimustes**

ALEKSANDR ŠABLINSKI



# CONTENTS

<b>INTRODUCTION</b> .....	<b>7</b>
<b>ABBREVIATIONS AND SYMBOLS</b> .....	<b>10</b>
<b>1. THEORETICAL BACKGROUND</b> .....	<b>13</b>
1.1. OIL-SHALE AS A FUEL .....	13
1.2. OIL-SHALE COMBUSTION .....	13
1.3. MODEL OVERVIEW .....	16
1.4. OBJECTIVES OF THE THESIS .....	25
<b>2. 2D RANS MODELLING OF UPWARD PARTICULATE PIPE FLOW</b> .....	<b>26</b>
2.1. 2-DIMENSIONAL REYNOLDS AVERAGED NAVIER-STOKES EQUATIONS.....	27
2.2. BOUNDARY CONDITIONS FOR THE RANS MODEL.....	30
2.3. NUMERICAL METHOD.....	31
2.4. RESULTS .....	31
2.5. CONCLUSIONS .....	33
<b>3. 2D RANS MODELLING OF FREEBOARD</b> .....	<b>39</b>
3.1. INTER-PARTICLE COLLISIONS AND TURBULENCE MODULATION.....	41
3.2. GOVERNING EQUATIONS FOR THE TWO DIMENSIONAL RANS MODEL: .....	42
3.3. RESULTS AND DISCUSSIONS.....	42
3.4. COMPARISON OF THE RESULTS .....	45
3.5. CONCLUSIONS .....	45
<b>4. 3D RANS MODELLING BY RSTM AND TWO WAY-COUPLING EFFECT</b> ..	<b>51</b>
4.1. TRANSPORT EQUATIONS OF AVERAGE VELOCITY OF CARRIER FLUID.....	52
4.2. TRANSPORT EQUATIONS OF REYNOLDS STRESSES OF CARRIER FLUID. ....	53
4.3. TRANSPORT EQUATIONS OF AVERAGE VELOCITY OF SOLID PHASE & PARTICLES FEEDBACK.....	58
4.4. BOUNDARY CONDITIONS.....	59
4.5. NUMERICAL METHOD AND RESULTS.....	61
4.6. CONCLUSIONS .....	63
<b>CONCLUSIONS</b> .....	<b>70</b>
<b>REFERENCES</b> .....	<b>71</b>
<b>LIST OF PUBLICATIONS</b> .....	<b>81</b>
<b>KOKKUVÕTE</b> .....	<b>84</b>
<b>ABSTRACT</b> .....	<b>86</b>
<b>CURRICULUM VITAE</b> .....	<b>88</b>

<b>ELULOOKIRJELDUS .....</b>	<b>89</b>
<b>DISSERTATIONS DEFENDED AT TALLINN UNIVERSITY OF TECHNOLOGY ON MECHANICAL ENGINEERING .....</b>	<b>93</b>

# INTRODUCTION

## *Motivation for the research*

Turbulent gas-solid particles flows in channels have numerous engineering applications ranging from pneumatic conveying systems to coal gasifiers, chemical reactor design and are one of the most thoroughly investigated subject in the area of the particulate flows. These flows are very complex and influenced by various physical phenomena, such as particle-turbulence and particle-particle interactions, deposition, gravitational and viscous drag forces, particle rotation and lift forces etc.

One of very interesting examples of the particulate flows is circulating fluidized bed (CFB), due to its enormous practical applications. The solid particles moving in a CFB reactors are considered as a shaker generating a flat profile of temperature of carrier fluid and thus a high mass transfer that results in high efficiency of a unit. Thus, CFB reactors are widely applied in industry [65].

The heat and mass transfer processes that take place in a CFB freeboard substantially affect the performance of a CFB reactor. Ash and inert materials that move along the freeboard are considered as a heat solid carrier that are separated further in cyclone and cooled in hear exchanger and those particles are come back into furnace. Since the heat capacity of ash is low, adding of inert solid particles rise the level of a heat capacity of a whole admixture. At the same time, it results to collisions of light ash and heavy inert particles that should be taken into account. However, the processes in a CFB freeboard are very complicated and still very poorly known due to a number of hydrodynamic phenomena occurred there. The particles of different sizes and different material densities, the particle-turbulence interaction and the balance of viscous drag and gravitation forces, the effect of high temperature etc. may contribute to processes in the CFB freeboard, and it is necessary to analyze and assess them. The design and projecting of the CFB reactors are totally empiric and, therefore, the numerical modelling is essential tool to facilitate them.

Thus, the main task of the given investigation is to study the mass transfer processes that occur in the CFB freeboard by means of the numerical simulation that allow to obtain data for further optimization of the flow inlet conditions and get more high efficiency of the processes in the CFB units.

### ***Scientific novelty***

In the scope of the present thesis the numerical simulation of the turbulent gas-solid particles flow has been performed within 2D and 3D Reynolds Averaged Navier-Stokes (RANS) Euler/Euler approach for the CFB freeboard.

The given approach has an advantage over of the Lagrange approach of the modelling of the CFB freeboard because of its direct acquisition of distributions of particle mass concentration. The scientific novelty of the thesis includes the numerical analysis of mechanisms occurred in CFB processes mainly focusing on the particle-particle collisions and particle-turbulence interactions. The applicant has analyzed for the first time the effect of variation of the densities of contacting materials in the mixture of oil-shale ash and sand particles along with effect of particle size distributions occurring for both materials. The results of the simulation describe the behaviour of oil-shale ash and sand particles in CFB, which could be helpful in improving the efficiency of the combustion.

## *Approbation*

Scientific results presented in the thesis have been previously presented at the following international conferences:

- The 7th International Symposium „Topical Problems in the Field of Electrical and Power Engineering“. Doctoral School of Energy and Geotechnology. Pärnu, Estonia, January 11-16, 2010.
- The 21st international conference on Fluidized Bed Combustion, Naples (Italy), 3.-6. June 2012.
- The 8th International Conference on Multiphase Flow 2013, Jeju (Korea), May 26-31, 2013.
- The 11th international conference of numerical analysis and applied mathematics 2013: ICNAAM 2013, Rhodes, Greece, 21–27 September 2013.

# ABBREVIATIONS AND SYMBOLS

## *Abbreviations*

2D	-	two dimensional
3D	-	three dimensional
AFBC-		Atmospheric Fluidized Bed Combustion
CFB-		Circulating Fluidized Bed
CFBC-		Circulating Fluidized Bed Combustion
DNS-		Direct Numerical Simulation
DPM-		Discrete Particle Model
DSMC-		Direct Simulation Monte Carlo
EMMS-		Energy-Minimization Multi-Scale
FBC-		Fluidized Bed Combustion
GF	-	Grate-Firing
ILU	-	Implicit Lower and Upper
MP-PIC-		Multi – Phase Particle – In – Cell
PDF-		Probability Density Function
PF	-	Pulverized Firing
PFBC-		Pressurized Fluidized Bed Combustion
RANS-		Reynolds Averaged Navies-Stokes
RSTM-		Reynolds Stress Turbulence Model
TBL-		Turbulent Boundary Layer
TFM-		Two Fluid Model

## *Roman symbols*

$A$	-	representative area of the droplet
$C$	-	mass concentration of the dispersed phase, $\text{kg}/\text{m}^2$
$C'_D$	-	factor of drag coefficient
$C_D$	-	drag coefficient
$C_M$	-	coefficient of Magnus force
$c$	-	mass loading, $\text{kg}/\text{kg}$
$f$	-	drag factor corrected to multiple particle effects
$f_c$	-	frequency of particulate collision
$\overline{F}$	-	force
$F_B$	-	buoyant force, $1/\text{s}$
$F_s$	-	Saffman force, $1/\text{s}$
$F_D$	-	drag force, $1/\text{s}$
$d_i, d_j$	-	diameter of colliding particle, $\text{m}$
$D$	-	pipe diameter, $\text{m}$
$D_p (d, \delta)$	-	particle diameter, $\text{m}$ (different sources)
$D_s$	-	coefficient of diffusion, $\text{m}^2/\text{s}$
$D_{ci}$	-	diffusion coefficient of particles, $\text{m}^2/\text{s}$
$E_d$	-	energy added per unit mass to the flow
$k$	-	turbulent energy, $\text{m}^2/\text{s}^2$

$k_i$	-	turbulent energy in the flow without particles, $m^2/s^2$
$k_n$	-	particle restitution coefficient
$k_s$	-	energy of dispersed phase from particle collision, $m^2/s^2$
$l$	-	characteristic length, m
$L$	-	integral turbulence length scale, m
$L_e$	-	length scale characteristic of the most energetic turbulent eddies, m
$L_\varepsilon$	-	is the dissipation length scale
$L_i$	-	dissipation length scale in the flow without particles, m
$L_h$	-	“hybrid“ length scale, m
$M$	-	mesh size, mm
$m^*$	-	mass loading, kg/kg
$n_{ij}$	-	concentration of the group of particles „j“, which may collide with the group of particles „i“
$p$	-	pressure, $kg/ms^2$
$P$	-	turbulence modulation
$P_d$	-	production due to particles
$P_i$	-	inherent production
$r$	-	radial coordinate, m
$R$	-	pipe radius, m
$Re$	-	Reynolds number
$Re_r$	-	Reynolds number based on the relative velocity
$t_c$	-	time scale of interparticle collision
$T$	-	the temperature of the flow, °C
$u$	-	axial velocity component, m/s (main symbol used for velocity, other symbols are also involved)
$u_i$	-	mass average velocity, m/s
$u_j^i$	-	axial velocity at grid points (i, j), m/s
$u_l$	-	velocity of the continuous phase, m/s
$\bar{u}$	-	gas velocity over cross-section, m/s
$\tilde{u}$	-	total axial velocity including drift turn, $\tilde{u} = u - D_s \frac{\partial \alpha}{\partial x}$ , m/s
$v$	-	radial velocity component, m/s
$v_j^i$	-	radial velocity at grid points (i, j), m/s
$v_l$	-	velocity of the particle, m/s
$v_*$	-	friction velocity of gas, m/s
$\bar{v}$	-	radial velocity over cross-section, m/s
$\tilde{v}$	-	total radial velocity including drift turn, $\tilde{v} = v - D_s \frac{\partial \alpha}{\partial y}$ , m/s
$V$	-	unit volume
$\vec{V}$	-	velocity vector
$V_i, V_j$	-	velocity of colliding particle, m/s
$x, x_i$	-	axial coordinate, m

## ***Greek symbols***

$\alpha$	-	particle mass concentration
$\alpha_c$	-	volume fraction of the continuous phase
$\varepsilon$	-	dissipation rate of turbulent energy, $\text{m}^2/\text{s}^3$
$\varepsilon_h$	-	rate of dissipation of the turbulent energy of the gaseous phase, $\text{m}^2/\text{s}^3$
$\Sigma$	-	summation over all particle fractions
$\rho$	-	density of gas, $\text{kg}/\text{m}^3$
$\rho_d$	-	dispersed phase density, $\text{kg}/\text{m}^3$
$\rho_c$	-	density of the continuous (conveying) phase, $\text{kg}/\text{m}^3$
$\rho_p$	-	density of gas and material of particles, $\text{kg}/\text{m}^3$
$\tau$	-	response time, s
$\tau_i$	-	response time for the “i” fraction of particles, s
$\tau_p$	-	particle response time, s
$\tau_V$	-	response time for the Stokes regime, s
$\tau_w$	-	shear stress
$\sigma$	-	turbulent energy for two-phase flow, $\text{m}^2/\text{s}^2$
$\sigma_o$	-	turbulent energy for single-phase flow, $\text{m}^2/\text{s}^2$
$\Omega$	-	angular velocity slip between gas- and dispersed phases, 1/s
$\nu$	-	kinematic viscosity, $\text{m}^2/\text{s}$
$\omega$	-	angular velocity, 1/s
$\Delta$	-	width of the control volume
$\Delta_u, \Delta_v, \Delta_w$	-	cross-section modifications of components of the Reynolds stress
$\lambda$	-	inter-particle spacing, m

## ***Subscripts***

$c$	-	continuous phase
$i$	-	i-th particle fraction of dispersed phase
$g$	-	gas
$g_i, g_j, g_k$	-	different gas phases
$k$	-	droplet/particle
$p$	-	particle property
$s_i$	-	i-th fraction of dispersed phase
$t$	-	turbulent
$0$	-	parameters of single-phase flow & dynamic friction
'	-	fluctuation & post-collision
$\omega$	-	rotation

# 1. THEORETICAL BACKGROUND

## 1.1. Oil-Shale as a fuel

Oil shale is a sedimentary rock containing organic matter. It is widely distributed around the world; more than 600 deposits are known to exist, with resources of over 500 Gt (in oil equivalent). The organic matter of oil shale contains large amounts of hydrogen and oxygen; it is insoluble in organic solvents. Oil shale is also a material rich in mineral matter. Carbonaceous, terrigenous-carbonaceous, and terrigenous oil shales have been found [85].

Oil shale is the most important energy resource in Estonia. The share of energy from oil shale has provided approximately 50 % of the primary energy consumption of Estonia and up to 90 % of electricity production in recent years, and the share of Estonian electricity exports to neighbouring countries has been approximately 20–30 % from total electricity production. Thus, oil shale usage provides guaranteed energy independence for the Estonian Republic and enhanced energy security in the Baltic region [106,115].

Estonian oil shale belongs to the carbonate class of fuels, which are known as low quality fuels. Due to the high content of carbonates, their calorific value is low, and their ash content is high [85]. The lower heating value of oil shale fired in Estonian power plants is approximately 8.2-8.6 MJ/kg, and the ash content of oil shale is up to 50 %. Firing that kind of fuel is associated with high CO<sub>2</sub> emissions and ash landfilling. Due to the decomposition of carbonate minerals, the specific emission of CO<sub>2</sub> is in the range of 0.95–1.12 t/MWh<sub>e</sub>, depending on the combustion technology. CO<sub>2</sub> emissions and ash landfilling are the most important environmental concerns related to oil shale firing [51, 3].

## 1.2. Oil-Shale combustion

Fuel combustion technology and boiler design are closely connected and have undergone extensive development to reach today's level. The development of oil shale combustion technology and boilers has been unique because of the special characteristics of oil shale compared to other solid fuels.

Several different combustion technologies are known. Their introduction has occurred in parallel, complementing each other. Combustion technique is in some sense “conservative” because of the long operational life and high cost of the equipment.

The start of intensive electrification at the beginning of the last century, which was accompanied by the erection of fossil fuel-fired power plants, accelerated the development of combustion technology. The service area of thermal power units was no longer limited to one plant or factory. The solution to the problem of long-distance power transmission facilitated the erection of high-capacity power plants, followed by the closure of many local power units.

A modern boiler and furnace (combustor) form an integral system. However, the furnace can still be considered stand-alone. A furnace is a device where fuel

combustion, release of heat, and formation of flue gas and ash take place. A modern furnace is also a heat exchange device with heat transfer surfaces. A solid-fuel furnace is also a separator, where a part of the ash formed during combustion is removed. The following three simultaneous processes take place in the furnace: fuel combustion, heat release, and formation of flue gas and ash; heat transfer from flue gas (flame) to heat exchange surface; and removal of some part of the ash.

Currently, the following three fuel combustion technologies are widely used: grate-firing (GF), pulverized firing (PF), and fluidized bed combustion (FBC). In addition, vortex and cyclone combustion are also used to a lesser extent [85].

### **Grate firing**

The oldest solid fuel combustion technology is grate firing. Coal, brown coal, peat, and wood, as well as oil shale, have been successfully burned using GF technology.

GF is characterized by high thermal inertia and the potential to regulate heat load by controlling air supply under the grate.

GF furnaces can be divided into the following categories:

- Furnace with bar grate (grate bars are fixed) and fixed bed.
- Furnace with bar-and-key grate (bars are fixed, grate moves); bed stands steady on grate.
- Furnace with movable bars (for instance, Krull-Lomshakov sloping movable-bar grate).

Among these types, the furnace with the movable bar grate is best suited for burning oil shale. The main problem with oil shale GF is achieving soot-free combustion. It may be accomplished in a specially designed furnace chamber with appropriate feeding of secondary air into the furnace.

A GF boiler has a certain ultimate capacity determined by the upper limit of the grate surface area. This fact limited the unit capacity of power plant turbogenerators. Using more boilers per turbogenerator somewhat alleviated the problem, but complicated the coordinated operation of units. The solution was found in the application of PF technology [85].

### **Pulverized firing**

While for GF technology, boiler capacity depends on the grate surface area, for PF technology, it is determined by the volume of the combustion chamber by increasing the furnace height.

At present, GF is preferred in small-scale boilers burning mainly biofuel and peat. There are two types of PF boiler furnaces: dry-bottom and wet-bottom or slagging-bottom units. Dry-bottom PF boilers are used most frequently, while wet-bottom furnaces are rather rare. The aim of using boilers with a wet-bottom furnace is to reduce the fly ash concentration in the flue gas and, in the case of burning fuels with active mineral matter, to reduce the chemical activity of the ash passing through the convection heat transfer surfaces of the boiler [101, 86]. PF boiler furnaces are mostly of a single-chamber type, with flue gas flow from bottom to top.

Slag falls on the cooled bottom of the furnace (so-called hopper-shaped bottom). As a rule, the flame core is located below the furnace center. Systems for preparing solid fuel for dry-bottom PF units burning volatile-rich fuels are divided into two large groups. The first group includes systems where fuel pulverizing takes place simultaneously with drying in high-temperature air. These systems can be successfully used for fuels of low or moderate moisture content. The second group includes furnaces where fuel pulverizing and simultaneous drying occur in a pulverizing fan that uses high-temperature flue gas taken from the upper part of the furnace. Fans grinding fuel at the same time create underpressure for the suction of flue gas into the mill. These systems have been widely used for pulverizing and drying brown coals of high moisture content [35, 7, 6]. Because the residence time of fuel particles in the PF boiler furnace is short, thermal inertia of the furnace is low. Since oil shale is of moderate moisture content, the principles of pulverized oil shale combustion in the PF boiler furnace, air drying, and direct dust feeding into the furnace is similar to that of coal combustion. Pulverizing and simultaneous drying of oil shale with air takes place in hammer mills. Gravitational or inertial classifiers are used for separating dust.

### **Vortex combustion**

Vortex combustion of fuel particles takes place in a swirl within the combustion chamber. Coarse-grained pulverized fuel is fed, together with primary air, through nozzles that are directed downward and located either in the front or rear wall. To create a vortex, a high volume of air is fed in through numerous air gaps located near the bottom of the combustion chamber [85].

### **Fluidized bed combustion**

With FBC, fuel combustion takes place in a bed of an inert material (sand, ash, etc.). The fuel concentration in the fluidized bed is not high (in the range 1 to 5 percent), depending on the fuel type and combustion technology. The combustion temperature in FBC is usually between 750 and 950°C. In comparison, the maximum flame temperature for PF in a dry-bottom furnace boiler can reach 1,500°C. The PF furnace is characterized by high gradient of flue gas temperature inside the combustor chamber. However, the temperature field in a fluidized bed is very homogeneous (the temperature difference in the FBC solid phase cross section does not exceed 20 to 30 K) because of the low concentration of combustible matter, intensive mixing of particles, and high intensity of mass and heat exchange between particles and the gas medium.

The highest temperature in FBC is determined by the sintering properties of fuel ash. FBC boilers are divided into two groups: atmospheric and pressurized. With atmospheric FBC, fuel combustion and other gas-side processes take place at atmospheric pressure. With pressurized combustion, the pressure in the furnace is usually more than 1.2 MPa. FBC boilers are also divided into classical or stationary and circulating FBC (CFBC) boilers.

In the classical FBC boiler, air (gas) superficial velocity in the bed is low; the majority of the particles stay in the bed, and the system behaves like a fluid. To keep the temperature below the allowed limit, some of the heat generated by fuel combustion in the bed has to be removed. Therefore, a portion of the heat released in the fluidized bed is transferred to the heat exchange surface immersed in the bed.

In the CFBC boiler, the air (gas) superficial velocity is higher; particles leave the bed and are transferred together with flue gas to the separator (cyclone), where most particles are captured and directed back to the furnace. Solid phase circulation takes place. Because of the low concentration of combustible matter, high heat capacity of the circulating material, and balance between the energy generated during fuel combustion and heat absorbed by heat exchanger surfaces of the furnace, there is no need to insert heat transfer surfaces into the bed. In a modern fluidized bed boiler, the heat capacity of the solid phase precipitated in the separator is effectively used to transfer energy into a heated medium (water, steam) in the boiler. This process occurs in an additional fluidized bed type heat exchanger. Such an arrangement of heat transfer enables the heat exchange surface area to be reduced in the convective section after the furnace and simplifies the maintenance and control of the temperature regime in the combustor.

Similar to atmospheric combustion, pressurized FBC (PFBC) can be divided into classical and CFBC technologies. The temperature within the combustion chamber is at the same level as that during atmospheric combustion.

During classical PFBC, flue gas leaving the furnace is cleaned from particles in a multistage cyclone or in a ceramic filter and is directed to the gas turbine, where it expands to reach the external pressure. The temperature level needed for FBC is maintained by removing generated heat from the bed. For that purpose, tube bundles of a heat exchanger are immersed in the fluidized bed. As heat transfer processes intensify and gas density increases with an increase in pressure, the dimensions of the PFBC boiler are several times less than those of the atmospheric fluidized bed combustion (AFBC) boiler of the same power capacity [85].

### **1.3. Model overview**

#### **1.3.1. Fluidized bed**

The fluidized bed is also another example of an important industrial operation involving multiphase flows. A fluidized bed consists of vertical cylinder containing particles where the gas is introduced through holes (distributor) in the bottom of the cylinder as shown in Fig. 1.1. The gas rising through the bed suspends the particles. At a given flow rate, the “bubbles”, which are regions of low particle concentration, appear and rise through the bed which intensifies mixing within the bed. Fluidized beds are used for many chemical processes such as coal gasification, combustion, liquefaction as well as the disposal of organic, biological and toxic wastes [17].

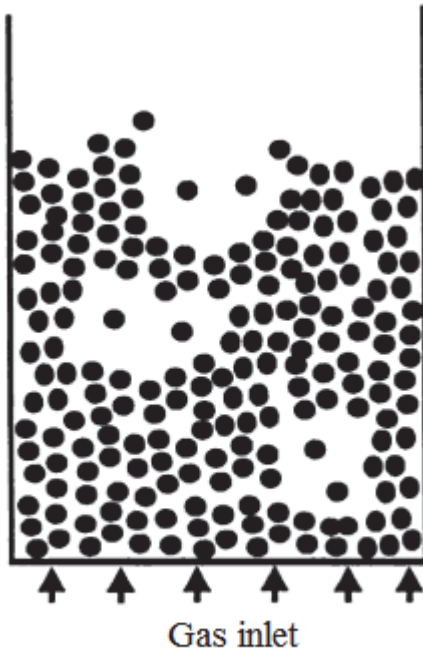


*Figure 1.1 Fluidized bed [17]*

### **1.3.2. Existing mathematical models**

There are several models developed to perform simulation of CFB-s. Full – loop TFM (Two Fluid Model) modelling of fluidized beds [140] is considered the state-of-the-art of simulated approaches. However, its accuracy has been questioned [140, 141, 142, 143], since the meso-scale structures induced under fluidization regimes, cannot be sufficiently considered. To improve its validity, sophisticated sub-grid models have been developed for the calculation of the drag force acting on particles [144]. The Energy-Minimization Multi-Scale (EMMS) model [69, 70] is employed in the Eulerian-Eulerian simulations of the hydrodynamics of a pilot scale CFB riser, with an implicit cluster diameter correlation accounting for the effect of sub-grid scale heterogeneity on inter-phase drag force. The simulated solid circulation flux, radial and axial solid concentration distributions and the radial particle velocity profile agree well with corresponding measurements. It presents a further step in establishing sub-grid scale models, which has been a focus in the study of gas-solid flows, on the basis of variation principles[50].

The recently revised EMMS model with an implicit cluster diameter correlation is combined with the Eulerian-Eulerian approach to simulate the heterogeneous gas-solid two-phase flows in a CFB riser. The resulting solid circulation fluxes, radial solid concentration and velocity profiles and the coexistence of a upper dilute region and a bottom dense region is well captured, demonstrating that the EMMS-based

sub-grid scale model for inter-phase drag force is a promising approach to coarse-grid simulations of CFB risers in the Eulerian-Eulerian framework [50].

Yet, another possible source of inaccuracy is the monosized approximation, used in the majority of TFM CFD works [140, 141, 142, 143, 108, 109].

To handle the complicated turbulent flow in a riser, various theoretical approaches have been proposed in the past. There are various models for the simulation of gas-particle multiphase flow. These models can be subdivided in two main classes: Euler-Euler and Euler-Lagrange models. The Euler-Euler model is also known as the two-fluid model and is used in many studies, because it requires relatively low computing resources. In this model, the solid phases as well as the gas phase are treated as interpenetrating continuous phases. The presence of each phase is described by a volume fraction. The Euler-Lagrange model also known as the discrete particle model (DPM) in which the dynamics of the gas phase is modelled in conjunction with a discrete description of each individual particle in the system. The interactions amongst the particles and between the particles and the gas phase are accounted for in the DPM. The particle dynamics are modelled with a hard-sphere collision model, soft-sphere collision model or the direct simulation Monte Carlo (DSMC) method. Compared with the discrete particle model, the two-fluid model cannot reveal the motion of individual particles. The DSMC method has large memory requirements, so it can only deal with reactors of very small size. The soft-sphere collision model requires small computational time steps to guarantee an accurate description of the collisions, which becomes very restrictive in systems with fast moving particles, such as risers [31].

This is applicable in Circulating Fluidized Bed (CFB) modelling but TFM formulation proved to be more efficient, as reported by Sundaresan [146], owed to the incorporation of the kinetic theory developed by Lun [147]. Here the Multi - Phase Particle - In - Cell (MP-PIC) is proposed by Patankar and Joseph [148].

The numerical simulations are mainly performed within the Lagrangian approach by the tracking of single particles or their packages in order to capture the particle-fluid interaction. For example, the two-dimensional gas-solid particles flow taken place in the CFB riser with a total volume concentration of solids 3% has been studied in [33] by the Lagrangian approach using the particles tracking method.

In the present work, another method is applied, namely, the two-fluid model, or the Eulerian approach or the model of coexisted flows. Within this approach the dispersed phase is considered as a continuous phase similar to carrier gas-phase fluid however with own parameters, namely, the velocities, the mass concentration etc., the parameters of the dispersed phase. The advantage of the Eulerian method is in direct modelling of the particle mass concentration and particles feedback of turbulence and average velocity of carrier fluid. This method does not depend on the number of the tracked particles which model the motion of the dispersed phase by the Lagrangian approach, which convergence is determined by the number of the tracked single particles that can be up to hundreds of thousands, which requires high computational capabilities. An implementation of an original closure model of linear and angular momentum of polydispersed solid phase [24, 57] based on the

interparticle collision in the Eulerian frame allows first of all directly describe four-way coupling effect in case of highly loaded flow, secondly, to take into account particle collisions which seem to be very significant with respect of high flow mass ratio and big range of particle size deviation. Finally, implementation of our model description [59] used for calculation of pneumatic transport to conditions of fluidized bed ( $T=850^{\circ}\text{C}$ ) considering low density of carrier gas ( $\rho=0.27\text{ kg/m}^3$ ) and its high coefficient of kinematic viscosity which is roughly 10 times larger than that at the normal conditions of  $T=20^{\circ}\text{C}$ , and the real geometry of the flow with respect of inlet size of 2.5 m allows to validate our numerical simulations and obtained results. Within the Eulerian approach the original collision model was used for closure of the transport equations by accounting the interparticle collision effect occurred in CFB due to high mass loading [42]. The numerical parametric study deals with the influence of various riser exit geometries on the hydrodynamics of the gas-solid two-phase flow taken place in the riser of CFB [42]. The problems of two-phase flows in the CFB risers are analyzed in the observed publications, but these studies do not consider the dependence of amount of the sensible heat carried by the ash solid particles on their concentration in gases. In the present work the gas-solid particles flow in conditions of CFB is studied, taking into account the amount of heat, which must be separated from the combustor by the sensible heat of the ash solid ash particles. This Eulerian approach enables to optimize the concentrations of the ash solid particles in fire gases.

In present work adding the process the second fraction of particles gives a significant change of the process due to different density of added particles and different particle size.

### 1.3.3. Mass conservation

The general statement for mass conservation is that the net efflux of mass from a control volume plus the rate of accumulation of mass flow in the volume is zero. The continuity equation, that, is

$$\frac{\partial}{\partial t}(\alpha_c \rho_c) + \frac{\partial}{\partial x_i}(\rho_c u_i) = 0, \quad (1.1)$$

### 1.3.4. Turbulence

Turbulence in a single-phase flow is generally characterized by the turbulence energy  $\kappa$  and the dissipation rate  $\varepsilon$ . This is known as the two-equation model. The equations for  $\kappa$  and  $\varepsilon$  are developed starting with Reynolds equations which are the equations for the fluctuating velocity components.

After numerous assumptions and clever physical reasoning, an equation is developed which relates the change in turbulence energy to terms representing the diffusion of turbulence energy, generation of energy and dissipation. The generation of turbulence energy results from velocity gradients in the flow and the dissipation from viscous effects. The dissipation equation comes from taking the curl of the

Reynolds equations which essentially gives the vorticity of the fluctuating velocity components. Once again the rate of change of dissipation is related to diffusion, generation and dissipation. There have been many modifications suggested to improve the  $\kappa - \varepsilon$  model but the essential features remain the same and it maintains a prominent role in the commercial fluid mechanics codes [129]. More recently, more attention has been developed to the turbulence models based on large eddy simulation as an improvement over the  $\kappa - \varepsilon$  model.

Turbulence modulation is the effect of particles or droplets on the turbulence of the carrier phase. Modulation is weak if the particle concentration is very low. Also, at very high concentrations, near the state of a packed bed, fluid turbulence is attenuated by the large viscous forces associated with the small Reynolds number based on the interparticle spacing. These limited cases are not addressed here. While the study of the particle dispersion in turbulence has a long history, the effect of the particles on fluid turbulence has been the subject of studies conducted over the past years. It was not until the 1970s that direct measurements of turbulence in the presence of particles were possible. Although these measurements were relatively new, practitioners in some engineering fields were already aware of the fact that the presence of particles can significantly change the rates of heat transfer and chemical reaction, which could not be explained except through the effect of the particles on the fluid turbulence. The drag reduction phenomenon observed in the pipe flows with low solids concentrations is another example which suggested that the particle phase modified the carrier phase turbulence.

The primary obstacle in obtaining fluid turbulence data in particulate flows was the difficulty with making fluid property measurements in the presence of solid particles. Before the invention of laser Doppler velocimetry, hot-wire or hot-film anemometry were the only means to acquire a direct measurement of fluid turbulence. Hot-wire probes cannot be used in flows with solid particles but a conical probe coated with a hot-film is durable, to some degree, in solid-liquid flows. For this reason the early data on fluid turbulence in the presence of solid particles were obtained in liquid-solid flows in connection with sediment transport. Some researchers attempted to use a hot-wire probe in gas-droplet free-jets in the study of a two-fluid atomizer and obtained results showing that particles (liquid droplets) suppress the turbulence intensity of gas.

Two papers [29, 34] summarize the available data on turbulence modulation. These papers suggest criteria for the suppression and enhancement of turbulence. One criterion is based on the length scale ratio  $d/L_e$ , where  $d$  is the particle diameter and  $L_e$  is the length scale characteristic of the most energetic turbulent eddies. Turbulence intensity is attenuated for  $d/L_e$  less than 0.1 while the turbulence level is increased for larger length scale ratios. Another criterion is based on the relative particle Reynolds number. The model suggests that particles with a low Reynolds number tend to suppress the fluid turbulence and particles with high particle Reynolds number tend to increase turbulence. Although some qualitative trends have been observed for the effects of particles on the turbulence energy of the carrier phase, there is currently no general model that can be used reliably to predict carrier phase turbulence in particle-laden flows.

The presence of particles can affect the carrier phase turbulence in several ways [18], such as:

- displacement of the flow field by flow around a dispersed phase element,
- generation of wakes behind particles,
- dissipation of turbulence transfer of turbulence energy to the motion of the dispersed phase,
- modification of velocity gradients in the carrier flow field and corresponding change in turbulence generation,
- introduction of additional length scales which may influence the turbulence dissipation,
- disturbance of flow due to particle-particle interaction.

Numerical models for turbulence modulation are still in development so no specific model has been adopted. The general approach is to modify the generation and dissipation terms in the  $\kappa - \varepsilon$  equations and develop Reynolds equations for the averaged quantities. This approach leads to a fallacy [15].

One approach which has been used to model the effect of particles on the carrier phase turbulence is direct numerical simulation (DNS). This approach is advantageous because it requires no Reynolds stress modelling. Squires and Eaton [113] used DNS with spectral methods to study the effect of particles on isotropic, homogeneous turbulence at low Reynolds numbers. Energy had to be added to maintain the turbulence. They modelled the effect of the particles by including a point forces (drag) in the flow field. It was found that the presence of the particles increases the turbulence dissipation rate. Squires and Eaton also found that the particles tend to concentrate in regions of high strain. Elghobashi and Truesdell [22] used a similar approach to model the effect of particles on turbulence. They also predicted that the rate of viscous dissipation is increased due to presence of the particles.

For gas-particle flows it can be shown that the energy transferred to particulate motion is negligible. The energy added per unit mass to the flow because of the dissipation of the work associated with drag is

$$\dot{E}_d = \frac{f}{\tau_V} \frac{\bar{\rho}_d}{\bar{\rho}_c} (u_1 - v_1)^2, \quad (1.2)$$

where  $f$  is drag factor corrected to multiple particle effects,  $\tau_V$  is response time for the Stokes regime,  $u_1$  is velocity of the continuous phase,  $v_1$  is velocity of the particle,  $\rho_d$  is dispersed phase density,  $\rho_c$  is density of the continuous (conveying) phase

The dissipation of energy is given by

$$\varepsilon = \frac{k^{3/2}}{L_\varepsilon}, \quad (1.3)$$

where  $L_\varepsilon$  is the dissipation length scale and  $k$  turbulent energy. However, in a two-phase mixture, several new length scales are introduced, the particle size and the interparticle spacing. If the interparticle spacing is less than the intrinsic length scale for the flow, then the interparticle spacing should influence the dissipation. Kenning & Crowe [55] defined a „hybrid“ length scale  $L_h$ , which approached the correct limits and used this for the dissipation length scale. They showed that the change in turbulence intensity for particles transported by air in a vertical duct should vary as,

$$\frac{\sigma - \sigma_o}{\sigma_o} = P = \left[ \frac{L_h}{L_i} + \frac{L_h}{k_i^{3/2}} \frac{f}{\tau_V} \frac{\bar{\rho}_d}{\bar{\rho}_c} (u_1 - v_1)^2 \right]^{1/3} - 1', \quad (1.4)$$

where  $L_i$  and  $k_i$  are the dissipation length scale and turbulence energy in the flow without particles.

The inability to model the local details of the continuous phase is dispersed phase flow necessitates the use of averaging. The three general categories of averaging are time, volume and ensemble. The conservation equations based on volume averaging illustrate the influence of the dispersed phase on the carrier phase through the coupling terms and volume fractions of each phase. The deviations of the continuous phase velocity from the average velocity give rise to a Reynolds stress in the same manner as time averaging yields the Reynolds stress in single-phase flow. Modelling the Reynolds stress in a dispersed phase flow is complicated by the length scales associated with the dispersed phase. Also the heat transfer through the mixture involves the heat transfer through both the continuous and dispersed phases. The presence of the particles or droplets in the field affects the turbulence of the carrier phase as a result of enhanced turbulence generation and dissipation.

### 1.3.5. Drag viscous force

The „steady-state“ drag is the drag force which acts on the particle in a uniform pressure field when there is no acceleration of the relative velocity between the particle and the conveying fluid. The force is quantified by the drag coefficient through the equation [17]:

$$F_D = \frac{1}{2} \rho_c C_D A |u_1 - v_1| (u_1 - v_1), \quad (1.5)$$

where  $\rho_c$  is the density of the continuous (conveying) phase,  $C_D$  is the drag coefficient,  $A$  is the representative area of the droplet and  $u_l$  and  $v_l$  are the velocities of the continuous phase and the droplet or particle, respectively.

Typically the area is projected area of the particle in the direction of the relative velocity.

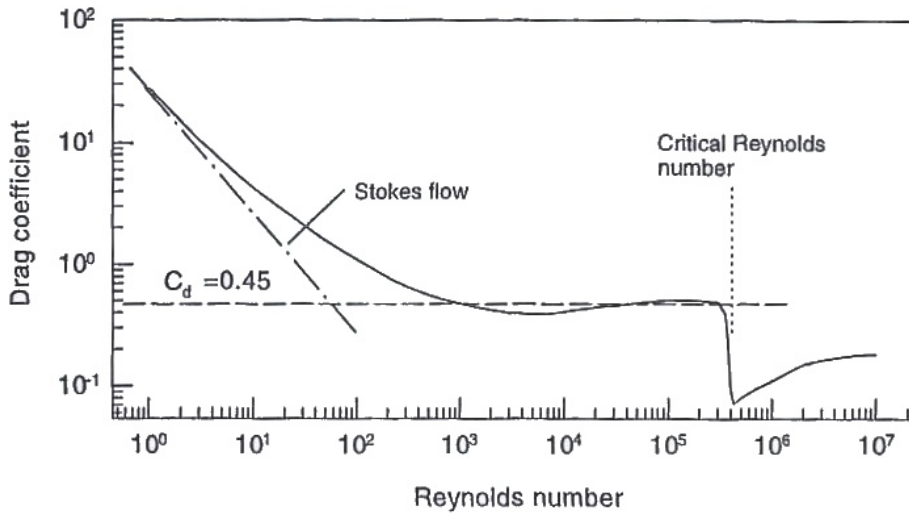


Figure 1.2 Variation of drag coefficient of a sphere with Reynolds number [17]

Using the drag force to solve for the drag coefficient in previous equation results in

$$C_D = \frac{24}{Re_r}, \quad (1.6)$$

where  $Re_r$  is the Reynolds number based on the relative velocity. This is the classic Stokes drag coefficient which is valid for  $Re_r < 1$ .

An extension of Stokes analysis for high particle Reynolds numbers is [12]. In this case the drag coefficient becomes is case of a uniform free stream velocity:

$$C_D = \frac{24}{Re_r} (1 + 0.15 \cdot Re_r^{0.687}), \quad (1.7)$$

Variation of drag coefficient of a sphere with Reynolds number is shown in Fig. 1.2

### **1.3.6. Lift forces**

Lift forces on a particle are due to particle rotation. This rotation may be caused by a velocity gradient or may be imposed from some other source such as particle contact and rebound from a surface. The effect of this force factor is small for modelling of the processes in freeboard CFB.

### **1.3.7. Particle-particle and particle-wall interactions**

Particle-particle interaction controls the motion of particles in dense particle flows. Also particle-wall interaction is important in dense flows as well as wall-dominated dilute flows.

#### **Particle-wall interaction**

The problem of particle-wall interaction is encountered when analyzing gas-particle flows contained within walls such as pipe flows, channel flows and fluidized beds. The particle-wall interaction considered here falls into two categories: hydrodynamic forces due to the proximity of a wall and the purely mechanical interaction in the absence of a fluid. The Saffman lift force due to velocity gradient near the wall is one example of the hydrodynamic interaction. Another example is the fluid force acting on a particle approaching the wall in the normal direction.

The treatment of the mechanical behaviour associated with particle-wall interaction depends on the inertia of the particle. When a massive particle collides with a wall, it rebounds but loses kinetic energy due to friction and inelasticity effects. For a very small particle approaching a wall, molecular forces become dominant compared with the inertial force. As a result, the particle is captured by the wall due to cohesive forces, and neither rebounds from nor slides along the wall. This cohesive force is identified as the van der Waals force.

#### **Particle-particle interaction**

Particle-particle collision is negligible in dilute gas-particle flows. As the particle concentration becomes higher, particles collide with each other and the loss of particle kinetic energy due to inter-particle collision cannot be neglected. Fortunately, as long as the particulate phase is dispersed, it is sufficient to consider only simple binary collisions, not multiple collisions.

Particle-particle interaction is the key element in dense phase flows. The two models for particle-particle interaction are the hard sphere and soft sphere models. With the hard sphere model the post-collision velocities and rotations are determined as a function of the pre-collision conditions, coefficient of restitution and coefficient of friction. The soft sphere model describes the particle history during the collision process and can be modelled with spring-damper arrangements. Particle-wall collisions are treated with the hard sphere model. A number of theoretical investigations devoted to study of inter-particle collision effect can be formally divided by the use of either Lagrangian or Euler approaches. Sommerfeld [65] presented a number of diagrams for the average and r.m.s. velocity shapes, which were obtained for a relatively large mean flow velocity, with no noticeable effect on

the velocity profiles due to the particle accumulation on the bottom wall. Sommerfeld and Zivkovic [112] estimated the effect of the particles' collision on a stochastic approach using a Lagrange frame of reference. The stochastic approach for the particles' collision model was also considered by Oesterle and Petitjean [88] as well as by Yamomoto [131]. The calculations in the last three studies were restricted to short pipe lengths. In similar studies, Simonin and co-workers [103,62,63] have used the PDF approach within the frame of the two-fluid model, to model the gas-solid flows with collisions. The effect of inter-particle collisions is obviously important for dense particulate flows where the ratio of particle response time is larger than the time of inter-particle collisions that is when  $\tau / t_c > 1$  with

$\tau = \left( \frac{18\rho\nu}{\rho_p d^2} C_D \right)^{-1}$  being the particle response time. The frequency of particulate collision  $f_c = 1/t_c$  may be calculated by the classical expression of Marble [80]:

$$f_c = \left( \frac{d_i + d_j}{2} \right)^2 |\vec{V}_i - \vec{V}_j| n_{ij},$$

where  $d_i$  and  $d_j$  are the diameters of colliding particles,

$V_i$  and  $V_j$  are the velocities of the particles and  $n_{ij}$  is the concentration (number of particles per unit volume) of the group of particles “j,” which may collide with the group of particles “i.” An order of magnitude estimate shows that the inequality  $\tau / t_c > 1$  is satisfied when the mass loading is higher than 10. Hence, inter-particle collisions play an important role in the transport processes when the loading ratio is higher than 10. There are a few particle collision models obtained in the Eulerian frame of reference, such as the ones by Louge [72], and Cao and Ahmadi [10]. In this paper, we also apply a two-fluid approach using a two-way coupling model. We introduce a collision model that considers the exchange of not only the linear momentum, but also the angular momentum. Hence, we obtain analytical formulae for the stress tensor components and the pseudoviscosity coefficients using an average procedure over the collision coordinates [58]. Wall roughness can be simulated with a local wall slope at the surface.

#### 1.4. Objectives of the thesis

The main goal of the thesis is focused on numerical analysis of the mass transfer in the CFB freeboard and determination of the optimal operating regimes of the CFB unit to increase its performance. The criterion of optimality is the uniform distribution of concentration of solid particles that occurs in the CFB freeboard.

There are following activities to accomplish the main goal:

1. Numerical simulation of the isothermal upward pipe particulate flow to determine the key force factors by 2D RANS modelling of the isothermal upward pipe particulate flow study.
2. 2D RANS modelling of the non-isothermal mass transfer for the CFB freeboard conditions study based on the data obtained at 2D RANS modelling of the isothermal upward pipe particulate flow study.
3. Assessment of effect of the flow geometry by 3D modelling of the square-section channel particulate flow study.

## 2. 2D RANS modelling of upward particulate pipe flow.

“Two-fluid model” was used in the modelling of dispersed two-phase systems, where the gas and the particles are considered as two coexisting phases that cover entire flow domain. To describe the flow of the particulate phase, one of the possibilities is the use of the Reynolds Averaged Navier-Stokes method. The general equations of this method were examined by plenty of experiments that showed good reasonable matching and they are feasible to be numerically implemented. In this work we use the RANS method with its’ closure equations to find on the output needful data: axial and radial velocities, turbulent energy, mass concentration.

Particulate flows in pipes have numerous engineering applications ranging from pneumatic conveying systems to coal gasifiers, chemical reactor design and are one of the most thoroughly investigated subjects in the area of multiphase flows. These flows are very complex and influenced by various physical phenomena, such as particle-turbulence and particle-particle interactions, deposition, by gravitational and viscous drag forces, particle rotation and lift force (fig. 2.1).

Numerous theoretical and experimental researches [93, 19, 29, 116, 13, 118, 113, 135, 28, 9, 134, 10, 16, 76, 105, 57, 77, 61, 62] are dedicated to various aspects of behaviour of gas and solid particles occurring in particulate pipe flows.

The aim of the present study is to focus on the research of the effect of variation of pipe diameter for constant Reynolds number applied for vertical particulate turbulent pipe flows. The numerical investigation, being discussed here, examined in details the effects of direct and indirect particle-turbulence interaction (no-coupling and coupling) and gravity for various flow mass loading. Additionally, the viscous drag force and the Magnus and Saffman lift forces are also taken into account.

The presented numerical model applies the following assumptions: two-fluid model [21, 99, 103, 20, 98], the Reynolds-averaged Navier-Stokes (RANS) approach [61, 62] applied to gas and solid particles.

Within the frame of the two-fluid model, the gas and the particles are considered as two coexisting phases that span the entire flow domain [61, 62]. Therefore, in order to describe the flow of the particulate phase within the two-fluid model, the presented model implements RANS approach, which is the most general and frequently used in modelling, and its closure equations have been verified by numerous experiments and the boundary conditions are easy to determine. The given modelling employs the model by Crowe [13], which is the most relevant model to account for mechanisms of a turbulence modulation caused by particles, since it includes both the turbulence enhancement and its attenuation by particles the particles. The inter-particle collisions is another mechanism accounted for capture properties of turbulent particulate pipe flows and which is modelled, e.g., by Kartushinsky and Michaelides [57]. These two models enable the comprehensive mathematical simulation of two-phase upward pipe flow.

The presented model allows covering 100 and more calibres of a pipe flow. This is the main advantage over the numerical models based, for example, on the direct numerical simulation (DNS) codes [73], that handle usually with a short pipe length up to 10-20 calibres with imposing upper limit for the flow Reynolds number.

The utilized two-fluid model with adoption of original collisional closure model by Kartushinsky and Michaelides [57] together with applied numerical method has been verified and validated in our previous research [61, 62] by comparison of numerical results with existing experimental data by Tsuji et al. [118]. By the given study, the effect of variation of pipe diameter (or transport velocity) at constant Reynolds number is numerically investigated in the particulate turbulent flow, and this is the step forward for an analyzing of external effect, namely, the flow configuration rather the internal effect with variation of the parameters of the flow.

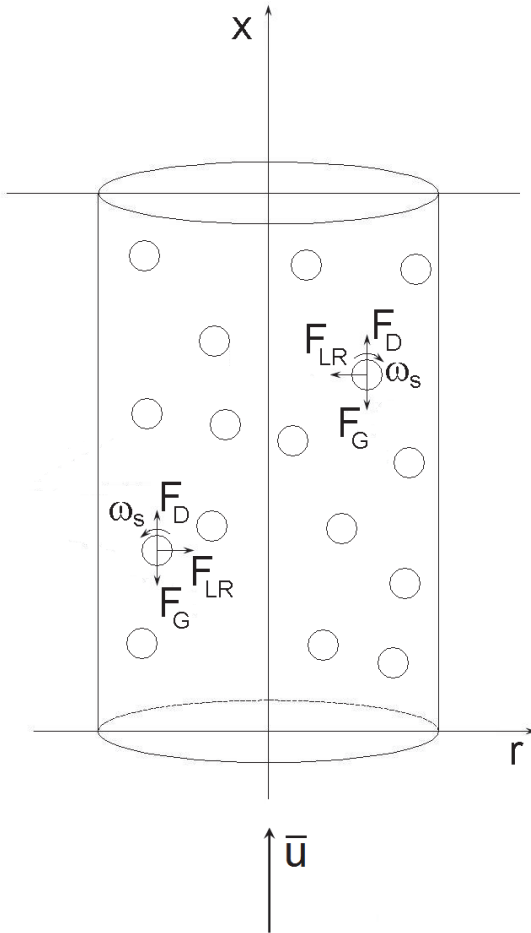


Figure 2.1 Upward turbulent particulate flow in a pipe

## 2.1. 2-Dimensional Reynolds Averaged Navier-Stokes equations

The model is based on the time averaged Navier-Stokes equations (RANS method), without any simplifications, such as the boundary layer simplifications. The vertical pipe flows are 2D unless the study of rotating flows. In general, the effect of the inter-particle collision can be taken into account in two-way: a) by

particle size distribution, or/and b) particle material density variation. In both cases, it can be described by motion of finite number on particle fractions denoted by subscript index “i”, that in particularly, in case of three particle fractions is varied in range of  $1 \leq i \leq 3$  [52]. In given chapter, we deal with motion of monodispersed solid particles, i.e. is supposed that  $i=1$ , then governing equations written for the axisymmetric round pipe flow are as follows:

1. Continuity equation for the gas phase:

$$\frac{\partial u}{\partial x} + \frac{\partial(rv)}{r\partial r} = 0, \quad (2.1)$$

where  $u$  and  $v$  are the longitudinal and radial velocity components of the gas phase.

2. Longitudinal linear momentum equation for the gas phase:

$$\frac{\partial}{\partial x} \left( u^2 - \tilde{\nu}_t \frac{\partial u}{\partial x} \right) + \frac{\partial}{r\partial r} r \left( uv - \tilde{\nu}_t \frac{\partial u}{\partial r} \right) = -\frac{\partial p}{\rho \partial x} + \frac{\partial}{\partial x} \tilde{\nu}_t \frac{\partial u}{\partial x} + \frac{\partial}{r\partial r} r \tilde{\nu}_t \frac{\partial v}{\partial x} - \alpha_i \left( \frac{u_r}{\tau'_i} + C_M \Omega_i v_{ri} \right) \quad (2.2)$$

where  $\tilde{\nu}_t = \nu_t + \nu$  is the effective viscosity, which is the sum of the turbulent and laminar viscosities, while  $\nu_t$  is calculated following to Boussinesq eddy-viscosity concept;  $p$  is the pressure;  $\alpha$  is the mass concentration of the particles.  $u_{ri} = u - u_{si}$  and  $v_{ri} = v - v_{si}$  are the particles relative velocities along the longitudinal and radial directions, respectively. Here  $\tau'_i = \tau_i / C'_{Di}$  is the particle response time that specifies the drag, defined by expression  $C'_{Di} = 1 + 0.15 Re_{si}^{0.687}$  for the non-Stokesian regime [100]. The particle Reynolds number and Stokesian particle response time are defined as  $Re_{si} = \delta_i |\vec{V}_{ri}| / \nu = \delta_i \sqrt{u_{ri}^2 + v_{ri}^2} / \nu$  and  $\tau = \rho_{pi} \delta_i^2 / (18\rho\nu)$ , respectively.  $\Omega_i = \omega_{si} - 0.5(\partial v / \partial x - \partial u / \partial r)$  is the angular velocity slip, with  $\omega_s$  being the angular velocity of the given particle fraction. The coefficient of the Magnus lift force  $C_M$  is calculated according to Crowe [16];  $\rho$  and  $\rho_p$  are the physical densities of air and the particle material, respectively.

3. Radial linear momentum equation for the gas phase:

$$\frac{\partial}{\partial x} \left( uv - \tilde{\nu}_t \frac{\partial v}{\partial x} \right) + \frac{\partial}{r\partial r} r \left( v^2 - \tilde{\nu}_t \frac{\partial v}{\partial r} \right) = -\frac{\partial p}{\rho \partial r} + \frac{\partial}{\partial x} \tilde{\nu}_t \frac{\partial u}{\partial r} + \frac{\partial}{r\partial r} r \tilde{\nu}_t \frac{\partial v}{\partial r} - \frac{2\tilde{\nu}_t v}{r^2} - \alpha_i \left( \frac{v_{ri}}{\tau'_i} - (C_M \Omega_i + F_{si}) u_{ri} \right), \quad (2.3)$$

$F_s$  is the coefficient for the Saffman lift force, which is due to the local shear of the flow, and it is given for finite values of the particle Reynolds numbers by correction of [75].

4. Turbulence kinetic energy equation for the gas phase:

$$\frac{\partial}{\partial x} \left( uk - \tilde{v}_t \frac{\partial k}{\partial x} \right) + \frac{\partial}{r \partial r} r \left( vk - \tilde{v}_t \frac{\partial k}{\partial r} \right) = 2\nu_t \left\{ \left( \frac{\partial u}{\partial x} \right)^2 + \left( \frac{\partial v}{\partial r} \right)^2 + \frac{1}{2} \left( \frac{\partial u}{\partial r} + \frac{\partial v}{\partial x} \right)^2 \right\} + \frac{\alpha}{\tau} (u_r^2 + v_r^2 + k_s) - \varepsilon_h \quad (2.4)$$

where  $k$  and  $k_s$  are the turbulence kinetic energy of the gas- and dispersed phases, respectively. The hybrid dissipation rate  $\varepsilon_h$  is calculated for the two-phase flow via hybrid turbulence length scale defined as harmonic average of the integral length scale of single-phase flow and inter-particle spacing [16].

5. Mass conservation equation for the particulate phase:

$$\frac{\partial}{\partial x} (\alpha \tilde{u}_{si}) + \frac{\partial}{r \partial r} r (\alpha \tilde{v}_{si}) = 0, \quad (2.5)$$

where  $\tilde{u}_s$  and  $\tilde{v}_s$  are the longitudinal and radial components of the drift particle velocity of the given fraction, given by expressions  $\tilde{u}_{si} = u_{si} - (D_t + D_c^x) \frac{\partial \ln \alpha_i}{\partial x}$ ,  $\tilde{v}_{si} = v_{si} - (D_t + D_c^r) \frac{\partial \ln \alpha_i}{\partial r}$ . Here  $D_t$  is coefficient of turbulent diffusion of particles, which is calculated by the model of Zaichik and Alipchenkov [136]. The pseudoviscosity diffusion coefficients along  $x$  and  $r$  directions  $D_c^{x,r}$  are stemmed from the particles collisions [52].

6. Momentum equation in the longitudinal direction for the particulate phase:

$$\frac{\partial}{\partial x} (\alpha u_{si} \tilde{u}_{si}) + \frac{\partial}{r \partial r} (r \alpha u_{si} \tilde{v}_{si}) = - \frac{\partial}{\partial x} (\alpha_i \overline{u_{si}^2}) - \frac{\partial}{r \partial r} (r \alpha_i \overline{u_{si}' v_{si}'}) + \alpha_i \left[ \frac{u_{ri}}{\tau_i'} + C_M \Omega v_{ri} - g \left( 1 - \frac{\rho}{\rho_{pi}} \right) \right] \quad (2.6)$$

where  $g$  is the gravitational acceleration.

7. Momentum equation in the radial direction for the particulate phase:

$$\frac{\partial}{\partial x} (\alpha_i v_{si} \tilde{u}_{is}) + \frac{\partial}{r \partial r} (r \alpha_i v_{si} \tilde{v}_{si}) = - \frac{\partial}{\partial x} (\alpha_i \overline{u_{si}' v_{si}'}) - \frac{\partial}{r \partial r} (r \alpha_i \overline{v_{si}^2}) + \alpha_i \left[ \frac{v_{ri}}{\tau_i'} - (C_M \Omega + F_s) u_{ri} \right], \quad (2.7)$$

where  $\overline{u_{si}'^2}$ ,  $\overline{u_{si}'v_{si}'}$ ,  $\overline{v_{si}'^2}$  are the velocity correlations due to the particle collisions and induce momentum swap in the longitudinal and radial motions of the given fraction [57].

8. Angular momentum equation in the longitudinal direction for the particulate phase:

$$\frac{\partial}{\partial x}(\alpha_i \omega_{si} \tilde{u}_{si}) + \frac{\partial}{r \partial r}(r \alpha_i \omega_{si} \tilde{v}_{si}) = -\frac{\partial}{\partial x}(\alpha_i \overline{u_{si}' \omega_{si}'}) - \frac{\partial}{r \partial r}(r \alpha_i \overline{v_{si}' \omega_{si}'}) - \alpha_i C_{\omega i} \frac{\Omega_i}{\tau_i'} \quad (2.8)$$

where  $\overline{u_{si}' \omega_{si}'}$  and  $\overline{v_{si}' \omega_{si}'}$  are the linear-angular velocity correlations of particles due to the inter-particle collisions calculated according to Kartushinsky and Michaelides [57].

## 2.2. Boundary conditions for the RANS model

As inlet boundary conditions, it is assumed that particles enter into the previously computed, fully developed flow domain of single-phase, having the initial longitudinal velocity determined by the lag coefficient. The equilibrium outlet boundary conditions were set at the exit cross-section  $x = 100D$ , i.e. the non-gradient derivatives from all velocities of all phases, turbulence kinetic energy and mass concentration over longitudinal coordinate were written according to Kartushinsky [62]. Since the particulate flow in vertical pipe is considered as axisymmetrical, the non-gradient boundary conditions were set at the pipe axis for the longitudinal velocity components of gas and particles, the turbulent energy and particle mass concentration. The boundary conditions were set zero at the pipe axis for the radial velocities of both phases and the particles angular velocity. The concept of “wall functions” [94] has been applied to set the boundary conditions at the wall. While applying the balance of the production and dissipation rate of kinetic energy “near wall” with using of the eddy-viscosity concept [92], it can link the friction velocity  $v_*$  and shear stress  $\tau_w$  through the turbulence kinetic energy as  $v_*^2 = \tau_w / \rho = c_\mu^{0.5} k$ . The computations near the wall were carried out at the half width of the control volume off the wall. Then, for the longitudinal velocity of gas phase and for the turbulent energy computed by means of its production  $P_k$  the following boundary conditions are as follows:

$$\left\{ \begin{array}{l} u = \sqrt{\frac{\tau_w}{\rho}} \frac{1}{\alpha} \ln(y^+) + C = v_* \frac{1}{\alpha} \ln\left(E \frac{y}{v} v_*\right) \quad 11.6 \leq y^+ < 500 \\ u = \frac{v_*^2 y}{v} \quad y^+ < 11.6 \end{array} \right. , \quad (2.9)$$

$$P_k = \tau_w \frac{\tau_w}{\rho \alpha c_\mu^{0.25} k^{0.5} y}, \quad (2.10)$$

where empirical constant  $\alpha = 0.41$ ;  $y = \Delta/2$  ( $\Delta$  is the width of the control volume).

The wall boundary conditions for dispersed phase have taken into account the particle's velocity lag determined through particles-wall interaction [62].

### 2.3. Numerical method

The control volume method was applied to solve mass and momentum equations of both phases by using the implicit lower and upper (ILU) matrix decomposition method with flux-blending differenced-correction and upwind-differencing schemes by Perić and Scheuerer [92]. Calculations were performed in dimensional form for all flow regimes. The number of the control volumes was varied from 280,000 to 1,120,000 corresponding to increase of pipe diameter from  $D=30.5$  mm to  $D=61$  mm, and their size remained constant across the pipe flow.

### 2.4. Results

The numerical results presented in the following figures have been obtained at the distance of  $x/D=100$  from the pipe entrance in Paper I. At this distance, it was reasonable to stipulate that the steady flow conditions have been reached and there was no influence of the entrance conditions. Mainly, the results presented here are dimensionless, but some of them are presented in dimensional form.  $250 \mu\text{m}$  coal particles (physical density,  $\rho_p=1600 \text{ kg/m}^3$ ) were used in investigations. The flow mass loading was  $m^* = 1$  and  $10 \text{ kg dust/kg air}$ . The applied particles were light enough to be responsive to the turbulent fluctuations of gas.

The Reynolds number  $Re$  was assigned as the constant through all calculations and set equalled  $4.4 \cdot 10^4$ . The pipe diameter  $D$  was  $30.5$ ,  $45.75$  and  $61$  mm for the gas average velocity  $\bar{u} = 21.6$ ,  $14.6$  and  $10.8$  m/s, respectively. The average longitudinal velocity and turbulence energy radial distributions calculated for these three regimes are shown in Figs 2.2 and 2.3.

The following figures show the influence of various force factors on radial distributions of the particles velocity lag, particle mass concentration and turbulence modulation originated from the particles. Separately, there is analyzed the effect of the direct (turbulence) and indirect (no-coupling and coupling) particle-turbulence interactions together with the singled out influence of gravity.

The longitudinal velocity lag is presented as the ratio of the longitudinal velocity slip  $u_r$  between the gas and particulate phases to the terminal velocity of particles,  $(u - u_s)/v_t$ , where  $v_t$  is the particles terminal velocity.

The analysis of behaviour of the normalized longitudinal velocity lag is shown in Fig. 2.4 for various force factors for 250  $\mu\text{m}$  particles at  $m^* = 1$ . If the motion of particles is exposed only by the viscous and gravitation forces (without the direct effect of turbulence, lift forces and coupling), the velocity lag between two phases approaches to the particles terminal velocity occurring in the steady-state flow domain, i.e. the ratio  $u_r / v_t$  converges to unity (the curve marked by triangles, Fig. 2.4). However, as the numerical simulation shows, if the motion of particles is exposed by combined effect of various force factors, the normalized longitudinal velocity lag increases above the particles terminal velocity.

Figure 2.5 shows the effect of the flow mass loading on the normalized longitudinal velocity lag. It is evident that increase of the flow mass loading results in reduce of  $u_r / v_t$  almost all over the cross-section of the pipe except the near-wall region.

Diminishing of the normalized longitudinal velocity lag observed for relatively dense flow ( $m^*=10$ , Fig. 2.5) clearly depicts the tendency of the turbulence attenuation by particles, or, in other words, decrease of direct effect of turbulence on the particles motion. The ratio between particle size and turbulence integral length scale is about 0.1 for the given 250  $\mu\text{m}$  coal particles and, according to Gore and Crowe [29], they attenuate turbulence. This effect becomes stronger with increase of the flow mass loading which results in converging of  $u_r / v_t$  to unity when considering only effect of gravity (Fig. 2.4).

In order to trace the effect of the flow mass loading on the turbulence modulation let us first examine the distribution of the particle mass concentration presented in Fig. 2.6. As one can see, the growth of the flow mass loading attenuates turbulence and makes radial distributions steeper with more pronounced tendency with respect of the particle size variation [57, 58].

Figure 2.7 explicitly addresses to the coupling effect, which was observed for two flow mass loadings,  $m^*=1$  and 10. Obviously, the higher mass loading leads to the higher rate of the turbulence modulation, i.e., if there is the turbulence attenuation due to the particles, then this process is intensified for the higher mass loading.

The next series of plots (Fig. 2.8–2.10) show the effect of the pipe diameter for the constant Reynolds number on distributions of the normalized velocity lag, the particle mass concentration and the turbulence modulation.

Figure 2.8 shows radial distributions of the normalized longitudinal velocity lag obtained for various pipe diameters. One can see that increase of the pipe diameter results in lower turbulence level (Fig. 2.3). This in turn leads to the smaller velocity lag with less deviation from particles terminal velocity, and, in fact, to the weaker particles involvement into the turbulent motion. This is proved by the data of Fig. 2.3 that shows that the larger pipe diameter corresponds to the lower level of the

turbulence energy, and, therefore, to the lower rate of the particles involvement by the gas flow.

One can see that the effect of the pipe diameter has the tendency to straighten the radial distributions of the particle mass concentration (Fig. 2.9). Increase of the pipe diameter leads to reduction of ratio between particle size and pipe diameter that results in intensification of particles turbulent diffusion leading to flattening of distributions of particles concentration [62].

The turbulence modulation caused by particles is shown in Fig. 2.10 for various pipe diameters at the flow mass loading  $m^*=10$ . As one can see, increase of the pipe diameter leads to lower rate of turbulence attenuation. This can be explained based on the analysis of Fig. 2.3. As it shows, increase of the pipe diameter results in decrement of turbulence kinetic energy  $k$ . Since the length scale of energy-containing eddies is proportional to turbulence kinetic energy ( $L_e \sim k^{\frac{3}{2}}$ ), the decrement of kinetic energy is followed by decrease of turbulence length scale. This, in turn, causes the growth of ratio between particle size and turbulence length scale, and finally results in lower rate of turbulence attenuation due to particles.

## 2.5. Conclusions

The two-dimensional RANS numerical approach fitted for upward turbulent particulate pipe flow supplied with the appropriate closure equations was applied for the computational investigation of parameters of gas and solid particles by the control volume method. The study covered the distance of 100 calibres from the pipe entrance.

The longitudinal velocity lag, turbulent kinetic energy of gas and particles mass concentration, effected by the gravity, viscous drag, the particle-turbulence, particle-particle, particle-wall interactions as well as the Saffman and Magnus lift forces, were examined for different pipe diameters with holding constant the flow Reynolds number for various flow mass loadings.

The obtained numerical results allow to draw the conclusions:

1. Simultaneous accounting of turbulence interactions effect and all force factors, impacting on solid particles, results in substantial excess of longitudinal velocity lag over their terminal velocity.

2. The increase of the pipe diameter appears as follows:

- it gives rise to decrease of the relative velocity lag;
- it flattens the radial distributions of particles velocity;
- it induces the decrease of the turbulence attenuation rate;

- it causes flattening the radial distributions of the particles mass concentration.

3. The increase of the flow mass loading causes:

- diminution of the relative velocity lag;
- increase of the rate of the turbulence attenuation
- steepening of the radial distributions of the particles mass concentration.

The presented model with applying of minimum number of assumptions and empiricism represents a more contemporary computational approach in turbulent particulate flow, as well as it is simpler and uses the state-of-the-art modelling and computational techniques and is more accurate owing to no applying of approximations. The given method allows computing the large particulate flow domains occurred in various practical devices.

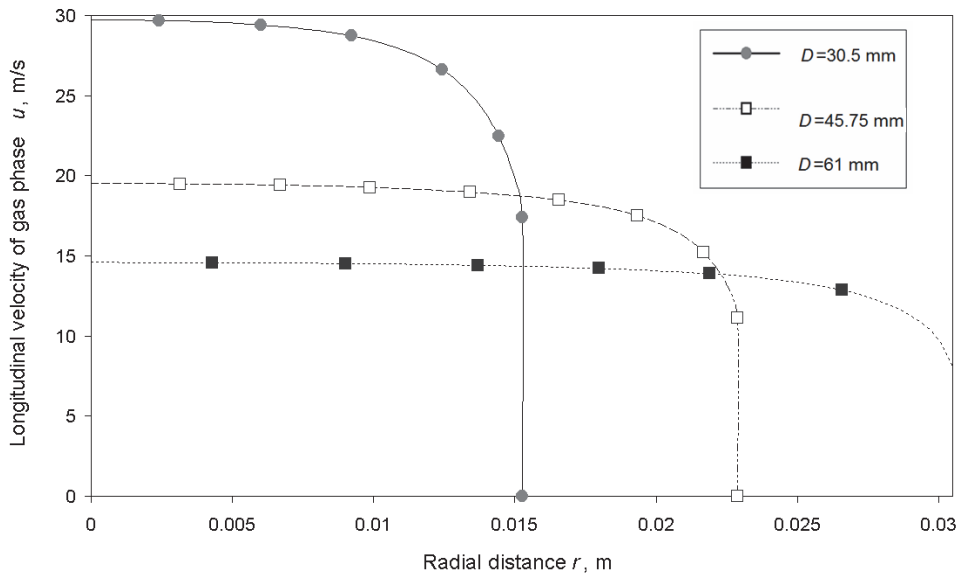


Figure 2.2 Radial distributions of the longitudinal gas velocity in the pipes  $D=30.5$ ,  $45.75$  and  $61$  mm,  $Re=4.4 \cdot 10^4$

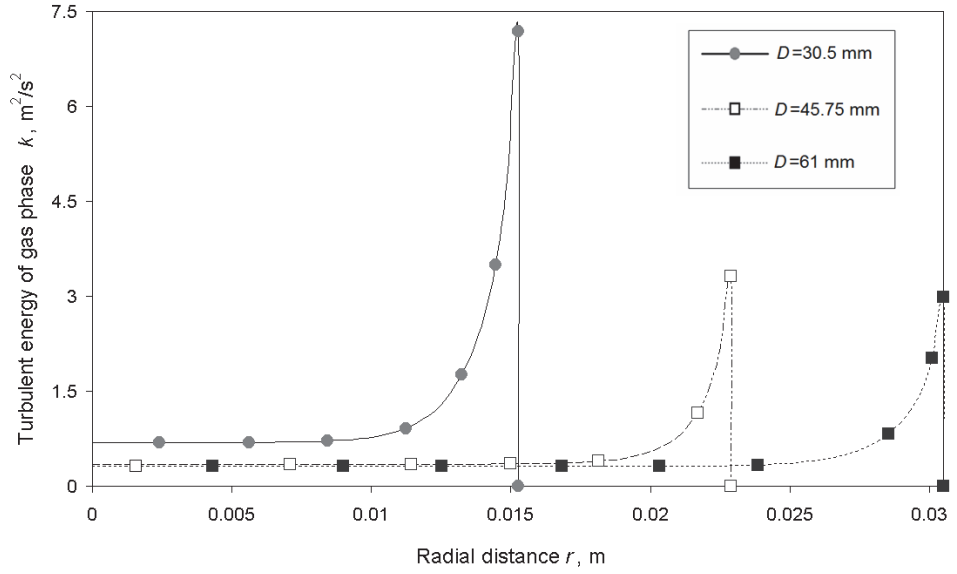


Figure 2.3. Radial distributions of the turbulence energy of gas in the pipes  $D=30.5$ ,  $45.75$  and  $61$  mm,  $Re=4.4 \cdot 10^4$

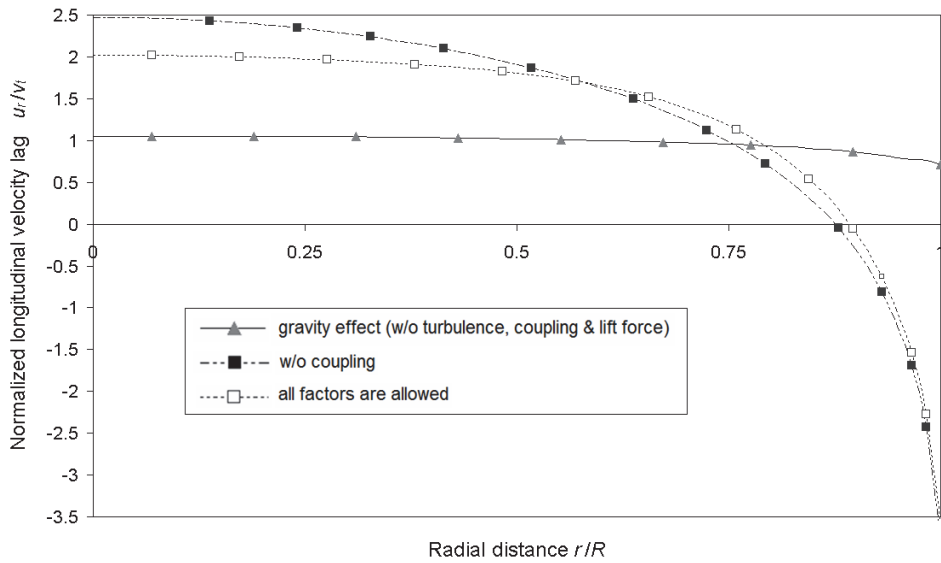


Figure 2.4. Radial distributions of normalized longitudinal velocity lag for  $250 \mu\text{m}$  coal particles obtained for various flow conditions,  $m^*=1$ ,  $D=45.75$  mm,  $Re=4.4 \cdot 10^4$

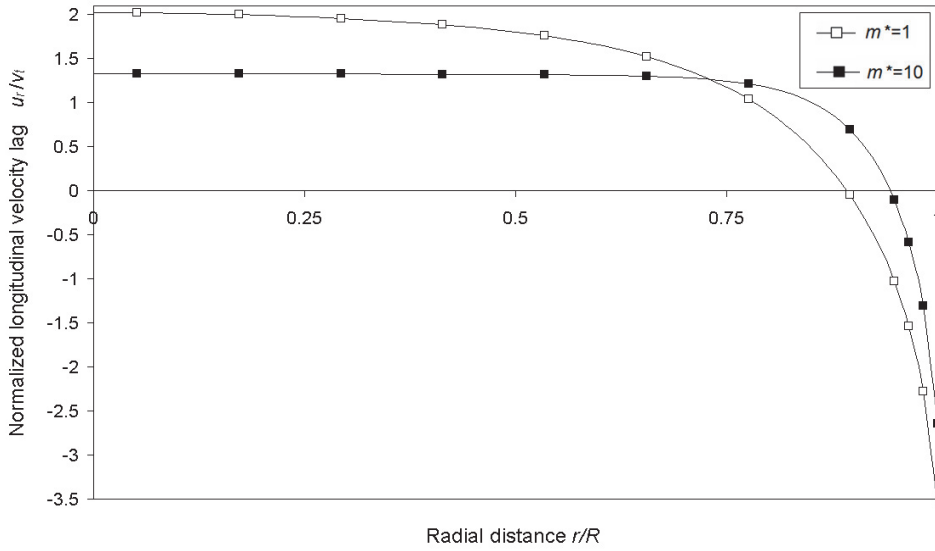


Figure 2.5. Radial distributions of normalized longitudinal velocity lag for 250  $\mu\text{m}$  coal particles obtained for the flow mass loadings  $m^*=1$  and  $m^*=10$ ,  $D=45.75$  mm,  $Re=4.4 \cdot 10^4$

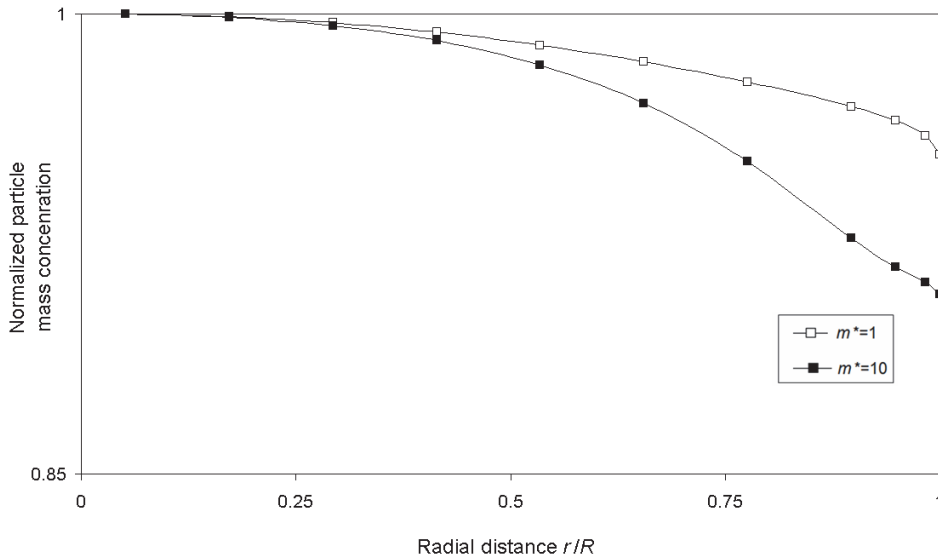


Figure 2.6 Radial distributions of the normalized mass concentration of 250  $\mu\text{m}$  coal particles obtained for the flow mass loadings  $m^*=1$  and  $m^*=10$ ,  $D=45.75$  mm,  $Re=4.4 \cdot 10^4$

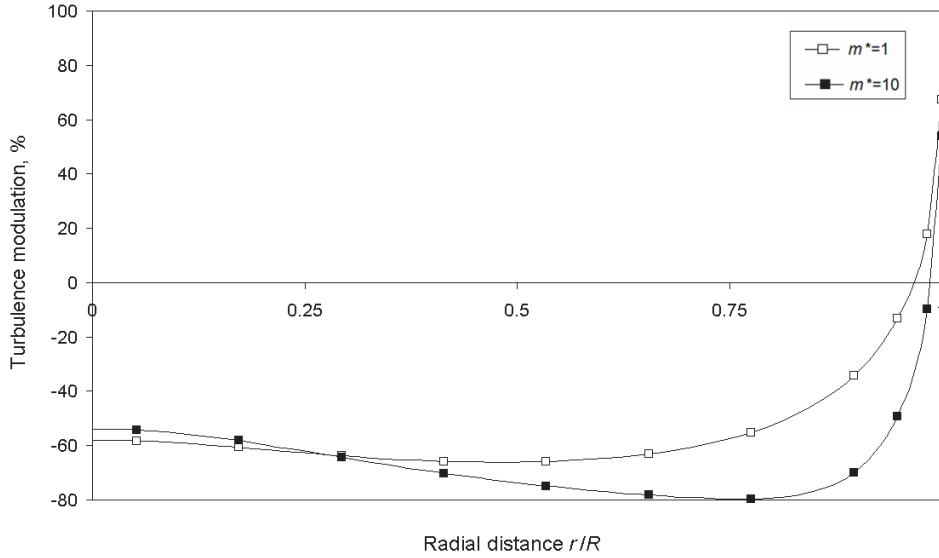


Figure 2.7 Effect of mass loading on the turbulence modulation by 250  $\mu\text{m}$  coal particles,  $m^*=1$  and  $m^*=10$ ,  $D=45.75$  mm,  $Re=4.4 \cdot 10^4$

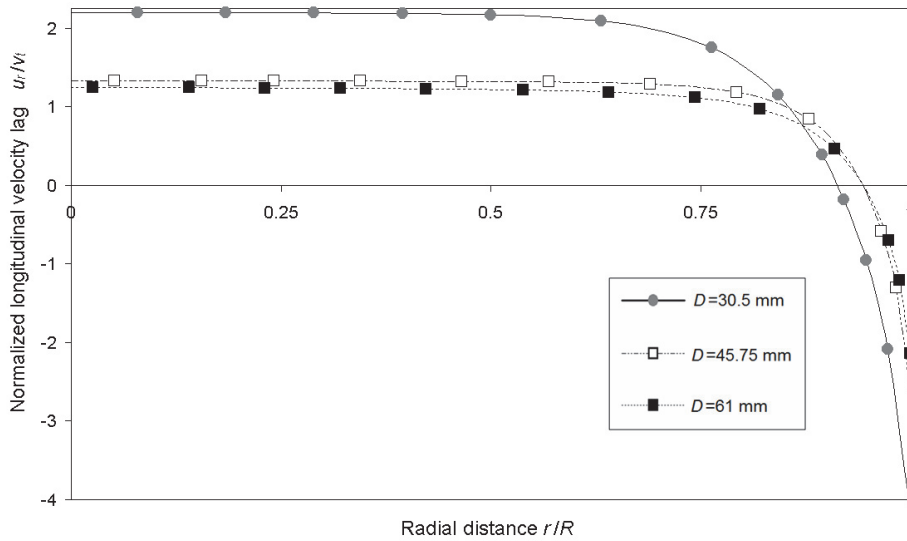


Figure 2.8 Radial distributions of normalized longitudinal velocity lag for 250  $\mu\text{m}$  coal particles in the pipes  $D=30.5$ , 45.75 and 61 mm,  $m^*=10$ ,  $Re=4.4 \cdot 10^4$

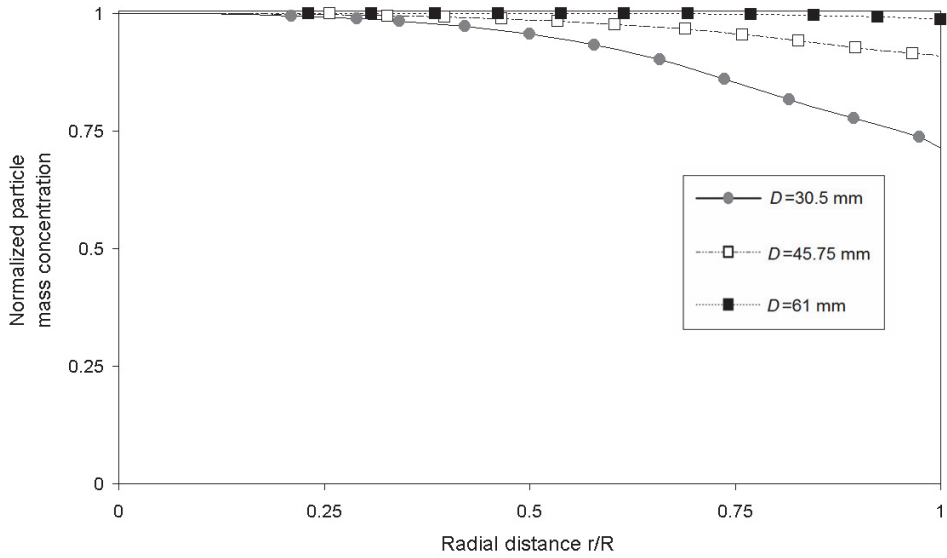


Figure 2.9 Radial distributions of normalized mass concentration for 250  $\mu\text{m}$  coal particles in the pipes  $D=30.5$ , 45.75 and 61 mm,  $m^*=10$ ,  $Re=4.4 \cdot 10^4$

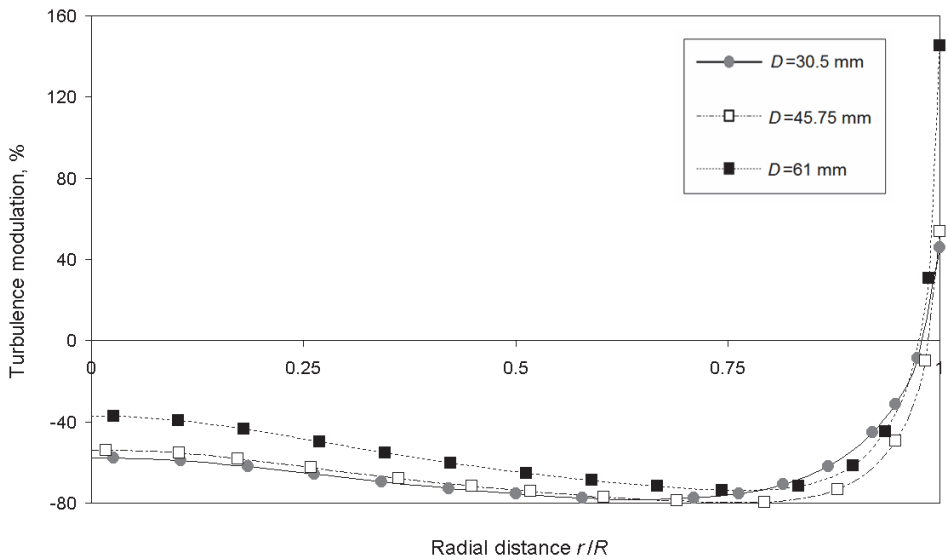


Figure 2.10 Radial distributions of the turbulence modulation for 250  $\mu\text{m}$  coal particles in the pipes  $D=30.5$ , 45.75 and 61 mm,  $m^*=10$ ,  $Re=4.4 \cdot 10^4$

### 3. 2D RANS MODELLING of FREEBOARD

The real CFB processes face not only with the particle size distributions, but also with particles of various gravities, and all this results in effect of four-way coupling should be taken into account along with effect of specific flow conditions (high temperature) on flow parameters (gas density & gas viscosity). To do this, firstly, the 2D numerical simulations are performed in isothermal conditions in upward pipe flow analyzing impact of various force factors effect of those are later on implemented to non-isothermal conditions of CFB. In addition, numerical simulation of effect of particle-turbulence interaction were performed in 3D flows focusing on effect of shape of flow cross-section, namely, effect of square channel cross-section versus cross-section of round pipe.

It is considered that solid admixture used in CFB is polydispersed solid admixture composed of light and heavy solid particles with taking into account also variation of their sizes which up rises in the turbulent pipe flow. This is the first step to evaluate the effect of variation of the particle material density on parameter distribution to develop further numerical modelling of such complicated flow where the heat conditions together with the real particle size distribution and real particle material composition which take place in real processes in CFB are included. 2D RANS modelling of freeboard CFB by polydispersed approach enables to optimize particle mass concentration of the ash solid particles in fire gases. For the numerical simulation of the uprising gas-solid particle flow occurred in the vertical riser the CFB conditions, namely temperature, the gas velocity, the particles concentration, are followed, and the particles of the Estonian oil shale ash (particle size, density) are chosen.

Within the given numerical investigations we focus attention on problem of the particles turbulent motion along with particles collision in case of polydispersed solid admixture. Considered polydispersed admixture is composition of light and heavy solid particles with variation of their sizes which up rises in the turbulent pipe flow. This is the first step to evaluate effect of variation of the particle material density on parameter distribution to develop further numerical modelling of such complicated flow where the heat conditions together with the real particle size distribution and real particle material composition which are taken plate in real processes in CFB will be included [85]. The approach enables to optimize particle mass concentration of the ash solid particles in fire gases. For the numerical simulation of the uprising gas-solid particle flow occurred in the vertical riser the CFB conditions, namely temperature, the gas velocity, the particles concentration, are followed, and the particles of the Estonian oil shale ash (particle size, density) will be chosen.

The previous numerical simulations have been performed within the two-phase turbulent boundary layer (TBL) approach [63]. This implies that the diffusive source terms were only retained in one direction, namely in transverse direction, and magnitude of the average transverse velocity components of the gas- and dispersed phases were much less than that of the longitudinal components of the corresponding velocities of gas- and dispersed phases. Such approach is thoroughly

valid and used in the pipe channel flows as well as in the turbulent round jets together with the flow past of the rigid shapes [40,24].

As opposed to Paper II, the given study assesses the impact of two coexisting particle fractions, namely ash (light) and sand (heavy) particles with variation in general case of their particle sizes. The problem is solved by applying of 2D RANS approach.

In comparison with Krupensky [64], the following practical initial data were used in calculations:

*Table 3.1. The initial data for calculations*

<b>Generic name</b>		<b>Dimension</b>	<b>Minimal</b>	<b>Maximal</b>
Pipe data	Diameter	m	0.030	0.03
	Height	m	3	3
Ash concentration		kg/kg air	5	10
Ash density		kg/m <sup>3</sup>	1020	1020
Ash particle size		m	0.00025	0.0004
Corundum density		kg/m <sup>3</sup>	4000	4000
Corundum particle size		m	0.00025	0.00025

The present research is continuation of our previous numerical study of processes occurred in CFB using two-fluid (Euler-Euler) approach applying to description of behaviour of solid particles as a continuous co-existed solid phase. 2D RANS modelling is currently applied with use of finite (control) volume method [23] to avoid common assumptions of turbulent boundary layer (TBL) approximation. RANS modelling originally performed for 2D single phase turbulent pipe flow was extended for modelling of two-phase flow with incorporated solid particle phase. The other popular approach now for modelling of dispersed phase is the Lagrangian particle tracking method. For use of the Lagrange method one can handle with huge number of tracking particles (up to several millions of particles depending on mass flow loading) to obtain solution convergence and to take into account of the particles feedback on primary (gas-phase) fluid on a contrary to the Euler approach one can obtain the direct impact of particles on fluid turbulent structure. The two-dimensional gas-solid particles flow taken place in the CFB riser with a total volume concentration of solids 3% was studied by the Lagrangian approach using the particles tracking method [33]. Also the Lagrangian approach of particle collisions was used by Sommerfeld [104] who introduced a stochastic inter-particle model when a fictitious particle and trace particles collide.

### 3.1. Inter-particle collisions and turbulence modulation.

A parameter that measures the importance of inter-particle collisions in a following gas-solid mixture is the ratio of the particle response time,  $1/\tau_p$ , to the time of inter-particle collision,  $t_c$ . For dense particulate flows,  $t_c/\tau_p < 1$ , and particle-to-particle collisions must be taken into account. There are many theoretical studies on the subject of the inter-particle collision phenomena: Williams and Crane [130] obtained an expression for the collision rate of the particles and their relative velocities in a turbulent flow in terms of the Stokes number. The Lagrangian approach of particle collisions was used by many researchers in the past including Sommerfeld [104] who introduced the stochastic inter-particle model when a fictitious particle and tracer particle collide. Jenkins and Savage [48] used the Eulerian approach that accounts for inter-particle collisions in the case of rapid granular flow. The so-called “granular temperature”, which is an analogue of the temperature obtained from a kinetic theory approach, may be calculated from the velocity distribution function of the particles. Other constitutive relations, also based on the kinetic theory, may be obtained by using the characteristic shape of the velocity distribution function. In the particular case of nearly elastic and frictionless inter-particle collisions this function may be assumed as to be Maxwellian. In such a case, an expression for the total stress of the particles collision may be obtained as Louge [72] who used closure equations that involve the pseudo-viscosity coefficients and the stress tensor components corresponding to the collision terms in the transport equations of the dispersed phase. In previous models for the closure of governing equations of the dispersed solid phase based on inter-particle collisions [43, 24], an approximation was used [7] that considers only one mechanism for the particle collisions that is collision without sliding friction at the point of contact surfaces. These authors also took into account the effect of surface roughness by using empirical roughness coefficient. This mechanism applies only to the motion of particle where the transverse component of the velocity is higher than the longitudinal (tangential) component at the moment of collision. It must be pointed out that the solution of such models cannot be achieved in the limiting case of the collision of identical particles because the computed pseudo-viscosity coefficient diverge since the time of inter-particle collisions becomes infinite. Matsumoto and Saito [74] investigated particle-wall collisions and determined two mechanisms of interactions namely, collisions with and without sliding friction at the point of surfaces contact. They also determined criteria for the application of these mechanisms. According to their investigation, if the ratio of transverse to tangential velocities is smaller than  $\frac{2}{7f(1+k_n)}$  a collision with sliding friction is observed.

Otherwise, a collision without sliding friction occurs and the tangential is zero at the point of impact. The analyses of particle-wall and particle-particle collisions considering various stages of the collision process are presented in Crowe [17]. They also considered separate expressions for the liner and angular velocity changes for both of these mechanisms within frame of so-called “hard sphere collision model”. In order to cover all plausible situations that may occur in a gas-solids flow, the model that accounts for the mechanism of collision with sliding friction has been

developed [57]. Besides the improvement of the former models for inter-particle collision, an important motivation for the development of such a model is that it may be applied to identical particles without divergence of the pseudo-viscosity coefficients or any other parameters. With a sliding type of collision friction, it is able to reduce the terms related to the angular velocity in the expressions of the stress tensors of dispersed phase in the linear-linear and linear-angular velocity correlations. This makes it possible to perform collision calculations for various sizes of particles as well as for various particle material densities that flow simultaneously in solids mixture. Thus, the model of Kartushinsky and Michaelides [57] is flexible to the variation of all the flow parameters and also may be applied in the case of polydispersed solid mixtures.

Here in given research it is assumed that the solid phase is polydispersed and composed of several fractions with known mass fractions, denoted by  $\alpha_i$ . These fractions may be of a single material density and have different sizes or they may be of different materials and sizes. Without any loss in generality, it is assumed that the mechanical effect of the size of each solid fraction may be characterized by a single parameter, the equivalent diameter of the fraction,  $\delta_i$ . In the formation of the governing equations that follows, two fractions, denoted as 1 and 2, have been assumed to be present. Any other number of fractions may be counted for by simple modifying the index “i” in the summation operation. The hydrodynamic forces, such as the drag and lift, act on all the particulate fractions as well as the gravitational force. The governing equations and boundary conditions for the three modelling particle fractions are given in the following sub-sections.

### **3.2. Governing equations for the two dimensional RANS model:**

This model is based on the complete averaged Navier-Stokes equations applied for axisymmetrical upward gas-solid particle turbulent pipe flow. The governing equations present the carrier fluid (gas-phase) and solid (polydispersed) phase that is considered as co-existed flow and consist of continuity equation for gas phase and mass conservation equation for dispersed phase together with momentum equations for both phases in streamwise and radial directions. In addition the moment of momentum equation for solid phase is included because of Magnus lift force and plausible particle rotation stemmed from the wall interaction. The solid phase is considered as polydispersed phase with two particle fractions – light (ash) particles and heavy (corundum) particles. The system of governing equations is taken from Kartushinsky and Michaelides [57, 58, 61].

The system equations are solved for the CFB flow conditions are given in chapter 2 eqs. (2.1-2.8).

### **3.3. Results and discussions**

The control volume method was used for the given RANS computations. The governing equations (2.1-2.8) were solved utilizing strong implicit procedure with lower and upper matrix decomposition and with an up-wind scheme [23]. The computations were run for 280000 uniformly distributed control volumes. The wall functions were incorporated at a dimensionless distance.

All computations were extended from the pipe entrance to a distance up to  $x/D=100$ . For the particulate phases, where the size of particles is often larger than the size of the viscous boundary sub-layer, we employed the numerical method developed by Hussainov et al [40]. All results are presented in the dimensionless way: the velocities of both phases are related to gas-phase velocity occurring at center of flow ( $r=0$ ), the turbulent energy – to square of gas-phase velocity at flow center, the particle mass concentration – to its value at flow domain center ( $r = 0$ ). It is known that the increase of the particle mass concentration as well as decrease of the particle size results in decrease of the velocity slip between average velocities of gas and dispersed phases [40]. The effect of the interparticle collisions is very important for the particulate flows of the mass ratio larger than 1 kg dust/kg air, when  $\tau_c / \tau_p < 1$ , where the time of the interparticle collision  $\tau_c$  is less than the particle response time  $\tau_p$ . We performed calculations taking into account the inter-particle collisions described by the analytically obtained stress tensor components  $\overline{v_{si}^k v_{sj}^k}$  and diffusion coefficient  $D_s^k$  which are not empirical in equations (Eqs. (4-6)); they are obtained by analytical solution from an original model of closure [57].

The results of the simulation are shown in following figures. Figure 3.1 shows the axial velocity of carrier fluid (gas-phase) and dispersed phase as a whole – average velocity of mixture of ash and corundum solid particles given as,  $\overline{u_s} = (\alpha_1 u_{s1} + \alpha_2 u_{s2}) / (\alpha_1 + \alpha_2)$ , where  $u_{s1}$  and  $\alpha_1$  are the axial linear velocity and particle mass concentration of ash particle fraction and  $u_{s2}$  and  $\alpha_2$  are the axial linear velocity and particle mass concentration of particle fraction. The profile of axial velocity of a single-phase flow is also shown in this figure. Two cases are examined, namely, the flow with solid particles of 250 microns of ash with mass loading  $c=5$  kg dust/kg air, and then mixture of large ash particles, of 400 microns and smaller corundum particles of 250 microns in case of higher mass loading,  $c=10$  kg/kg. The distribution of average velocity of dispersed phase  $\overline{u_s}$  is almost flat across the flow that versus typical velocity profiles of gas-phase. The increase of mass loading and variation of particle sizes of solid phase makes small impact on a change of shape of average velocity of solid phase. The increase of the velocity close to the wall is due to higher rate of interparticle collisions occurred for solid mixture of ash and corundum particles of different particle sizes.

The axial velocity components of different solid particles are shown in fig. 3.2. The particle velocity profiles are in consistence with their motion, so the small and lighter ash particles move faster than the same heavy 250  $\mu\text{m}$  corundum particles (cf. dashed bold and bold lines). This tendency is observed even for larger but lighter 400  $\mu\text{m}$  ash particles versus the heavy smaller 250  $\mu\text{m}$  particles (cf. dash-dotted and sold lines) that occurs for high mass loading of 10 kg dust /kg air. However, it is observed that velocity difference decreases in this case.

Figure 3.3 shows the distribution of radial velocity of gas and dispersed phases, namely, the profiles of ash and corundum particles plotted separately together with their average radial velocity, which is calculated in the same manner as previously axial velocity,  $\overline{v_s} = (\alpha_1 v_{s1} + \alpha_2 v_{s2}) / (\alpha_1 + \alpha_2)$  for different mass loadings,  $c = 5$  and  $10 \text{ kg/kg}$ , where  $v_{s1}$  is the radial linear velocity of ash particle fraction and  $v_{s2}$  is the radial linear velocity of corundum particle fraction. As one can see, radial velocity of dispersed phase has larger magnitude versus the gaseous phase. Besides, smaller and lighter ash particle have higher radial velocity than those of heavy corundum particles (cf. bold dashed line and bold solid line). Increase of mass loading results in decrease of radial velocity of dispersed phase (cf. lines for average velocity  $\overline{v_s}$  obtained for  $c = 5$  and  $10 \text{ kg/kg}$ ) which is linked with higher rate of turbulence attenuation observed for higher mass loading. The distribution of radial velocity of dispersed phase is much of importance because of impact on the mixing process.

Figure 3.4 shows distribution of angular velocity of dispersed phase for ash and corundum particles when the particles obtain rotation owing their impact with the pipe wall. As Figure 3.4 demonstrates, the angular velocity gradually increased towards the wall. The light ash particles have higher rotation in the wall vicinity than those of heavy corundum particles. Figure 3.4 also shows the average angular velocity calculated similarly to the previously for linear particle velocity components,  $\overline{\omega_s}$  and  $\overline{v_s}$ ,  $\overline{\omega_s} = (\alpha_1 \omega_{s1} + \alpha_2 \omega_{s2}) / (\alpha_1 + \alpha_2)$ , where  $\omega_{s1}$  is the radial linear velocity of ash particle fraction and  $\omega_{s2}$  is the radial linear velocity of corundum particle fraction. The effect of decrease of the particles rotation is obvious due to inertia effect of corundum particles. The particle rotation intensifies mixture process owing to the particles radial migration across the flow.

Figure 3.5 shows the distribution of turbulent energy in the single phase pipe flow and in gas-solid loaded pipe flows for different regimes: for the same particle sizes of as and corundum of 250 microns for different mass loadings  $c = 5$  and  $10 \text{ kg/kg}$  and for different particles sizes of ash of 400 microns and corundum of 250 microns for higher mass loading of  $10 \text{ kg/kg}$ . The whole trend shows that particles in all observed regimes attenuate turbulence almost along entire cross-section and they generate turbulence in wall vicinity. This is owing to their small sizes and less inertia. Following to Crowe [13] criteria the ratio of largest particle size (400 microns) to integral length scale is on the domain where particles should damp turbulence or it lays close to edge of turbulence attenuation/generation effect by presence of particles. The increase of polydispersity (variation of particle size 400 microns of ash and 250 microns of corundum together with variation of particle material density) raises the level of turbulence in tow-phase flow (cf. dashed bold line and solid bold line). Such tendency is observed with increase of mass flow ratio (cf. solid line and bold solid line in fig. 3.5). To make turbulence enhancement it would be better to use larger particles like increase at least twice their size which probably occurred in real process, for example in CFB (circulating fluidized beds).

Because of higher turbulence level leads to higher process of mixture and, thus, higher efficiency of the CFB combustion process.

Finally, Figure 3.6 shows distribution of particle mass concentration across the flow in considered flow regimes. All regimes show the general tendency of decrease of mass concentration towards the wall because of higher gravitation and less axial velocity component of the dispersed phase near the wall. The light ash particle themselves together with their average concentration  $\bar{\alpha} = \alpha_1 + \alpha_2$  for regime with the same particles of ash and corundum of 250 microns shows less accumulation of mass concentration near the wall than those with high polydispersity in particle sizes (400  $\mu\text{m}$  of ash and 250  $\mu\text{m}$  of corundum). The increase of flow mass ratio is less pronounced than those regimes with particle size variation. The particle size distribution is also very important factor for CFB efficiency. The gradient profiles of mass concentration may raise obstacles for better combustion process therefore account of corundum mass fraction distribution is needed to be done for improvement combustion cycles.

The effect of solid particles onto turbulence modulation of gas-phase is considered by Crowe & Gilland model [16] which accounts for both turbulence generation and its attenuation by presence of particles. The two additional terms are taken into account in transport equation of turbulence energy which are proportional to square of the average velocity slip between gas and particles times the particle concentration divided by particle response time and modified dissipation rate of turbulent energy. The last term is calculated via introduced hybrid length scale computed as harmonic average of integral turbulence length scale of single-phase flow and inter-particle spacing which is determined by particle mass concentration. By given the so-called “k-L” model of closure one can account both effects of particles impact on turbulence – its generation and/or its attenuation depending on the value of Stokes number, how big or small particles are, or depending on their inertia.

### 3.4. Comparison of the results

Comparing the obtained results with one by Krupenski [64], where the theoretical initial data were used, one can notice the next remarkable facts:

- the presence of the second particle fraction, namely, the heavier sand particles, results in intensification of dispersion of both lighter and heavier particles, and these results is next complicated step in comparison with Krupenski [64], where only one light particle fraction (ash particles) was considered;
- the account of lighter and heavier particle fractions is more close to real process in CFB units.

### 3.5. Conclusions

The numerical simulation of particulate flow performed by Euler/Euler (2D RANS) approach showed the importance of inclusion of second solid fraction (ash

and corundum particles) in forming of whole process occurred in CFB. The main contribution to the flow formation stemmed from the interparticle collisions and four-way coupling turbulence modulation due to the solids. The other forces exerted on the motion of solids are the gravitation, viscous drag and lift forces. On the basis of the performed calculations one can define the effects arisen from the presence of second fraction:

a) decrease of elevation rate of motion of polydispersed phase along with the velocity of carrier fluid;

b) variation of particle size in polydispersed admixture decreases its radial velocity and increases turbulence level due to interparticle collision;

c) variation of particle size in polydispersed admixture results in aligning the profiles of mass concentration in flow cross-sections because of high dispersion rate.

The obtained results can be applied for real scaled uprising CFB risers with real ash solid particles of Estonian shale if sizes of two main particle fractions will be raised.

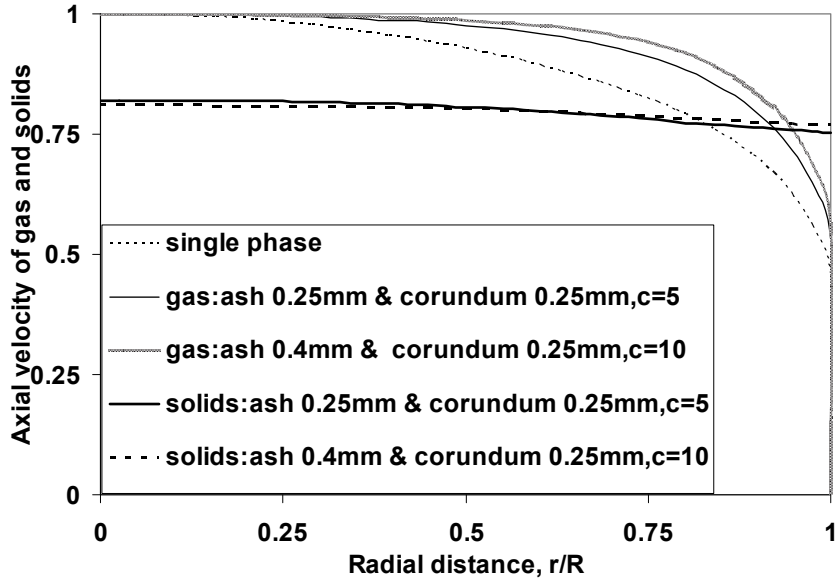


Figure 3.1. Axial velocity distribution of gas- and dispersed phases for different material densities and sizes: for ash particles 0.25 mm and 0.4 mm,  $\rho_p=1020 \text{ kg/m}^3$  and corundum particles (0.25 mm and 0.4 mm,  $\rho_p=4000 \text{ kg/m}^3$ ) and for two mass flow ratios: 5 and 10 kg/kg.

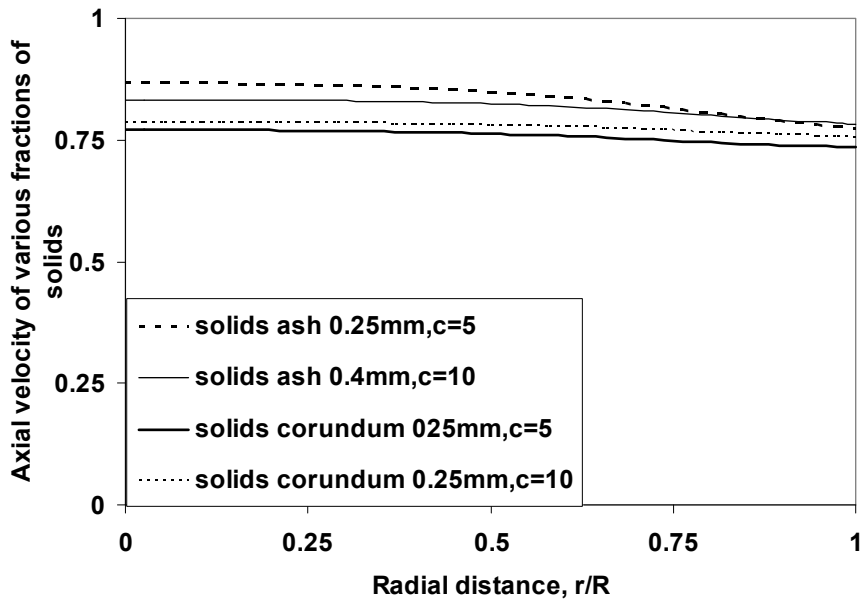


Figure 3.2. Axial velocity profiles of ash and corundum particles for various particle sizes (0.25 and 0.4mm) and mass loadings ( $c=5$  and  $10 \text{ kg/kg}$ ).

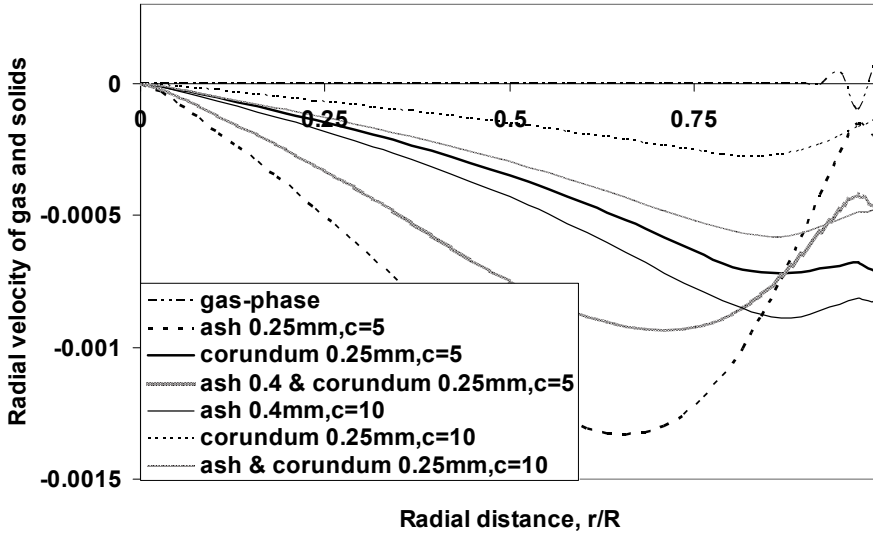


Figure 3.3. Radial velocity profiles of gas- and dispersed phases for ash and corundum particles of sizes (0.25mm and 0.4 mm) and various mass loadings ( $c=5$  and  $10$  kg/kg) and profiles of average radial of mixture of solid components,  $\overline{v}_s$  for various flow mass ratios ( $c=5$  and  $10$  kg/kg).

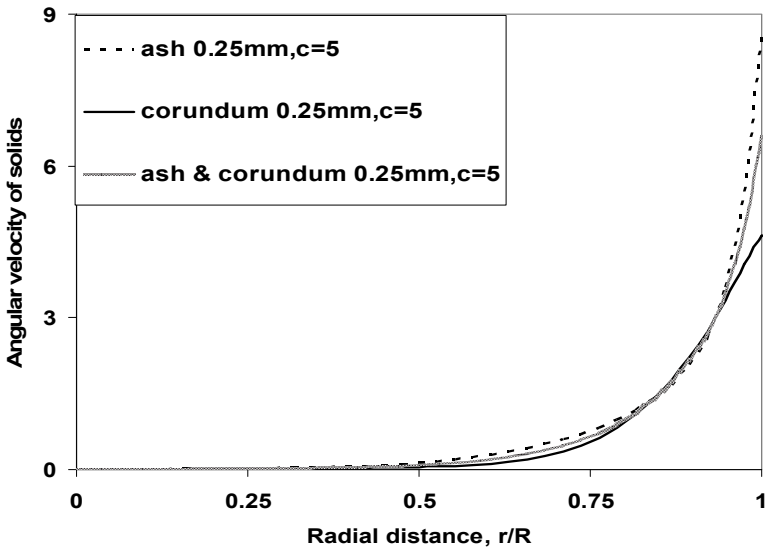


Figure 3.4. Angular velocity profiles of ash and corundum particles (0.25mm) and average profile of mixture of particles  $\overline{\omega}_s$  for mass loading  $c=5$  kg/kg.

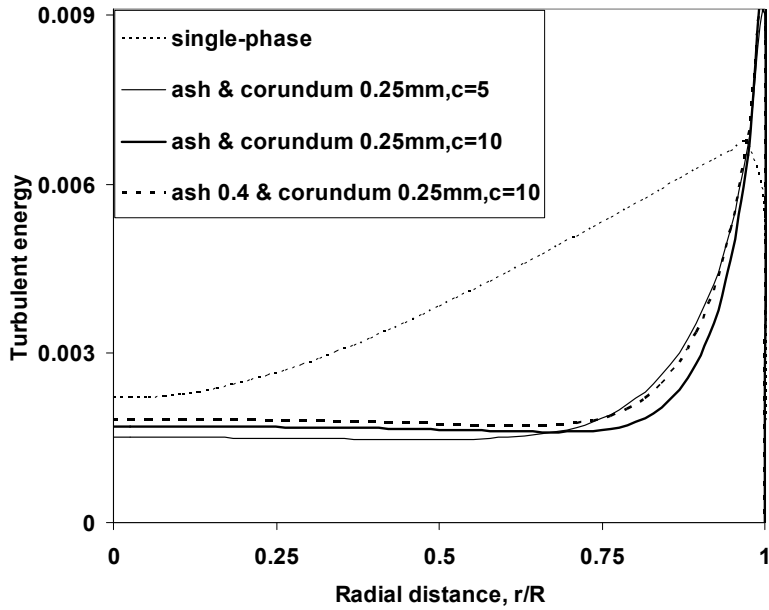


Figure 3.5. Turbulent energy profiles of single and gas phases for mixture of ash and corundum particles of the same size of 0.25 mm for flow mass ratios  $c=5$  and 10 kg/kg and for mixture of ash and corundum with different particle sizes: ash 0.4mm and corundum 0.25 mm for mass flow ratio  $c=10$  kg/kg.

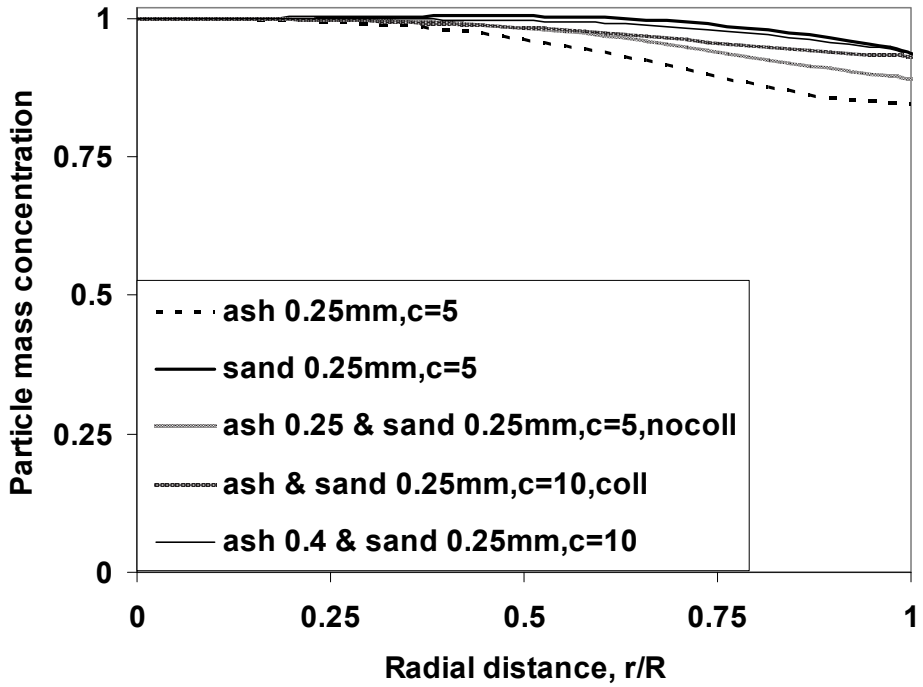


Figure 3.6. Distribution of particle mass concentration for different mixture components: for ash and corundum particles of 0.25 mm for mass ratios  $c=5$  and 10 kg/kg and for average mass concentration  $\bar{\alpha}$  for the same (ash and corundum 0.25 mm) and different particle sizes (ash 0.25 and corundum 0.4mm) for mass ratio  $c=5$  kg/kg (without particles collision) and  $c=10$  kg/kg (with particles collision).

#### **4. 3D RANS MODELLING by RSTM and TWO WAY-COUPLING EFFECT**

The 3D Reynolds stress turbulence model (RSTM) based on the 3D RANS numerical approach has been elaborated for the grid-generated turbulence in particulate downward channel flow domain. The influence of the particulate phase on the turbulence modification, namely the modification of three normal components of the Reynolds stress occurred in axial direction and in the flow cross-section, was examined for two different values of the length scale of the initial turbulence, which was set by the mesh size of the turbulence generating grid.

The presented numerical model applies the following assumptions: two-fluid model [21, 99, 103, 20, 98], the Reynolds-averaged Navier-Stokes (RANS) approach [61, 62] applied to gas and solid particles.

Within the frame of the two-fluid model, the gas and the particles are considered as two coexisting phases that span the entire flow domain [61,62]. Therefore, in order to describe the flow of the particulate phase within the two-fluid model, the presented model implements RANS approach, which is the most general and frequently used in modelling, and its closure equations have been verified by numerous experiments and the boundary conditions are easy to determine. The given modelling employs the model [13], which is the most relevant model to account for mechanisms of a turbulence modulation caused by particles, since it includes both the turbulence enhancement and its attenuation by particles the particles. The inter-particle collisions is another mechanism accounted for capture properties of turbulent particulate pipe flows and which is modelled, e.g., by Kartushinsky and Michaelides [57]. These two models enable the comprehensive mathematical simulation of two-phase upward pipe flow.

The presented model allows covering 100 and more calibres of a pipe flow. This is the main advantage over the numerical models based, for example, on the direct numerical simulation (DNS) codes[73], that handle usually with a short pipe length up to 10-20 calibres with imposing upper limit for the flow Reynolds number.

The utilized two-fluid model with adoption of original collisional closure model [57] together with applied numerical method has been verified and validated in our previous research [61,62] by comparison of numerical results with existing experimental data by Tsuji[118]. By the given study, the effect of variation of pipe diameter (or transport velocity) at constant Reynolds number is numerically investigated in the particulate turbulent flow, and this is the step forward for an analyzing of external effect, namely, the flow configuration rather the internal effect with variation of the parameters of the flow.

The numerical simulation of the stationary incompressible 3D turbulent particulate flow in the square cross-section channel was performed by the 3D RANS model with applying of the 3D Reynolds stress turbulence model for the closure of the governing equations of gas, while the particulate phase was modelled in a frame

of the 3D Euler approach with the equations closed by the two-way coupling model [16] and eddy-viscosity concept.

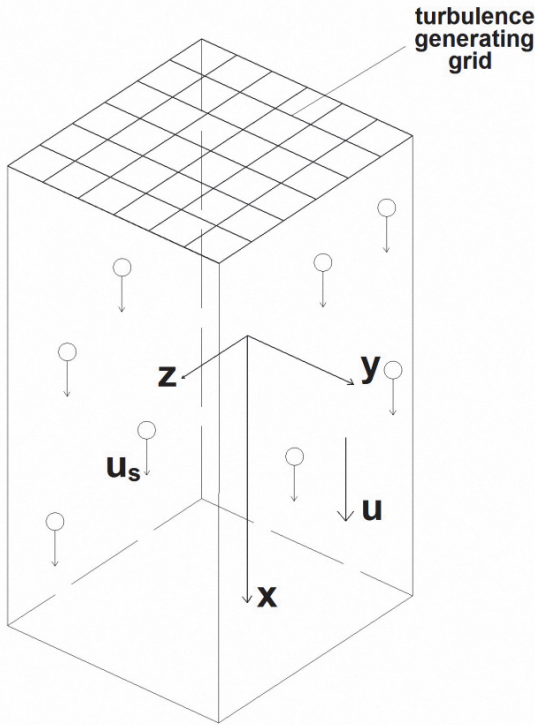


Figure 4.1 Downward grid-generated turbulent particulate flow in a pipe.

#### 4.1. Transport equations of average velocity of carrier fluid.

The particles were brought into the developed isotropic turbulent flow set-up in channel domain, which has been preliminary computed to obtain the flow velocity field. The system of the momentum and closure equations of the gas phase are identical for the unladen while the particle-laden flows under impact of the viscous drag force. Therefore, here is only presented the system of equations of the gas phase written for the case of the particle-laden flow in the Cartesian coordinates.

3D governing equations for stationary gas phase of the laden flow are written together with the closure equations as follows:

continuity equation:

$$\frac{\partial u}{\partial x} + \frac{\partial v}{\partial y} + \frac{\partial w}{\partial z} = 0, \quad (4.1)$$

where  $u$ ,  $v$  and  $w$  are the axial, transverse and spanwise time-averaged velocity components of the gas phase, respectively.

$x$ -component of the momentum equation:

$$\begin{aligned} \frac{\partial u^2}{\partial x} + \frac{\partial uv}{\partial y} + \frac{\partial uw}{\partial z} &= \frac{\partial}{\partial x} \left( 2v \frac{\partial u}{\partial x} - \overline{u'^2} \right) + \frac{\partial}{\partial y} \left[ v \left( \frac{\partial u}{\partial y} + \frac{\partial v}{\partial x} \right) - \overline{u'v'} \right] \\ &+ \frac{\partial}{\partial z} \left[ v \left( \frac{\partial u}{\partial z} + \frac{\partial w}{\partial x} \right) - \overline{u'w'} \right] - \frac{\partial p}{\rho \partial x} - \alpha C'_D \frac{(u - u_s)}{\tau_p}, \end{aligned} \quad (4.2)$$

$y$ -component of the momentum equation:

$$\begin{aligned} \frac{\partial uv}{\partial x} + \frac{\partial v^2}{\partial y} + \frac{\partial vw}{\partial z} &= \frac{\partial}{\partial x} \left[ v \left( \frac{\partial u}{\partial y} + \frac{\partial v}{\partial x} \right) - \overline{u'v'} \right] + \frac{\partial}{\partial y} \left( 2v \frac{\partial v}{\partial y} - \overline{v'^2} \right) \\ &+ \frac{\partial}{\partial z} \left[ v \left( \frac{\partial v}{\partial z} + \frac{\partial w}{\partial y} \right) - \overline{v'w'} \right] - \frac{\partial p}{\rho \partial y} - \alpha C'_D \frac{(v - v_s)}{\tau_p}, \end{aligned} \quad (4.3)$$

$z$ -component of the momentum equation:

$$\begin{aligned} \frac{\partial uw}{\partial x} + \frac{\partial vw}{\partial y} + \frac{\partial w^2}{\partial z} &= \frac{\partial}{\partial x} \left[ v \left( \frac{\partial u}{\partial z} + \frac{\partial w}{\partial x} \right) - \overline{u'w'} \right] + \frac{\partial}{\partial y} \left[ v \left( \frac{\partial v}{\partial z} + \frac{\partial w}{\partial y} \right) - \overline{v'w'} \right] \\ &+ \frac{\partial}{\partial z} \left( 2v \frac{\partial w}{\partial z} - \overline{w'^2} \right) - \frac{\partial p}{\rho \partial z} - \alpha C'_D \frac{(w - w_s)}{\tau_p}, \end{aligned} \quad (4.4)$$

## 4.2. Transport equations of Reynolds stresses of carrier fluid.

The transport equation of the  $x$ -normal component of the Reynolds stress:

$$\begin{aligned} &\frac{\partial(\overline{uu'^2})}{\partial x} + \frac{\partial(\overline{vu'^2})}{\partial y} + \frac{\partial(\overline{wu'^2})}{\partial z} \\ &= \frac{\partial}{\partial x} \left[ (C_s T \overline{u'^2} + \nu) \frac{\partial \overline{u'^2}}{\partial x} + C_s T \left( \overline{u'v'} \frac{\partial \overline{u'^2}}{\partial y} + \overline{u'w'} \frac{\partial \overline{u'^2}}{\partial z} \right) \right] + \frac{\partial}{\partial y} \left[ (C_s T \overline{v'^2} + \nu) \frac{\partial \overline{u'^2}}{\partial y} \right. \\ &\quad \left. + C_s T \left( \overline{u'v'} \frac{\partial \overline{u'^2}}{\partial x} + \overline{v'w'} \frac{\partial \overline{u'^2}}{\partial z} \right) \right] + \frac{\partial}{\partial z} \left[ (C_s T \overline{w'^2} + \nu) \frac{\partial \overline{u'^2}}{\partial z} + C_s T \left( \overline{u'w'} \frac{\partial \overline{u'^2}}{\partial x} + \overline{v'w'} \frac{\partial \overline{u'^2}}{\partial y} \right) \right] \end{aligned}$$

$$+ P_{uu} + R_{uu} + \alpha C'_D \frac{(u - u_s)^2}{\tau_p} - \varepsilon_h, \quad (4.5)$$

The transport equation of the  $y$ -normal component of the Reynolds stress:

$$\begin{aligned} & \frac{\partial(\overline{uv'^2})}{\partial x} + \frac{\partial(\overline{vv'^2})}{\partial y} + \frac{\partial(\overline{wv'^2})}{\partial z} \\ &= \frac{\partial}{\partial x} \left[ (C_s T \overline{u'^2} + \nu) \frac{\partial \overline{v'^2}}{\partial x} + C_s T \left( \overline{u'v'} \frac{\partial \overline{v'^2}}{\partial y} + \overline{u'w'} \frac{\partial \overline{v'^2}}{\partial z} \right) \right] + \frac{\partial}{\partial y} \left[ (C_s T \overline{v'^2} + \nu) \frac{\partial \overline{v'^2}}{\partial y} \right. \\ & \left. + C_s T \left( \overline{u'v'} \frac{\partial \overline{v'^2}}{\partial x} + \overline{v'w'} \frac{\partial \overline{v'^2}}{\partial z} \right) \right] + \frac{\partial}{\partial z} \left[ (C_s T \overline{w'^2} + \nu) \frac{\partial \overline{v'^2}}{\partial z} + C_s T \left( \overline{u'w'} \frac{\partial \overline{v'^2}}{\partial x} + \overline{v'w'} \frac{\partial \overline{v'^2}}{\partial y} \right) \right] \\ & + P_{vv} + R_{vv} + \alpha C'_D \frac{(v - v_s)^2}{\tau_p} - \varepsilon_h, \end{aligned} \quad (4.6)$$

The transport equation of the  $z$ -normal component of the Reynolds stress:

$$\begin{aligned} & \frac{\partial(\overline{uw'^2})}{\partial x} + \frac{\partial(\overline{vw'^2})}{\partial y} + \frac{\partial(\overline{ww'^2})}{\partial z} \\ &= \frac{\partial}{\partial x} \left[ (C_s T \overline{u'^2} + \nu) \frac{\partial \overline{w'^2}}{\partial x} + C_s T \left( \overline{u'v'} \frac{\partial \overline{w'^2}}{\partial y} + \overline{u'w'} \frac{\partial \overline{w'^2}}{\partial z} \right) \right] + \frac{\partial}{\partial y} \left[ (C_s T \overline{v'^2} + \nu) \frac{\partial \overline{w'^2}}{\partial y} \right. \\ & \left. + C_s T \left( \overline{u'v'} \frac{\partial \overline{w'^2}}{\partial x} + \overline{v'w'} \frac{\partial \overline{w'^2}}{\partial z} \right) \right] + \frac{\partial}{\partial z} \left[ (C_s T \overline{w'^2} + \nu) \frac{\partial \overline{w'^2}}{\partial z} + C_s T \left( \overline{u'w'} \frac{\partial \overline{w'^2}}{\partial x} + \overline{v'w'} \frac{\partial \overline{w'^2}}{\partial y} \right) \right] \\ & + P_{ww} + R_{ww} + \alpha C'_D \frac{(w - w_s)^2}{\tau_p} - \varepsilon_h, \end{aligned} \quad (4.7)$$

The transport equation of the  $xy$  shear stress component of the Reynolds stress:

$$\frac{\partial(\overline{uu'v'})}{\partial x} + \frac{\partial(\overline{vu'v'})}{\partial y} + \frac{\partial(\overline{wu'v'})}{\partial z}$$

$$\begin{aligned}
&= \frac{\partial}{\partial x} \left[ \left( C_s T \overline{u'^2} + \nu \right) \frac{\partial \overline{u'v'}}{\partial x} + C_s T \left( \overline{u'v'} \frac{\partial \overline{u'v'}}{\partial y} + \overline{u'w'} \frac{\partial \overline{u'v'}}{\partial z} \right) \right] + \frac{\partial}{\partial y} \left[ \left( C_s T \overline{v'^2} + \nu \right) \frac{\partial \overline{u'v'}}{\partial y} \right. \\
&+ C_s T \left( \overline{u'v'} \frac{\partial \overline{u'v'}}{\partial x} + \overline{v'w'} \frac{\partial \overline{u'v'}}{\partial z} \right) \left. \right] + \frac{\partial}{\partial z} \left[ \left( C_s T \overline{w'^2} + \nu \right) \frac{\partial \overline{u'v'}}{\partial z} + C_s T \left( \overline{u'w'} \frac{\partial \overline{u'v'}}{\partial x} + \overline{v'w'} \frac{\partial \overline{u'v'}}{\partial y} \right) \right] \\
&+ P_{uv} + R_{uv}, \tag{4.8}
\end{aligned}$$

The transport equation of the  $xz$  shear stress component of the Reynolds stress:

$$\begin{aligned}
&\frac{\partial (\overline{uu'w'})}{\partial x} + \frac{\partial (\overline{vu'w'})}{\partial y} + \frac{\partial (\overline{wu'w'})}{\partial z} \\
&= \frac{\partial}{\partial x} \left[ \left( C_s T \overline{u'^2} + \nu \right) \frac{\partial \overline{u'w'}}{\partial x} + C_s T \left( \overline{u'v'} \frac{\partial \overline{u'w'}}{\partial y} + \overline{u'w'} \frac{\partial \overline{u'w'}}{\partial z} \right) \right] + \frac{\partial}{\partial y} \left[ \left( C_s T \overline{v'^2} + \nu \right) \frac{\partial \overline{u'w'}}{\partial y} \right. \\
&+ C_s T \left( \overline{u'v'} \frac{\partial \overline{u'w'}}{\partial x} + \overline{v'w'} \frac{\partial \overline{u'w'}}{\partial z} \right) \left. \right] + \frac{\partial}{\partial z} \left[ \left( C_s T \overline{w'^2} + \nu \right) \frac{\partial \overline{u'w'}}{\partial z} + C_s T \left( \overline{u'w'} \frac{\partial \overline{u'w'}}{\partial x} + \overline{v'w'} \frac{\partial \overline{u'w'}}{\partial y} \right) \right] \\
&+ P_{uw} + R_{uw}, \tag{4.9}
\end{aligned}$$

The transport equation of the  $yz$  shear stress component of the Reynolds stress:

$$\begin{aligned}
&\frac{\partial (\overline{uv'w'})}{\partial x} + \frac{\partial (\overline{vv'w'})}{\partial y} + \frac{\partial (\overline{wv'w'})}{\partial z} \\
&= \frac{\partial}{\partial x} \left[ \left( C_s T \overline{u'^2} + \nu \right) \frac{\partial \overline{v'w'}}{\partial x} + C_s T \left( \overline{u'v'} \frac{\partial \overline{v'w'}}{\partial y} + \overline{u'w'} \frac{\partial \overline{v'w'}}{\partial z} \right) \right] + \frac{\partial}{\partial y} \left[ \left( C_s T \overline{v'^2} + \nu \right) \frac{\partial \overline{v'w'}}{\partial y} \right. \\
&+ C_s T \left( \overline{u'v'} \frac{\partial \overline{v'w'}}{\partial x} + \overline{v'w'} \frac{\partial \overline{v'w'}}{\partial z} \right) \left. \right] + \frac{\partial}{\partial z} \left[ \left( C_s T \overline{w'^2} + \nu \right) \frac{\partial \overline{v'w'}}{\partial z} + C_s T \left( \overline{u'w'} \frac{\partial \overline{v'w'}}{\partial x} + \overline{v'w'} \frac{\partial \overline{v'w'}}{\partial y} \right) \right] \\
&+ P_{vw} + R_{vw}, \tag{4.10}
\end{aligned}$$

The transport equation of the dissipation rate of the turbulence kinetic energy:

$$\frac{\partial u_0 \varepsilon_0}{\partial x} + \frac{\partial v_0 \varepsilon_0}{\partial y} + \frac{\partial w_0 \varepsilon_0}{\partial z} = \frac{\partial}{\partial x} \left[ \left( C_\varepsilon T_0 \overline{u_0'^2} + \nu \right) \frac{\partial \varepsilon_0}{\partial x} + C_\varepsilon T_0 \left( \overline{u_0'v_0'} \frac{\partial \varepsilon_0}{\partial y} + \overline{u_0'w_0'} \frac{\partial \varepsilon_0}{\partial z} \right) \right]$$

$$\begin{aligned}
& + \frac{\partial}{\partial y} \left[ \left( C_\varepsilon T_0 \overline{v'^2} + \nu \right) \frac{\partial \varepsilon_0}{\partial y} + C_\varepsilon T_0 \left( \overline{u'_0 v'_0} \frac{\partial \varepsilon_0}{\partial x} + \overline{v'_0 w'_0} \frac{\partial \varepsilon_0}{\partial z} \right) \right] + \frac{\partial}{\partial z} \left[ \left( C_\varepsilon T_0 \overline{w'^2} + \nu \right) \frac{\partial \varepsilon_0}{\partial z} \right. \\
& \left. + C_\varepsilon T_0 \left( \overline{u'_0 w'_0} \frac{\partial \varepsilon_0}{\partial x} + \overline{v'_0 w'_0} \frac{\partial \varepsilon_0}{\partial y} \right) \right] + C_{\varepsilon_1} \frac{P \varepsilon_0}{k_0} - C_{\varepsilon_2} \frac{\varepsilon_0^2}{k_0}, \tag{4.11}
\end{aligned}$$

The given system of the transport equations (Eqs. 4.1–4.11) is based on the model by Launder [66] with applying of the numerical constants taken from Pope [94]:  $C_R=1.8$ ,  $C_2=0.6$ ,  $C_s=0.22$ ,  $C_\varepsilon=0.18$ ,  $C_{\varepsilon_1}=1.44$ ,  $C_{\varepsilon_2}=1.92$ .

Here  $T_0 = \frac{k_0}{\varepsilon_0}$  and  $T = \frac{k}{\varepsilon}$  are the turbulence integral time scales for the

unladen and particle-laden flows, respectively.  $k = 0.5(\overline{u'^2} + \overline{v'^2} + \overline{w'^2})$  and  $k_0 = 0.5(\overline{u_0'^2} + \overline{v_0'^2} + \overline{w_0'^2})$  are the turbulence kinetic energy of gas in the particle-laden and in the unladen flows, respectively;  $\varepsilon$  and  $\varepsilon_0$  are the dissipation rates of the turbulence kinetic energy in the particle-laden and unladen flows, respectively;  $\tau_p$  is the Stokesian particle response time,

$\tau_p = \frac{\rho_p \delta^2}{18 \rho \nu}$ ;  $\nu$  is the gas viscosity;  $(u - u_s)$ ,  $(v - v_s)$  and  $(w - w_s)$  are the components of the slip velocity.

The additional terms of Eqs. (4.2–4.7) pertain to presence of particles in the flow and contain the particle mass concentration  $\alpha$ . The influence of particles on gas is considered by the aerodynamic drag force in the momentum equations (the last term of the right-hand sides of Eqs. (4.2–4.4), and by the turbulence generation and attenuation effects contained in the transport equations of components of the Reynolds stress (the penultimate and last terms of the right-hand sides of Eqs. (4.5–4.7), respectively). The given model applies the two-way coupling approach by Crowe & Gilland [16], where the turbulence generation terms are proportional to the squared slip velocity, and the turbulence attenuation terms are expressed via the hybrid length scale  $L_h$  and the hybrid dissipation rate  $\varepsilon_h$  of the particle-laden flow, where  $L_h$  is calculated as the harmonic average of the integral length scale of the unladen flow  $L_0$  and the interparticle distance  $\lambda$ . Here  $\lambda = \delta \left( \sqrt[3]{\pi \rho_p / 6 \rho \alpha} - 1 \right)$ ,

$$L_0 = \frac{k_0^{3/2}}{\varepsilon_0}, \quad L_h = \frac{2L_0 \lambda}{L_0 + \lambda}, \quad \varepsilon_h = \frac{k^{3/2}}{L_h}.$$

The particles influence on the shear Reynolds stress components is considered in Eqs. (4.8–4.10) indirectly via the averaged velocity flow field  $(u, v, w)$ .

The production terms  $P$  are determined according to Pope [94] as follows:

$$P_{uu} = -2 \left( \overline{u'^2} \frac{\partial u}{\partial x} + \overline{u'v'} \frac{\partial u}{\partial y} + \overline{u'w'} \frac{\partial u}{\partial z} \right), \quad (4.12)$$

$$P_{vv} = -2 \left( \overline{u'v'} \frac{\partial v}{\partial x} + \overline{v'^2} \frac{\partial v}{\partial y} + \overline{v'w'} \frac{\partial v}{\partial z} \right), \quad (4.13)$$

$$P_{ww} = -2 \left( \overline{u'w'} \frac{\partial w}{\partial x} + \overline{v'w'} \frac{\partial w}{\partial y} + \overline{w'^2} \frac{\partial w}{\partial z} \right), \quad (4.14)$$

$$P_{uv} = - \left( \overline{u'^2} \frac{\partial v}{\partial x} + \overline{u'v'} \frac{\partial v}{\partial y} + \overline{u'w'} \frac{\partial v}{\partial z} + \overline{u'v'} \frac{\partial u}{\partial x} + \overline{v'^2} \frac{\partial u}{\partial y} + \overline{v'w'} \frac{\partial u}{\partial z} \right), \quad (4.15)$$

$$P_{uw} = - \left( \overline{u'^2} \frac{\partial w}{\partial x} + \overline{u'v'} \frac{\partial w}{\partial y} + \overline{u'w'} \frac{\partial w}{\partial z} + \overline{u'w'} \frac{\partial u}{\partial x} + \overline{v'w'} \frac{\partial u}{\partial y} + \overline{w'^2} \frac{\partial u}{\partial z} \right), \quad (4.16)$$

$$P_{vw} = - \left( \overline{u'v'} \frac{\partial w}{\partial x} + \overline{v'^2} \frac{\partial w}{\partial y} + \overline{v'w'} \frac{\partial w}{\partial z} + \overline{u'w'} \frac{\partial v}{\partial x} + \overline{v'w'} \frac{\partial v}{\partial y} + \overline{w'^2} \frac{\partial v}{\partial z} \right), \quad (4.17)$$

$$P = \frac{1}{2} (P_{uu} + P_{vv} + P_{ww}) = \overline{u'^2} \frac{\partial u}{\partial x} + \overline{u'v'} \frac{\partial u}{\partial y} + \overline{u'w'} \frac{\partial u}{\partial z} + \overline{u'v'} \frac{\partial v}{\partial x} + \overline{v'^2} \frac{\partial v}{\partial y} + \overline{v'w'} \frac{\partial v}{\partial z} + \overline{u'w'} \frac{\partial w}{\partial x} + \overline{v'w'} \frac{\partial w}{\partial y} + \overline{w'^2} \frac{\partial w}{\partial z}. \quad (4.18)$$

The diffusive or second order partial differentiation over Cartesian coordinates, i.e. the first three terms in Eqs. (5 - 11) are given, e.g. by [94]. The anisotropy terms  $R$  of the normal and shear components of the Reynolds stress  $\overline{u'^2}$ ,  $\overline{v'^2}$ ,  $\overline{w'^2}$ ,  $\overline{u'v'}$ ,  $\overline{u'w'}$ ,  $\overline{v'w'}$ , are defined by various pressure-rate-of-strain models of the isotropic turbulence written in terms of variation of constants  $C_R$  and  $C_2$  [94] as follows:

$$R_{uu} = - \frac{(C_R - 1)}{T} \left( \overline{u'^2} - \frac{2}{3} k \right) - C_2 \left( P_{uu} - \frac{2}{3} P \right), \quad (4.19)$$

$$R_{vv} = - \frac{(C_R - 1)}{T} \left( \overline{v'^2} - \frac{2}{3} k \right) - C_2 \left( P_{vv} - \frac{2}{3} P \right), \quad (4.20)$$

$$R_{ww} = - \frac{(C_R - 1)}{T} \left( \overline{w'^2} - \frac{2}{3} k \right) - C_2 \left( P_{ww} - \frac{2}{3} P \right), \quad (4.21)$$

$$R_{uv} = -\frac{(C_R - 1)\overline{u'v'}}{T} - C_2 P_{uv}, \quad (4.22)$$

$$R_{uw} = -\frac{(C_R - 1)\overline{u'w'}}{T} - C_2 P_{uw}, \quad (4.23)$$

$$R_{vw} = -\frac{(C_R - 1)\overline{v'w'}}{T} - C_2 P_{vw} \quad (4.24)$$

The relative friction coefficient  $C'_D$  is expressed as  $C'_D = 1 + 0.15 Re_s^{0.687}$  for the non-Stokesian streamlining of particle. The particle Reynolds number  $Re_s$  is calculated according to [100] as  $Re_s = \delta \sqrt{(u - u_s)^2 + (v - v_s)^2 + (w - w_s)^2} / \nu$ .

### 4.3. Transport equations of average velocity of solid phase & particles feedback

3D governing equations for the particulate phase are written as follows:

- the particle mass conservation equation:

$$\frac{\partial(\alpha u_s)}{\partial x} + \frac{\partial(\alpha v_s)}{\partial y} + \frac{\partial(\alpha w_s)}{\partial z} = \frac{\partial}{\partial x} D_s \frac{\partial \alpha}{\partial x} + \frac{\partial}{\partial y} D_s \frac{\partial \alpha}{\partial y} + \frac{\partial}{\partial z} D_s \frac{\partial \alpha}{\partial z}, \quad (4.25)$$

- x-component of the momentum equation:

$$\begin{aligned} \frac{\partial(\alpha u_s^2)}{\partial x} + \frac{\partial(\alpha u_s v_s)}{\partial y} + \frac{\partial(\alpha u_s w_s)}{\partial z} &= \frac{\partial}{\partial x} \alpha \left( 2v_s \frac{\partial u_s}{\partial x} - \frac{2}{3} k_s \right) + \frac{\partial}{\partial y} \left[ \alpha v_s \left( \frac{\partial u_s}{\partial y} + \frac{\partial v_s}{\partial x} \right) \right] \\ &+ \frac{\partial}{\partial z} \left[ \alpha v_s \left( \frac{\partial u_s}{\partial z} + \frac{\partial w_s}{\partial x} \right) \right] + \alpha C'_D \frac{(u - u_s)}{\tau_p} - \alpha g \left( 1 - \frac{\rho}{\rho_p} \right), \end{aligned} \quad (4.26)$$

- y-component of the momentum equation:

$$\begin{aligned} \frac{\partial(\alpha u_s v_s)}{\partial x} + \frac{\partial(\alpha v_s^2)}{\partial y} + \frac{\partial(\alpha v_s w_s)}{\partial z} &= \frac{\partial}{\partial x} \left[ \alpha v_s \left( \frac{\partial u_s}{\partial y} + \frac{\partial v_s}{\partial x} \right) \right] + \frac{\partial}{\partial y} \left[ \alpha v_s \left( \frac{\partial v_s}{\partial y} - \frac{2}{3} k_s \right) \right] \\ &+ \frac{\partial}{\partial z} \left[ \alpha v_s \left( \frac{\partial v_s}{\partial z} + \frac{\partial w_s}{\partial y} \right) \right] + \alpha C'_D \frac{(v - v_s)}{\tau_p}, \end{aligned} \quad (4.27)$$

- z-component of the momentum equation:

$$\begin{aligned} \frac{\partial(\alpha u_s w_s)}{\partial x} + \frac{\partial(\alpha v_s w_s)}{\partial y} + \frac{\partial(\alpha w_s^2)}{\partial z} &= \frac{\partial}{\partial x} \left[ \alpha \nu_s \left( \frac{\partial u_s}{\partial z} + \frac{\partial w_s}{\partial x} \right) \right] + \frac{\partial}{\partial y} \left[ \alpha \nu_s \left( \frac{\partial v_s}{\partial z} + \frac{\partial w_s}{\partial y} \right) \right] \\ &+ \frac{\partial}{\partial z} \alpha \left( 2\nu_s \frac{\partial w_s}{\partial z} - \frac{2}{3} k_s \right) + \alpha C'_D \frac{(w - w_s)}{\tau_p}. \end{aligned} \quad (4.28)$$

The closure model for the transport equations of the particulate phase was applied to the PDF model by Zaichik and Alipchenkov [136], where the turbulent kinetic energy of dispersed phase, the coefficients of the turbulent viscosity and turbulent diffusion of the particulate phase are determined as follows, respectively:

$$\begin{aligned} k_s &= \left[ 1 - \exp\left(-\frac{T_0}{\tau'_p}\right) \right] k, \\ \nu_s &= \left( \nu_t + \frac{\tau'_p k}{3} \right) \left[ 1 - \exp\left(-\frac{T_0}{\tau'_p}\right) \right], \\ D_s &= \frac{2k}{3} \left( 1 + \frac{T_0}{\tau} \right) \left[ 1 - \exp\left(-\frac{T_0}{\tau}\right) \right] \end{aligned} \quad (4.29)$$

where  $\nu_t$  is the turbulent viscosity,  $\nu_t = 0.09 \frac{k_0^2}{\varepsilon_0}$  and  $\tau'_p = \tau_p / C'_D$  is the particle response time with respect of correction of the particles motion to the non-Stokesian regime.

#### 4.4. Boundary conditions.

The flow being discussed here is vertical, and it is symmetrical with respect to the vertical axis. Therefore, the symmetry conditions are set at the flow axis, and the wall conditions are set at the wall.

The axisymmetric conditions are written as follows:

for  $y=0$ :

$$\frac{\partial u}{\partial y} = \frac{\partial \overline{u^2}}{\partial y} = \frac{\partial \overline{v^2}}{\partial y} = \frac{\partial \overline{w'^2}}{\partial y} = \frac{\partial \varepsilon}{\partial y} = \frac{\partial u_s}{\partial y} = \frac{\partial \alpha}{\partial y} = v = w = \overline{u'v'} = \overline{u'w'} = \overline{v'w'} = v_s = w_s = 0, \quad (4.30)$$

for  $z=0$ :

$$\frac{\partial u}{\partial z} = \frac{\partial \overline{u'^2}}{\partial z} = \frac{\partial \overline{v'^2}}{\partial z} = \frac{\partial \overline{w'^2}}{\partial z} = \frac{\partial \varepsilon}{\partial z} = \frac{\partial u_s}{\partial z} = \frac{\partial \alpha}{\partial z} = v = w = \overline{u'v'} = \overline{u'w'} = \overline{v'w'} = v_s = w_s = 0 \quad (4.31)$$

The wall conditions are written as follows:

$$\text{for } y = 0.5h : \quad u^+ = \frac{u}{v_*} = \begin{cases} y^+ \\ \frac{1}{\alpha} \ln y^+ + B \end{cases}, \quad (4.32)$$

$$\text{for } z = 0.5h : \quad u^+ = \frac{u}{v_*} = \begin{cases} z^+ \\ \frac{1}{\alpha} \ln z^+ + B \end{cases}, \quad (4.33)$$

$$v = w = 0, \quad (4.34)$$

where  $h$  is the channel width;  $v_*$  is the friction velocity of gas; the empirical constant  $\alpha = 0.41$ ; the wall coordinates  $y^+$  and  $z^+$  correspond to the transverse and spanwise directions, respectively:

$$y^+ = \frac{v_* \Delta y}{2\nu}, \quad z^+ = \frac{v_* \Delta z}{2\nu}.$$

Here  $\Delta y$ ,  $\Delta z$  are the width and height of the control volume; the numerical constant  $B$  equals 5.2 for the smooth wall of the channel.

The friction velocity of gas  $v_*$  can be determined according to Peric and Scheuerer [92] as follows:

$$v_* = (c_\mu/2)^{0.25} \sqrt{k},$$

where  $c_\mu$  is the numerical constant of the  $k - \varepsilon$  model,  $c_\mu = 0.09$ .

For the normal and shear stresses and dissipation rate of the unladen flow calculated at the wall, the boundary conditions are set based on the “wall-function” according to Pope [94] with the following relationships for the production and dissipation terms:

for  $y = 0.5h$  :

$$P_{uu} = -\overline{u'v'} \frac{\partial u}{\partial y}, \quad P_{vv} = P_{ww} = P_{uv} = P_{uw} = P_{vw} = 0, \quad (4.35)$$

$$\varepsilon = \frac{2c_{\mu}^{0.75} k^{1.5}}{\alpha \Delta y}, \quad (4.36)$$

for  $z = 0.5h$  :

$$P_{uu} = -\overline{u'w'} \frac{\partial u}{\partial z}, \quad P_{vv} = P_{ww} = P_{uv} = P_{uw} = P_{vw} = 0, \quad (4.37)$$

$$\varepsilon = \frac{2c_{\mu}^{0.75} k^{1.5}}{\alpha \Delta z} \quad (4.38)$$

The boundary conditions for the particulate phase are set at the wall as follows:

$$\text{for } y = 0.5h : \quad \frac{\partial u_s}{\partial y} = -\lambda u_s, \quad \frac{\partial w_s}{\partial y} = -\lambda w_s, \quad \frac{\partial \alpha}{\partial y} = D_s \alpha, \quad v_s = 0, \quad (4.39)$$

$$\text{for } z = 0.5h : \quad \frac{\partial u_s}{\partial z} = -\lambda u_s; \quad \frac{\partial v_s}{\partial z} = -\lambda v_s, \quad \frac{\partial \alpha}{\partial z} = D_s \alpha; \quad w_s = 0. \quad (4.40)$$

At the exit of the channel the following boundary conditions are set:

$$\frac{\partial u}{\partial x} = \frac{\partial v}{\partial x} = \frac{\partial w}{\partial x} = \frac{\partial u^2}{\partial x} = \frac{\partial v^2}{\partial x} = \frac{\partial w^2}{\partial x} = \frac{\partial uv}{\partial x} = \frac{\partial uw}{\partial x} = \frac{\partial vw}{\partial x} = \frac{\partial \varepsilon}{\partial x} = \frac{\partial u_s}{\partial x} = \frac{\partial v_s}{\partial x} = \frac{\partial w_s}{\partial x} = \frac{\partial \alpha}{\partial x} = 0 \quad (4.41)$$

Additionally, the initial boundary conditions are set for three specific cases:

- 1) the low level of the initial intensity of turbulence that usually occurs at the axis of the channel turbulent flow;
- 2) the high level of the initial turbulence generated by two different grids:
  - a) small grid of the mesh size  $M=4.8$  mm;
  - b) large grid with mesh size of  $M=10$  mm.

#### 4.5. Numerical method and results.

The control volume method was applied to solve the 3D partial differential equations written for the unladen flow (Eqs. 4.1 – 4.11) and the particulate phase (Eqs. 4.26 – 4.29), respectively, with taking into account the boundary conditions (Eqs. 4.30 – 4.41). The governing equations were solved using the implicit lower and upper (ILU) matrix decomposition method with the flux-blending differenced-correction and upwind-differencing schemes by Perić and Scheuerer [92]. This method is utilized for the calculations of the particulate turbulent flows in channels

of the rectangular and square cross-sections. The calculations were performed in the dimensional form for all the flow conditions. The number of the control volumes was 1120000.

The presented RSTM model has been verified and validated by comparison of the numerical results with the experimental data got by Hussainov et al. [44] for the grid-generated turbulent downward vertical channel flow of 200 mm square cross-section loaded with 700- $\mu\text{m}$  glass beads of the physical density  $\rho_p=2500 \text{ kg/m}^3$ . The mean flow velocity  $U$  was 9.5 m/s, the flow mass loading  $m^*$  was 0.14 kg dust/kg air. The grids of the square mesh size  $M = 4.8$  and 10 mm were used for generating of the flow initial turbulence length scale.

The validity criterion is based on the satisfactory agreement of the axial turbulence decay curves occurring behind different grids in the unladen and particle-laden flows obtained by the given RSTM model and by the experiments of Hussainov et al. [44]. Figure 4.2 demonstrates such agreement for the grid  $M = 4.8$  mm.

Figure 4.3 shows the decay curves calculated by the presented RSTM model for the grids  $M=4.8$  and 10 mm. As follows from Fig. 4.2 and 4.3, the pronounced turbulence enhancement by particles is observed for both grids. The character of the turbulence attenuation occurring along the flow axis agrees with the behaviour of the decay curves in the grid-generated turbulent flows described by Hinze [36]. Figures 4.4–4.9 show the cross-section modifications of three components of the Reynolds stress,  $\Delta_u$ ,  $\Delta_v$ ,  $\Delta_w$ , caused by 700  $\mu\text{m}$  glass beads, calculated by the presented RSTM model at two locations of the initial period of the grid-generated turbulence decay  $x/M = 46$  and 93 as well as beyond it for  $x/M \approx 200$ . Here:

$$\Delta_u = \frac{\overline{u'^2} - \overline{u_0'^2}}{\overline{u_0'^2}} \%, \quad \Delta_v = \frac{\overline{v'^2} - \overline{v_0'^2}}{\overline{v_0'^2}} \%, \quad \Delta_w = \frac{\overline{w'^2} - \overline{w_0'^2}}{\overline{w_0'^2}} \%, \quad (4.42)$$

One can see that the turbulence enhancement occupies over 75 percents of the half-width of the channel, that takes place at the initial period of the turbulence decay of the particle-laden flow as compared to the unladen flow. Along with, the distributions of  $\Delta_u$ ,  $\Delta_v$  and  $\Delta_w$  are uniform that corresponds to the initial grid-generated homogeneous isotropic turbulence, which decays downstream (Fig. 4.2 and 4.3). The distributions of modification of  $\Delta_u$ ,  $\Delta_v$  and  $\Delta_w$  remain uniform downstream. At the same time, the cross-section extent of uniformity of distributions of components of the Reynolds stress and the degree of the particles effect on turbulence decrease, since the turbulence level decreases downstream (cf. data presented for  $x/M = 46$  and 93 in Fig. 4.4–4.9).

The distributions of modification of  $\Delta_u$ ,  $\Delta_v$  and  $\Delta_w$  taken place beyond the initial period of the turbulence decay (location  $x/M \approx 200$  at Fig. 4.4–4.9) are typical of the channel turbulent particulate flow. One can see that in this case the turbulence enhancement becomes slower, since here the turbulence level is substantially smaller as compared with the initial period of decay, i.e. for  $x/M < 100$  (Fig. 4.2 and 4.3). This means that the grid-generated turbulence of the particulate flow decays downstream, and this causes the decrease of the rate of turbulence enhancement due to the particles occurred beyond the initial period of the turbulence decay. As a result, the turbulence is attenuated, that is expressed in terms of decrease of  $\Delta_u$  towards the pipe wall (Fig. 4.7). Such tendency has been shown qualitatively by Kartushinsky et al. [62].

The certain increase of  $\Delta_u$ ,  $\Delta_v$  and  $\Delta_w$ , that is observed verge towards the wall (Fig. 4.4–4.9), arises from the growth of the slip velocity (curves 1, 2, 3 in Fig. 4.10). The decrease of  $\Delta_u$ ,  $\Delta_v$  and  $\Delta_w$  taken place in the immediate vicinity of the wall is caused by the decrease of the length scale of the energy-containing vortices and, thus, the increase of the dissipation of the turbulence kinetic energy.

The analysis of Fig. 4.11 shows that the increase of the grid mesh size results in the weaker contribution of particles to the turbulence enhancement and dissipation of the kinetic energy taking place over the cross-section for the initial period of the turbulence decay. This can be explained by the higher rate of the particles involvement into the turbulent motion due to the longer residence time that comes from the larger size of the eddies.

## 4.6. Conclusions

3D Reynolds stress turbulence model (RSTM) based on the 3D RANS numerical approach has been elaborated for the grid-generated turbulence in particulate downward channel flow domain.

The influence of the particulate phase on the turbulence modification, namely the modification of three normal components of the Reynolds stress occurred in axial direction and in the flow cross-section, was examined for two different values of the length scale of the initial turbulence, which was set by the mesh size of the turbulence generating grid.

The obtained numerical results allow to draw the following conclusions:

1. The presence of the considered solid particles at the initial period of the turbulence decay results in the pronounced turbulence enhancement that observed for both turbulence generating grids.

2. The character of modification of the normal components of the Reynolds stress taken place at the initial period of the turbulence decay are uniform almost all over the channel cross-section. As the turbulence level diminishes downstream, the extent of this uniformity (plateau width) and the degree of the particles effect on turbulence decrease.

3. The rate of the turbulence enhancement, that occurs beyond the initial period of the turbulence decay, reduces. The character of the turbulence modification changes from initially uniform distributions of the normal components of the Reynolds stress to the ones that are inherent in the turbulent channel flow.

4. The increase of the grid mesh size slows down the rate of the turbulence enhancement which is caused by particles.

The presented model considers both the enhancement and attenuation of turbulence by means of the additional terms of the transport equations of the normal Reynolds stress components. It allows to carry out calculations covering long distance of the channel length without using algebraic assumptions for various components of the Reynolds stress.

The presented model, with applying of minimum number of assumptions and empiricism, represents a more contemporary computational approach in turbulent particulate flow, as well as it is simpler and uses the state-of-the-art modelling and computational techniques and is more accurate owing to no applying of approximations.

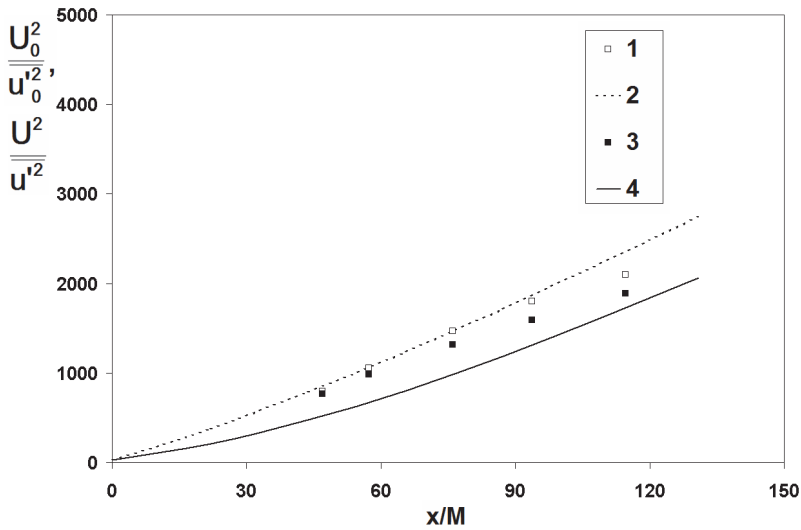


Figure 4.2 Axial turbulence decay behind the grid  $M = 4.8$  mm: 1 and 3 are the data by Hussainov [44] got for the unladen and particle-laden flows, respectively; 2 and 4 are the numerical data obtained for the same conditions.

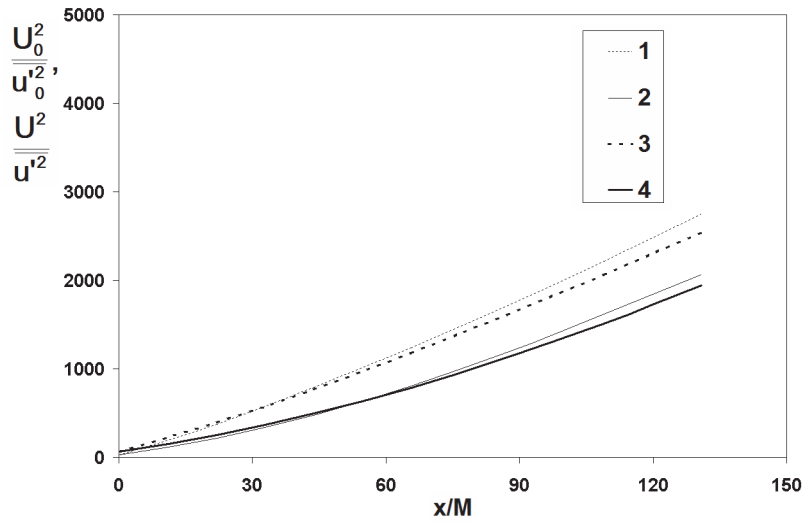


Figure 4.3 The calculated axial turbulence decay behind the grids: 1 and 2 are the data got for the unladen and particle-laden flow, respectively, at  $M=4.8$  mm, 3 and 4 are the data obtained for the same conditions at  $M=10$  mm.

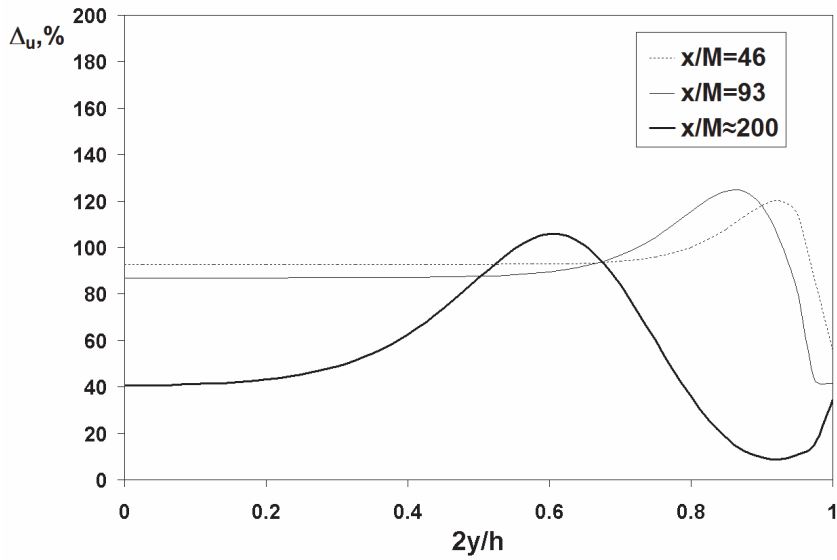


Figure 4.4 Effect of particles on the modification of the x-normal component of the Reynolds stress:  $M=4.8$  mm,  $z=0$ .

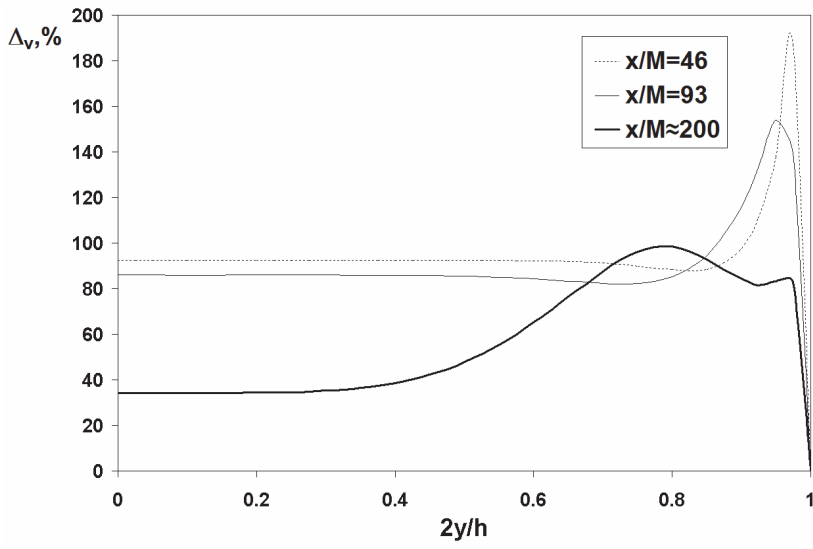


Figure 4.5 Effect of particles on the modification of the y-normal component of the Reynolds stress:  $M=4.8$  mm,  $z=0$ .

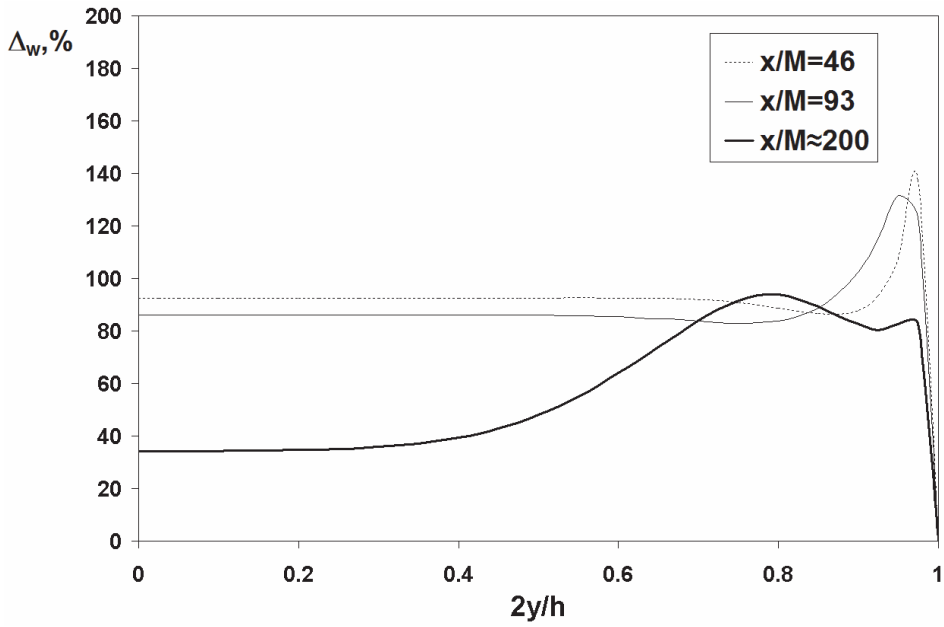


Figure 4.6 Effect of particles on the modification of the z-normal component of the Reynolds stress:  $M=4.8$  mm,  $z=0$ .

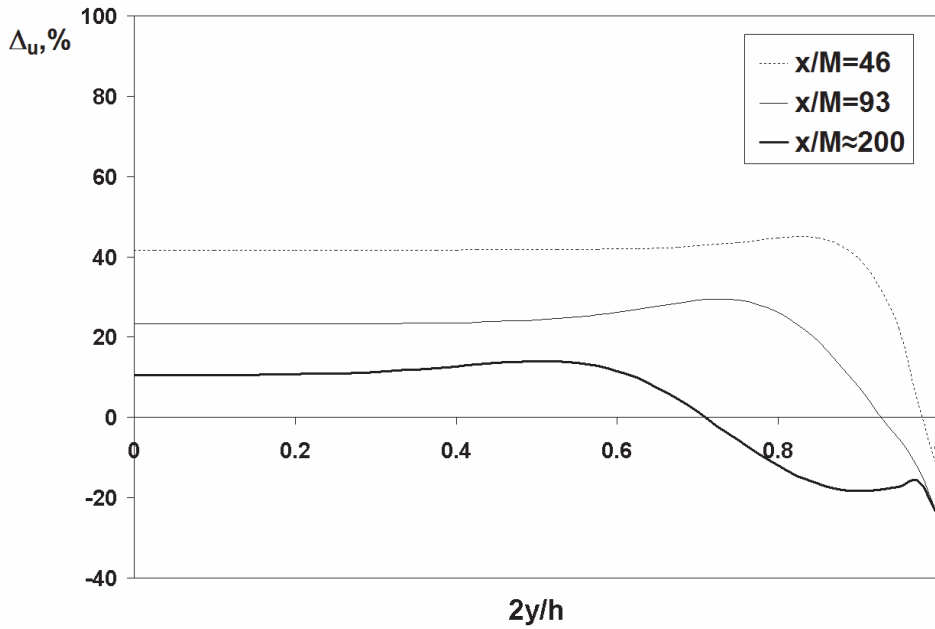


Figure 4.7 Effect of particles on the modification of the x-normal component of the Reynolds stress:  $M=10$  mm,  $z=0$ .

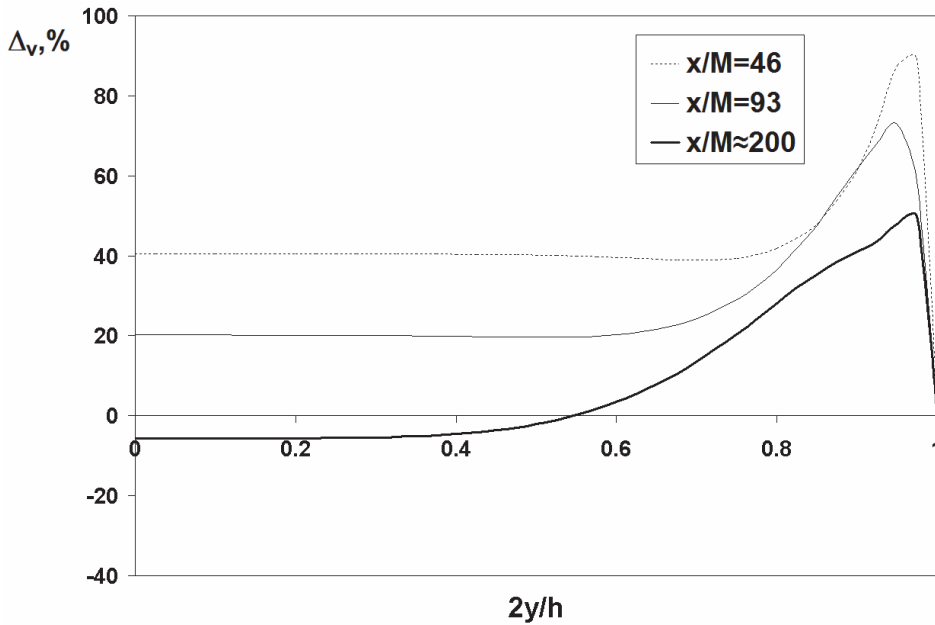


Figure 4.8 Effect of particles on the modification of the y-normal component of the Reynolds stress:  $M=10$  mm,  $z=0$ .

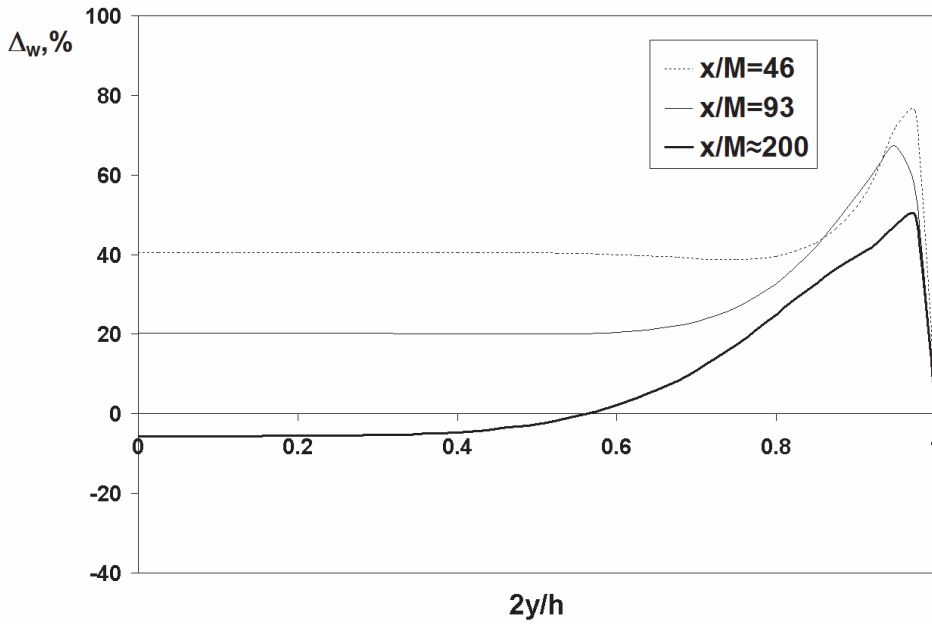


Figure 4.9 Effect of particles on the modification of the z-normal component of the Reynolds stress:  $M=10$  mm,  $z=0$ .

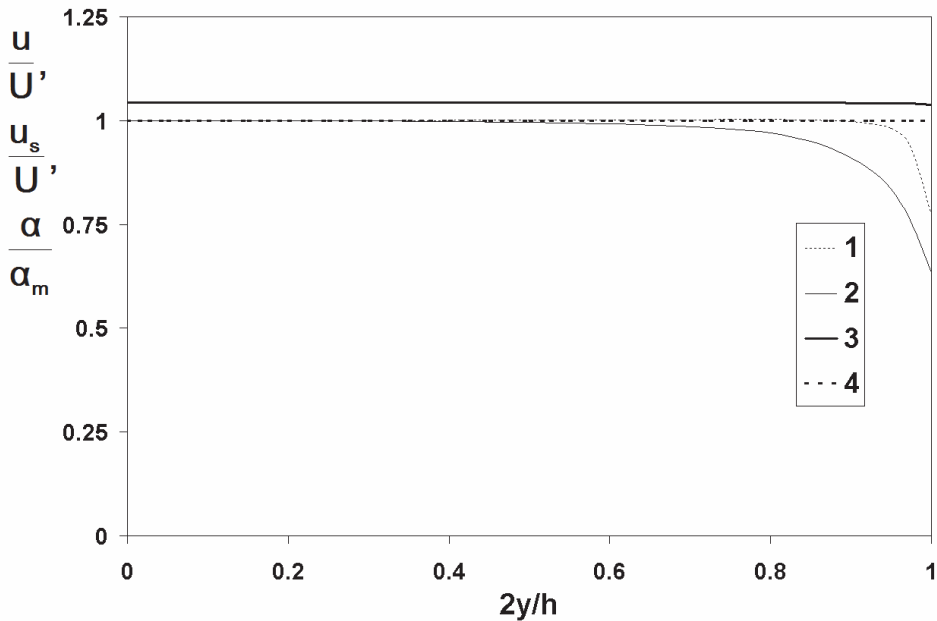


Figure 4.10 The cross-section distributions of the axial gas and particles velocities and particles mass concentration for the grid  $M=4.8$  mm: 1  $-u/U$  for  $x/M=46$ ; 2  $-u_s/U$ , 3  $-u_s/U$  and 4  $-\alpha/\alpha_m$  for  $x/M \approx 200$ . Here  $\alpha_m$  is the value of the mass concentration occurring at the flow axis.

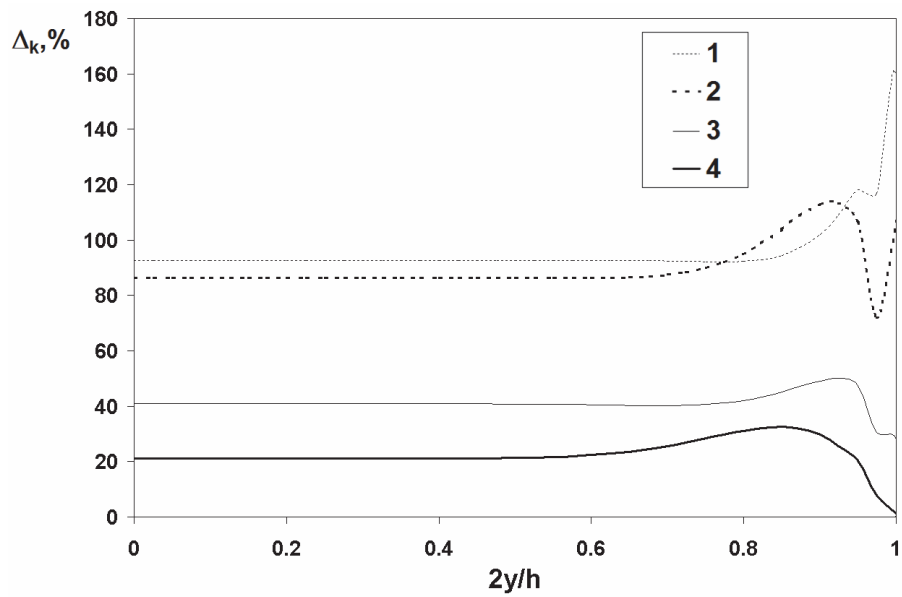


Figure 4.11 Effect of particles on the modification of the turbulence kinetic energy: 1 –  $M=4.8$  mm,  $x/M=46$ ; 2 –  $M=4.8$  mm,  $x/M=93$ ; 3 –  $M=10$  mm,  $x/M=46$ ; 4 –  $M=10$  mm,  $x/M=93$ .

## 5. CONCLUSIONS

The numerical analysis of the mass transfer in the CFB freeboard was performed to determine the optimal operating regimes of the CFB unit for increase its performance. The particulate phase, which is the heat carrier, was modelled both by the ash and sand particles having their own size and material density distributions.

Based on the results presented in chapters 1, 2, 3 and 4 one can conclude:

1. The direct and reasonable results concerning behaviour of the flow parameters (velocities, concentration, turbulence energy) were obtained by means of the Euler-Euler (two-fluid) model applied for the mathematical description of the confined turbulent particulate flows. The importance of the inherent effects, such as the particle-turbulence and particle-particle interactions, is shown with their significant role in exchange of the mass- and heat processes in turbulent particulate flows in pipes, channels as well as in the freeboard of CFB. For example, substantial increase of the particles mass loading with the simultaneous decrease of the particle size reduces the effect of the gas turbulence that leads to reduction of the combustion efficiency in the freeboard of CFB.
2. The four-way coupling approach is the most appropriate for modelling of transport of the particulate phase. This approach allows to capture and improve the theoretical description of the real processes in the CFB freeboard. It was obtained that the particle-particle collision is the key issue of the processes in the CFB freeboard. The presented simulation considers the collisions both between the particles of various size and material density. Thus, the effect of the presence of two fractions of solid particles in the CFB freeboard is successfully resolved by the presented theoretical analysis.
3. Applying the joined 3D RANS and RSTM modelling approaches it was solved the problem of the effect of a turbulence anisotropy that occurs near the walls of the CFB freeboard. The numerical simulation of the grid-generated particulate turbulent flow performed by the joined modelling approach is considered as the first step of the given research.
4. As showed the numerical analysis, the particles size and the flow mass ratio are the key issues for optimization of the mass- and heat exchange processes in CFB, since they are responsible for the uniform distribution of concentration of solid particles that occurs in the CFB freeboard.

## REFERENCES

1. Arro, H., Prikk, A., Pihu, T., Calculation of qualitative and quantitative composition of Estonian oil shale and its combustion products. Part 1. Calculation on the basis of heating value. *Fuel*, 2003, 82, 2179-2195
2. Arro, H., Prikk, A., Pihu, T. Calculation of qualitative and quantitative composition of Estonian oil shale and its combustion products. Part 2. Calculation on the basis of technical analysis data. *Fuel*, 2003, 82/18, 2197-2204
3. Arro, H., Prikk, A., Pihu, T. Calculation of CO<sub>2</sub> emission from CFB boilers of oil shale power. *Oil Shale*, 2006, 23/4, 356-365
4. Arro, H., Pihu, T., Prikk, A., Rootamm, R., Konist, A., 2009, Comparison of ash from PF and CFB boilers and behavior of ash in ash fields. *Proceedings of the 20th International Conference on Fluidized Bed Combustion*, no. 2, pp. 1054-1060.
5. Andrews IV, Arthur T., 2007, Filtered models for gas-particle flow hydrodynamics.
6. Allardice D.J., Newell B.S., Industrial Implications of Properties of Brown Coals – *The Science of Victorian Brown Coal*, Butterworths, Oxford, 1991, pp. 651-701.
7. Babukha, G., Shraiber, A., 1972, An interaction of particles of polydisperse composition of material in a two-phase flow. *Naukova Dumka*, Kiev, 176.
8. Bernstein W., Forschungsarbeiten zum Einsatz schwieriger Brennstoffe in Kraftwerken – *Kraftwerkstechnisches Kolloquium, Nutzung schwieriger Brennstoffe in Kraftwerken*, Stoba Druck GmbH, Lamperswalde, 2000, pp. 3-23.
9. Cabrejos, F. J., Klinzing, G. E. 1994, Pickup and saltation mechanisms of solid particles in horizontal pneumatic transport. *Powder Technol.*, vol.79, pp. 173-186.
10. Cao, J., Ahmadi, G., 1995, Gas-particle two-phase turbulent flow in vertical duct, *I International Journal of Multiphase Flows*, vol. 21, pp. 1203–1228.
11. Chen, Y.-M., Jang, C.-S., Cai, P., Fan, L.-S., 1991, On the formation and disintegration of particle clusters in a liquid–solid transport bed. *Chemical Engineering Science*, vol. 46 (9), pp. 2253–2268.
12. Clift, R., Grace, J.R., Weber., M.E. 1978, Bubbles, drops and particles. *Academic Press*, New York.
13. Crowe, C. T. On models for turbulence modulation in fluid-particle flows. 2000, *Int. J. Multiphase Flow*, vol. 26, pp. 719-727.
14. Crowe, C.T., Stock, D.E., Sharma, M.P., 1977, The particle-source-in cell PSI-CELL model for gas-droplet flows. *ASME, Transactions, Series I - Journal of Fluids Engineering*, vol. 99, pp. 325-332.
15. Crowe C. T., Troutt, T. R., Chung J. N., 1996, Numerical Models for Two-Phase Turbulent Flows. *Ann. Rev. Fluid Mech.*, vol. 28, pp. 11-43.

16. Crowe, C. T., Gillandt, I., 1998, Turbulence modulation of fluid-particle flows – a basic approach. *Third ICMF*, Lyon.
17. Crowe, C., Sommerfeld, M., Tsuji, Y., 1998, Multiphase flows for droplets and particles. CRC Press LLC, Boca Raton, Florida.
18. Crowe C. T., 1993, Modelling Turbulence in Multiphase Flows. *Engineering Turbulence Modelling and Experiments*, vol. 2, pp. 899-913.
19. Davies, J. T., 1987, Calculation of critical velocities to maintain solids in suspension in horizontal pipes. *J. Chem. Eng. Sci.*, vol., 42, pp. 1667–1670.
20. Deutsch, E. and Simonin, O., 1991, Large eddy simulation applied to the motion of particles in stationary homogeneous fluid turbulence. *In Proceedings of the 1st ASME/JSME Fluids Engineering Conference, Portland, USA, June 23–27, 1991 (Michaelides, E. E., Fukano, T. and Serizawa, A., eds.)*, pp. 35–42. American Society of Mechanical Engineers, New York, Series FED, 110.
21. Elghobashi, S. E. and Abou-Arab, T. W., 1983, A two-equation turbulence model for two-phase flows. *J. Phys. Fluids*, vol. 26, pp. 931–938.
22. Elgobashi, S., Truesdell, G. C., 1993, On the two-way interaction between homogeneous turbulence and dispersed solid particles. *I. Turbulence Modification. Physics of Fluids*, vol. 5, pp. 1790-1801.
23. Ferziger J. H., Perić M., 1996, *Computational methods for fluid dynamics*. New York: Springer-Verlag, 356 p.
24. Frishman, F., Hussainov, M., Kartushinsky, A., Mulgi, A., 1997, Numerical simulation of a two-phase turbulent pipe-jet flow loaded with polyfractional solid admixture. *Int. J. Multiphase Flow*, vol. 23, no. 4, pp. 765-796.
25. Grace, J.R., Tuot, J., 1979, A theory for cluster formation in vertically conveyed suspensions of intermediate density. *Transactions of Industrial and Chemical Engineering*, vol. 57, pp. 49–54.
26. Gunn, D.J., Malik, A.A., 1967, The structure of fluidized beds in particulate fluidization. *Proceedings of the International Symposium on Fluidization*, Einhoven, pp. 52–65.
27. Gerolymos, G. A. and Vallet, I., 2003, Contribution to single-point-closure Reynolds-stress modelling of inhomogeneous flow. *In Proceedings of the 4th ASME/JSME Joint Fluids Summer Engineering Conference (FEDSM 2003)*, Honolulu, Hawaii, USA, July 6–10, 2003, FEDSM2003-45346, CD-ROM.
28. Gidaspow, D., 1994, Multiphase Flow and Fluidization: Continuum and Kinetic Theory Descriptions. *Acad. Press*, Boston.
29. Gore, R. A. and Crowe, C. T., 1989, Effect of particle size on modulating turbulent intensity. *Int. J. Multiphase Flow*, vol. 15, pp. 279–285.
30. Happel, M., Brenner, H., 1973, Low Reynolds Number Hydrodynamics: with special applications to particulate media. *Mechanics of Fluids and Transport Processes*.
31. He, Y., Deen, N.G., van Sint Annaland, M., J.A.M. Kuipers, J.A.M., 2008, Gas-solid turbulent flow in a circulating fluidized bed riser; numerical

study of binary particles mixtures. *9th International Conference on Circulating Fluidized Beds*, Germany.

32. Helland, E., Occelli, R., Tadriss, L., 2002. Computational study of fluctuating motions and cluster structures in gas-particle flows. *International Journal of Multiphase Flows*, vol. 28/2, pp. 199–223.

33. Helland, E., Occelli, R., Tadriss, L., 2000, Numerical study of cluster formation in a gas-particle circulating fluidized bed. *Powder Technology*, vol. 100, pp. 210-221.

34. Hestroni, G., 1989, Particles-turbulent interaction. *International Journal of Multiphase Flow*, vol. 15, pp. 735-747.

35. Hennecke H., Heitmüller W., Firing Equipment of Brown Coal Boilers, Mills, Recirculation, Ducts, Pulverized Fuel Ducts and Burners – Selected Contributions on Power Station Technology, Vulkan/Verlag, Essen, 1980, pp. 181-193.

36. Hinze, J. O. 1975, Turbulence. McGraw-Hill, New York.

37. Hoomans, B.P.B., Kuipers, J.A.M., Van Swaaij, W.P.M., 1998, Granular dynamics simulation of cluster formation in dense riser flow. *Third International Conference on Multiphase Flow*, Lyon, France, pp. 2.7–9.

38. Horio, M., Clift, R., 1992, A note on terminology: “clusters” and “agglomerates”. *Powder Technology*, vol. 70, p. 196.

39. Horio, M., Kuroki, H., 1994, Three-dimensional flow visualization of dilutely dispersed solids in bubbling and circulating fluidized beds. *Chemical Engineering Science*, vol. 49 (15), pp. 2413–2421.

40. Hussainov, M., Kartushinsky, A., Mulgi, A., Rudi, Ü., 1996, Gas-solid flow with the slip velocity of particles in a horizontal channel. *J. Aerosol Science*, vol. 27, no. 1, pp. 41-59.

41. Hussainov, M., Kartushinsky, A., Rudi, Y., Shcheglov, I. and Tisler, S., 2005, Experimental study of the effect of velocity slip and mass loading on the modification of grid-generated turbulence in gas-solid particles flows. *Proc. Estonian Acad. Sci. Eng.*, vol. 11, pp. 169–180.

42. Hussainov, A., Ani, F. N., Darus, A. N., Mustafa, A., Salema, A. A., Proceedings of the 18th International Conference on Fluidized Bed Combustion, *ASME Publication*, 2005. p. 1-7.

43. Hussainov, M., Kartushinsky, A., Mulgi, A., Rudi, Ü., Tisler, S., 1995, Experimental and Theoretical Study of the Distribution of Mass Concentration of Solid Particles in the Two-Phase Laminar Boundary Layer on a Flat Plate, *International Journal of Multiphase Flow*, vol. 21, no. 6, pp. 1141-1161.

44. Hussainov, M., 2005. Effect of Solid Particles on Turbulence of Gas in Two-Phase Flows. *Ph.D. thesis*, Tallinn University of Technology.

45. Hussainov, M., Kartushinsky, A., Martins, A., Rudi, Ü., Shcheglov, I., Tisler, S., Krupenski, I., Siirde, A., 2008, Numerical simulation of uprising gas-solid particles flow in circulating fluidized bed. *Oil-Shale*, vol. 2, pp. 125-138.

46. Ito, M., Tsukada, M., Shinamura, J., Horio, M., 1998, Prediction of cluster size and slip velocity in circulating fluidized beds by a DSMC model. *Fluidization IX*, Durango, USA, pp. 525–532.
47. Jayaweera, K.O.L.F., Mason, B.J., Slack, G.W., 1964, The behaviour of clusters of spheres falling in a viscous fluid. Part I. *Experiment. Journal of Fluid Mechanics*, vol. 20, pp. 121–128.
48. Jenkins J.T., Mancini F., 1989, Kinetic theory for binary mixtures of smooth, nearly elastic spheres. *Physics of Fluids*, vol. 31, pp. 2050–2057.
49. Joseph, D.D., 2002, Interrogations of direct numerical simulation of solid–liquid flow, University of Minnesota. <http://www.efluids.com/efluids/books/joseph.htm>.
50. Junwu Wang, Changjian Cheng and Wei Ge, 2008, Eulerian-Eulerian simulation of CFB risers using an EMMS-based sub-grid scale model with an implicit cluster diameter correlation. *9th International Conference on Circulating Fluidized Beds*.
51. Kallaste, T., Liik, O., Ots, A. Possible Energy Sector Trends in Estonia. *Context of Climate Change*. Stockholm Environment Institute Tallinn Centre, Tallinn, 1999, 190 p.
52. Kavidass, S. Szumania, M. J., Alexander, K. C., 1996, Design conditions of Babcock & Wilcox industrial and utility size reheat/non-reheat IR-CFB boilers. *POWER-Gen Asia '96 Exhibition & Conference*, New Delhi, India, 12p.
53. Kattai, V., Saadre, T., Savitski, L. Geological Survey of Estonia. *Estonian Oil Shale*, Tallinn, 2000, 226 p. [In Estonian]
54. Kaye, B.H., Boardman, R.P., 1962, Cluster formation in dilute suspensions. *Proceedings of the Symposium on Interaction between Fluids and Particles*, British Institute of Chemical Engineers, London, pp. 17–21.
55. Kenning, V., Crowe, C., 1996, Brief communication on the effect of particles on carrier phase turbulence in gas-particles flow.
56. Kartushinsky, A., Michaelides, E. E., Rudi, Y. A., Tisler, S. V. and Shcheglov, I. N. **2001**, Numerical simulation of three-dimensional gas-solid particle flow in a horizontal pipe. *A.I.Ch.E. J.*, vol. 57, pp. 2977–2988.
57. Kartushinsky, A., Michaelides, E. E., **2004**, An analytical approach for the closure equations of gas-solid flows with inter-particle collisions. *Int. J. Multiphase Flow*, vol. 30, pp. 159–180
58. Kartushinsky, A., Michaelides, E. E. **2006**, Particle-laden gas flow in horizontal channels with collision effects. *J. Powder Technol.*, vol. 168, pp. 89–103.
59. Kartushinsky, A., Michaelides, E. E., **2007**, Gas-solid particle flow in horizontal channel: decomposition of the particle-phase flow and inter-particle collision effect. *Journal of Fluids Engineering, the Transaction of ASME*, vol. 129, no. 6, pp. 702-712.
60. A. Kartushinsky, E. E. Michaelides, M., Hussainov, Rudi, Y. Effects of the variation of mass loading and particle density in gas-solid particle flow in pipes, *Journal of Powder Technology* **2009**. Vol. 193, P. 176-181.

61. Kartushinsky, A., Michaelides, E. E. and Zaichik, L. I. **2009a**, Comparison of the RANS and PDF methods for air-particle flows. *Int. J. Multiphase Flow*, vol. 35, pp. 914–923.
62. Kartushinsky, A., Michaelides, E. E., Hussainov, M. T., Rudi, Y. **2009b**, Effects of the variation of mass loading and particle density in gas-solid particle flow in pipes. *J. Powder Technol.*, vol. 193, pp. 176–181.
63. Kartushinsky, A., Martins, A., Rudi, Ü., Stseglov, I., Tisler, S., Krupenski, I. and Siirde, A. Numerical simulation of uprising gas-solid particle flow in circulating fluidized bed, *Oil-Shale*, **2009**. Vol. 26, No. 2. P. 125-138.
64. Krupenski, I., Kartushinsky, A., Siirde, A., Rudi, Ü., **2010**, Numerical simulation of uprising gas-solid particle flow by 2D RANS for fluidized bed conditions. *Oil-Shale*
65. Kunii, D., Levenspiel, O., 1991, Fluid Engineering. *Butterworth Heinemann series in Chemical Engineering*, London, UK.
66. Launder, B. E., Reece, G. J., Rodi, W. 1975, Progress in the development of a Reynolds-stress turbulence closure. *J. Fluid Mech.*, vol. 68, pp. 537–566.
67. Leighton, R., Walker, D. T., Stephens, T., Garwood, G. 2003, Reynolds stress modelling for drag reducing viscoelastic flows. *In Proceedings of the 4th ASME/JSME Joint Fluids Summer Engineering Conference (FEDSM 2003)*, Honolulu, Hawaii, USA, July 6–10, 2003, FEDSM2003-45655, CD-ROM.
68. Fortes, A.F., Joseph, D.D., Lundgren, T.S., 1987, Nonlinear mechanics of fluidization of beds of spherical particles. *Journal of Fluids Mechanics*, vol. 177, pp. 467–483.
69. Li J, Tung Y, Kwauk M., 1988, Multi-scale modelling and method of energy minimization in particle-fluid two-phase flow. *In Circulating Fluidized Bed Technology II*, ed. P Basu, JF Large, pp. 89-103. Pergamon Press.
70. Li J, Kwauk M. ,1994, Particle-fluid two-phase flow: the energy-minimization multi-scale method. *Metallurgical Industry Press*. Beijing, P. R. China.
71. Li, J., Kuipers, J.A.M., 2002, Flow structure formation in high velocity gas-fluidized beds. *Fluidization X*, Beijing, China.
72. Louge, M.Y., Mastorakos, E., Jenkins, J.T., 1991, The role of particle collisions in pneumatic transport, *Journal of Fluid Mechanics*, vol. 231, pp. 345–359.
73. Marchioli, C., Giusti, A., Salvetti, M.-V., Soldati, A. 2003, Direct numerical simulation of particle wall transfer and deposition in upward turbulent pipe flow. *Int. J. Multiphase Flow*, vol. 29, pp. 1017–1038.
74. Matsumoto and Saito, 1970, Monte Carlo simulation of horizontal pneumatic conveying based on the rough wall model. *Journal of chemical engineering of Japan*. Vol.3 no 2 .1970. 223-230

75. Mei, R., 1992, An approximate expression for the shear lift force on a spherical particle at finite Reynolds number. *Int. J. Multiphase Flow*, vol. 18, pp. 145–147.
76. Michaelides, E. E., 1984, A model for the flow of solid particles in gases. *Int. J. Multiphase Flow*, vol. 10, pp. 61–77.
77. Michaelides, E. E., 2006, Particles, Bubbles and Drops – Their Motion, Heat and Mass Transfer. *World Scientific Publishers*, New Jersey.
78. Mukin, R. V., Zaichik, L. I. 2012, Nonlinear algebraic Reynolds stress model for two-phase turbulent flows laden with small heavy particles. *Int. J. Heat Fluid Flow*, vol. 33, pp. 81–91.
79. Manger, E., 1996, Modelling and simulation of gas/solid flow in curvilinear coordinates. *Ph.D. thesis*, Telemark Institute of Technology, Norway.
80. Marble, F.E., 1964, Mechanism of particle collision in one-dimensional dynamics of gas-particle admixture, *Phys. Fluids*, vol. 7, pp. 1270–1282.
81. Mathiesen, V., Solberg, T., Arastoopour, H., Hjertager, B.H., 1999, Experimental and computational study of multiphase gas/particle flow in a CFB riser. *A.I.Ch.E. Journal*, vol. 45, pp. 2503–2518.
82. Mathiesen, V., Solberg, T., Hjertager, B.H., 2000, An experimental and computational study of multiphase flow behavior in a circulating fluidized bed. *International Journal of Multiphase Flow*, 26, 387-419.
83. Matsen, J.M., 1982, Mechanisms of choking and entrainment. *Powder Technology*, vol. 32, pp. 21–33.
84. Munson, B., Young, D., Okiishi, T., 1998, Fundamentals of fluid mechanics, 877p.
85. Ots, A., 2006, Oil Shale Fuel Combustion, 883p.
86. Ots A., Processes in Steam Generators During the Burning of Oil Shale and Kansk-Achinsk Coals, *Энергия*, Москва, 1977
87. O'Brien, T.J., Syamlal, M., 1991. In: Gaden, E.L., Weimer, A.W. (Eds.), Advances in Fluidized Systems, *A.I.Ch.E. Symposium Services*, vol. 281(87), pp. 127–136.
88. Oesterle, B., Petitjean, A., 1993, Simulation of particle to particle interactions in gas–solid flows, *International Journal of Multiphase Flows*, vol. 19, pp 199–211.
89. Oil shale perspectives within energy production, Estonia. Outline proposal for 100 MWth demonstration CFB boiler. *Lurgi Energie und Umwelt GmbH*, Frankfurt am Main, 1995, 25p.
90. Ouyang, J., Li, J., 1999, Discrete simulations of heterogeneous structure and dynamic behavior in gas–solidfluid ization. *Chemical Engineering Sciences*, vol. 54, pp. 5427–5440.
91. Pan, T.W., Joseph, D.D., Bai, R., Glowinski, R., Sarin, V., 2002, Fluidization of 1204 spheres: simulation and experiment. *Journal of Fluid Mechanics*, vol. 451, pp. 169–191.

92. Perić, M., Scheuerer, G. 1989. CAST – A finite volume method for predicting two-dimensional flow and heat transfer phenomena. *GRS - Technische Notiz* SRR–89–01.
93. Pfeffer, R., Rosetti, S., Licklein, S. 1966, Analysis and correlation of heat transfer coefficient and heat transfer data for dilute gas-solid suspensions. *NASA Rep.* TND–3603.
94. Pope, S. B. 2008. *Turbulent Flows*. Cambridge University Press, Cambridge – New York.
95. Pourahmadi, F., Humphrey, J. A. C. 1983, Modelling solid-fluid turbulent flows with application to predicting erosive wear. *Phys. Chem. Hydrodyn.*, vol. 4, pp. 191–219.
96. Richardson, J.F., Zaki, W.N., 1954, Sedimentation and fluidization: Part 1. *Transactions of Institute of Chemical Engineers*, vol. 32, pp. 35–53.
97. Reeks, M. W. 1991, On a kinetic equation for the transport of particles in turbulent flows. *J. Phys. Fluids A*, vol. 3, pp. 446–456.
98. Reeks, M. W. 1992, On the continuum equations for dispersed particles in nonuniform flows. *J. Phys. Fluids A*, vol. 4, pp. 1290–1303.
99. Rizk, M. A., Elghobashi, S. E., 1989, A two-equation turbulence model for dispersed dilute confined two-phase flows. *Int. J. Multiphase Flow*, vol. 15, pp. 119–133.
100. Schiller, L., Naumann, A. 1933, Über die grundlegenden Berechnungen bei der Schwerkraftaufbereitung. *Zeitschrift des Vereines deutscher Ingenieure*, vol. 77, pp. 318–320.
101. Sharlovskaja M., Rivkin A., Influence of Siberian Coal's Mineral Matter on the Fouling of Steam Generators Heating Surfaces, *Издательство "Наука"*, Новосибирск, 1973.
102. Shraiber, A. A., Yatsenko, V. P., Gavin, L. B. and Naumov, V. A. 1990. *Turbulent Flows in Gas Suspensions*. Hemisphere Pub. Corp., New York.
103. Simonin, O. 1990. Eulerian formulation for particle dispersion in turbulent two-phase flows. In *Proceedings of the 5th Workshop on Two-Phase Flow Predictions, Erlangen, Germany, March 19-22, 1990 (Sommerfeld, M. and Wennerberg, D. eds.)*, pp. 156–166. Forschungszentrum Jülich, Jülich.
104. Sommerfeld, M. 2001, Validation of a stochastic lagrangian modelling approach for inter-particle collisions in homogeneous isotropic turbulence. *Int. J. Multiphase Flow*, vol. 27, pp. 1829–1858.
105. Sommerfeld, M. 2003, Analysis of collision effects for turbulent gas-particle flow in a horizontal channel. Part I: Particle transport. *Int. J. Multiphase Flow*, vol. 29, pp. 675–699.
106. Statistical Office of Estonia. Tallinn, 2012. <http://www.stat.ee> (12.03.2012)
107. Sharma, A.K., Tuzla, K., Matsen, J., Chen, J.C., 2000, Parametric effects of particle size and gas velocity on cluster characteristics in fast fluidized beds. *Powder Technology*, vol. 111, pp. 114–122.
108. Shuai, W., Guodong, L., Huilin, L., Juhui, C., Yurong, H. and Jiaying, W., 2011a, *Fuel Processing Technology*, 385-393

109. Shuai, W., Pengfei, X., Huilin, L., Yunchao, Y., Lijie, Y. and Jiaying, W., 2011b, *Chemical Engineering Science*, 593-603
110. Simonin, O., Deutsch, E., Minier, J.-P., 1993, Eulerian prediction of the fluidparticle correlated motion in turbulent two-phase flows, *Appl. Sci. Res.*, vol. 51, pp. 275–283.
111. Simonin, O., 2001, Statistical and continuum modelling of turbulent reactive particulate flows—part i: theoretical derivation of dispersed phase eulerian modelling from probability density function kinetic equation, *in: J.-M. Buchlin (Ed.), Von Karman Institute Lecture Series*, Brussels, Belgium.
112. Sommerfeld, M., Zivkovic, G. 1992, Recent advances in the numerical simulation of pneumatic conveying through pipe systems, *Comp. Meth. Appl. Sci. Elsevier Sci. Publ. B.V.*, pp. 201–212.
113. Squires K. D., Eaton, J. K., 1990, Particle response and turbulence modification in isotropic turbulence. *Physics of Fluids*, A2, pp. 1191-1203.
114. Taulbee, D. B., Mashayek, F. and Barré, C., 1999, Simulation and Reynolds stress modelling of particle-laden turbulent shear flows. *Int. J. Heat Fluid Flow*, vol. 20, pp. 368–373.
115. The annual report for installed electricity capacities. By the Estonian transmission system operator Elering, 2011. [http://elering.ee/public/Elering\\_Tootmispiisavuse\\_aruanne\\_2011.pdf](http://elering.ee/public/Elering_Tootmispiisavuse_aruanne_2011.pdf) (22.05.2012).
116. Thermal calculation of power generators (Standard method). Moskva, 1973, 295p.
117. Tsuji, Y., Morikawa, Y., 1982, LDV measurements of an air-solid two-phase flow in a horizontal pipe. *J. Fluid Mech.*, vol. 120, pp. 385–409.
118. Tsuji, Y., Morikawa, Y., Shiomi, H. 1984, LDV measurements of an air-solid two-phase flow in a vertical pipe. *J. Fluid Mech.*, vol. 139, pp. 417–434.
119. Tisler, S., 2006, Deposition of Solid Particles from Aerosol Flow in Laminar Flat-Plate Boundary Layer. *Ph.D. thesis*, Tallinn University of Technology.
120. Tsuji, Y., Tanaka, T., Yonemura, S., 1998, *Powder Technology*, vol. 95, pp. 254–264.
121. Tsuo, Y.P., Gidaspow, D., 1990, Computation of flow patterns in circulating fluidized beds. *A.I.Ch.E. Journal*, vol. 36, pp. 885–896.
122. Valk, M. (Editor). Atmospheric Fluidized Bed Coal Combustion Research, *Development and Application*. Amsterdam – Lausanne – New York – Oxford – Shannon – Tokyo, 1995, 462p.
123. van Den Moortel, T., Santini, R., Tadriss, L., Pantaloni, J., 1998, *Fluidisation IX*, Durango, CO, pp. 157–162.
124. van der Hoef, M.A., Ye1, M., van Sint Annaland, M., Andrews IV, A.T., Sundaresan S., Kuipers, J.A.M., 2006, Multiscale modelling of gas-fluidized beds. *Advances in Chemical Engineering*, vol. 31
125. van Swaaij, W. P. M., 1985, Chemical reactors. Fluidization *Academic Press*, London, UK (J. F. Davidson, and R. Clift, Eds.).

126. Wang, S., Liu, H., Lu, H., Liu, W., Jiamin, D. and Li, W., 2005, Flow behaviour of clusters in a riser simulated by direct simulation Monte Carlo method. *Chemical Engineering Journal*, vol. 106, pp. 197-211.
127. Wilhelm, R.H., Kwauk, M., 1948, Fluidization of solid particles. *Chemical Engineering Progress*, vol. 44, p. 201.
128. Wachmann, B., Kalthoff, W., Schwarzer, S., Herrmann, H.J., 1998, Collective drag and sedimentation: comparison of simulation and experiment in two and three dimensions. *Granular Matter*, vol. 1, pp. 75–82.
129. Wilcox, D.C. 1998. Turbulence Modelling for CFD. La Canada, Calif.: *DCW Industries, Inc.*
130. Williams J. J. E., Crane R. I., 1983, Particle collision rate in turbulent flow, *Int. J. Multiphase Flow* 9, 421
131. Yamamoto, Y., Potthoff, M., Tanaka, T., Kajishima, T., Tsuji, Y., 2001, Large-eddy simulation of turbulent gas-particle flow in a vertical channel: effect of considering inter-particle collisions, *Journal of Fluid Mechanics*, vol. 442, pp. 303–334.
132. Yerushalmi, J., Tuner, D.H., Squires, A.M., 1976, The fast fluidized bed. *Industrial Engineering Chemical Process Design and Development*, vol. 15, pp. 47–53.
133. Young, D., Munson, B., Okiishki, T., Huebsch, W., 2007, A brief introduction to fluid mechanics.
134. Yarin, L. P. , Hetsroni, G., 1994, Turbulence intensity in dilute two-phase flows. Parts I, II and III. *Int. J. Multiphase Flow*, vol. 20, pp. 1–44.
135. Yuan, Z., Michaelides, E. E., 1992, Turbulence modulation in particulate flows - a theoretical approach. *Int. J. Multiphase Flow*, vol. 18, pp. 779–791.
136. Zaichik, L. I. and Alipchenkov, V. M. 2005, Statistical models for predicting particle dispersion and preferential concentration in turbulent flows. *Int. J. Heat and Fluid Flow*, vol, 26, pp. 416–430.
137. Zaichik, L. I., Vinberg, A. A. 1991, Modelling of particle dynamics and heat transfer in turbulent flows using equations for first and second moments of velocity and temperature fluctuations. In *Proceedings of the 8th International Symposium on Turbulent Shear Flows, Munich, Germany, September 9-11, 1991 (Durst, F., Friedrich, R., Launder, B. E., Schmidt, F. W., Schumann, U., Whitelaw, J. H. eds.)*, 1, 1021–1026. FRG, Munich.
138. Zaichik, L. I., Fede, P., Simonin, O. and Alipchenkov, V. M. 2007. Comparison of two statistical approaches for modelling collision in bidisperse mixture of particles settling in homogeneous turbulent flows. In *Proceedings of the 6th International Conference on Multiphase Flow, Leipzig, Germany, July 9–13, 2007 (Sommerfeld, M. ed.)*, CD-ROM.
139. Zhang, W., 1992, Particle flow pattern in circulating fluidized bed boilers.
140. Zhang, N., Lu, B., Wang, W. and Li, J., 2008, *Particology*, 529-539
141. Nikolopoulos, A., Atsonios, K., Nikolopoulos, N., Grammelis, P. and Kakaras, E., 2010a, *Chemical Engineering Science*, 4089-4099

142. Nikolopoulos, A., Papafotiou, D., Nikolopoulos, N., Grammelis, P. and Kakaras, E., 2010b, *Chemical Engineering Science*, 4080-4088
143. Wang, J., Ge, W. and Li, J., 2008, *Chemical Engineering Science*, 1553-1571
144. Ge, W., Wang, W., Dong, W., Wang, J., Lu, B., Xiong, Q. and Li, J., 2008, *Proceedings of the 9th International Conference on Circulating Fluidized Beds 19-37*
145. Nikolopoulos a,b, A., Nikolopoulos a, N., Grammelis a, P., Kakaras a,b, E. PSD incorporation in full - loop CFD modelling of CFBs. *21th Conference*
146. Sundaresan, S., 2011, 10th Conference on Circulating Fluidized Beds and Fluidization Technology - *CFB10, 21-40*
147. Lun, C. K. K., Savage, S. B., Jeffrey, D. J. and Chepurniy, N., 1984, *Journal of Fluid Mechanics*, 223-256
148. Patankar, N. A. and Joseph, D. D., 2001, *International Journal of Multiphase Flow*, 1659-1684

## ***List of publications***

The results of this work were presented at publications:

1. Kartushinsky, A.; Rudi, Y.; Stock, D.; Hussainov, M.; Shcheglov, I.; Tisler, S.; Shablinsky, A. (2013). Numerical simulation of particulate grid-generating turbulence by 3D RSTM. Proceedings of the Estonian Academy of Sciences, 62(3), 161 - 174.

2. Kartushinsky, A.; Rudi, Y.; Tisler, S.; Shcheglov, I.; Shablinsky, A. (2013). Numerical study of upward particulate pipe flows at constant Reynolds number. Proceedings of the Estonian Academy of Sciences, 62(2), 97 - 108.

3. Kartushinsky, A.; Siirde, A.; Rudi, Ü.; Shablinsky, A. (2011). Mathematical model of two-phase flows loaded with light and heavy particles to analyze CFB processes. Oil Shale, 28(1s), 169 - 180.

4. Kartushinsky, A.; Rudi, Y.; Stock, D.; Hussainov, M.; Shcheglov, I.; Tisler, S.; Shablinsky, A. (2013). Reynolds stress turbulence model for particulate grid-generated turbulence. 8th International Conference on Multiphase Flow 2013, Jeju (Korea), May 26-31, 2013.

5. Shablinsky, A.; Kartushinsky, A.; Krupenski, I.; Siirde, A.; Rudi, Ü. (2012). Numerical Simulation of Uprising Gas-Solid Particles Turbulent Flow in Circulating Fluidized Bed. In: *The 21st international conference on Fluidized Bed Combustion, Proceedings: The 21st international conference on Fluidized Bed Combustion, Naples (Italy), 3.-6. June 2012.*, 946 - 953.

## *The personal contribution of the author*

The contribution of the author to the papers included in the thesis is as follows:

I. Alexander Shablinsky has participated in writing the paper. The author has run the codes and mastered afterwards the numerical data to plot results in 2D & 3D coordinates using for that MatLab codes and utilities.

II. Alexander Shablinsky has participated in writing the paper and discussed of obtained numerical results. He has prepared and presented results at the international conferences (Naples) and local meetings.

III. Alexander Shablinsky is author of three the papers. He was responsible for the literature overview, analysis, calculation, graphical part and conclusions. He has contributed a major role in preparation and writing all three journal papers and two international meetings.

IV. Alexander Shablinsky has participated in writing the paper and discussed of obtained numerical results.

V. Alexander Shablinsky has participated in writing the paper and discussed of obtained numerical results. He has prepared and presented results at the international conferences (Naples)

## *Acknowledgements*

I would like to express his gratitude to everyone who has in one way or another contributed to this work. The author would like to express his deepest gratitude to his supervisors, Prof. A. Siirde and DSc A. Kartushinsky, for their excellent guidance and support during this research.

I would like to thank my family and friends for constant support, understanding and encouragement at different stages of the present work.

The work has been partially supported by the Estonian grant project ETF9343. This study is related to the activity of the European network action COST MP1106.

# KOKKUVÕTE

## Turbulentsete voolude matemaatiline RANS modelleerimine keevkihi tingimustes

Antud töö eesmärgiks on massivahetusprotsesside uurimine tsirkuleeriva keevkihtkatla (CFB) kihipealses ruumis, et määrata katla optimaalseid režiime ja suurendada tootlikkust. Optimaalsuskriteeriumiks on tahkete osakeste kontsentratsiooni ühtlase jaotuse kindlustamine kihipealse ruumi ristlõikes.

Uuring teostati 2D ja 3D keskmistatud Reynoldsi Navier'-Stokes'i Euler/Euler (RANS) lähenduses numbrilise modelleerimise abil, sest sellel on eelis Lagrange'i lähenduse ees keevkihi pealse ruumi modelleerimisel osakeste masskontsentratsiooni jaotuste leidmisel. Osakeste faasi, mis on soojuskandja, modelleeriti nii põlevkivi tuha ja liiva osakestega, millel oli oma suuruse ja ainetiheduse jaotused.

Dissertatsiooni teaduslik uudsus sisaldab CFB-s protsessides avalduvate mehhanismide numbrilist analüüsi, mille peatähelepanu koondus osake-osake põrgetele ja osake-turbulents vastasmõjule. Esmakordselt on analüüsitud tuha- ja liivaosakeste segus kontakteeruvate ainete tiheduse muutumise mõju koos osakeste suuruse jaotuse mõjuga.

Töö koosneb neljast peatükist ja kokkuvõttest.

Esimeses peatükis esitatakse antud uurimisteamiga seotud eelnevate tööde ülevaade, analüüsitakse uusi faktoreid, mis avaldavad mõju soojus- ja massivahetusprotsessidele CFB-s ja püstitatakse antud uurimistöö ülesanded.

Teises peatükis esitatakse ümmarguses torus tõusva kahefaasilise isotermilise vooluse 2D RANS põhjaliku modelleerimise tulemused. Näidatakse, et turbulentsi mõju tahkete osakeste liikumisele ja ka nende omavahelised põrkumised mängivad tähtsat rolli vooluse mõõdukate ja suurte koormatuste korral. Neid tulemusi kasutati CFB kihipealse ruumi protsesside järgneva analüüsiks.

Kolmandas peatükis on toodud 2D RANS modelleerimisega saadud CFB kihipealse ruumi kahefaasilise mitteisotermilise vooluse soojus- ja massivahetusprotsesside numbriline analüüs. On välja toodud põhifaktorid, mis avaldavad mõju tahkete osakeste masskontsentratsiooni jaotuse formeerumisele kihipealse ruumi ristlõikes.

Neljandas peatükis esitatakse riskülikukujulises kanalis, mis oma geomeetria poolest on maksimaalselt sarnane reaalse CFB kihipealse ruumiga, kahefaasilise kolmemõõtmelise vooluse numbrilise modelleerimise tulemused. Saadud tulemuste analüüs näitas vooluse anisotropia olulist mõju kahefaasilise vooluse parameetrite jaotuste formeerumisele, sealhulgas tahkete osakeste

kontsentratsiooni jaotustele. Selline ristkülikulise ristlõikega kanali kolmemõõtmelise kahefaasilise CFB kihipealse ruumi vooluse esitatud analüüs on oluliseks eelduseks reaalsete 3D soojus- ja massivahetusprotsesside arvutusmudeli loomisel Euleri kirjelduse raamides.

Dissertatsiooni kokkuvõttes osas on tehtud järgmised järeldused:

1. Vooluse parameetreid (kiirus, kontsentratsioon, turbulentne energia) iseloomustavad tulemused on saanud Euler-Euler (kahe vedeliku) mudeliga, mida rakendati turbulentsete osakesi sisaldavate piiratud vooluste matemaatiliseks kirjeldamiseks. Sisemiste efektide (osake-turbulents ja osake-osake vastasmõju) olulisust on näidatud soojus- ja massivahetusprotsessidele turbulentsetes toru- ja kanalvoolustes kui ka keevkihtkolletes.
2. Kõige korrektsem modelleerimine eeldab kõikide vastasmõjude (osake-osake, osake-voolus, osake-sein, osake-turbulents) arvestamist. Selline lähendus võimaldab leida ja täiustada CFB reaalsete protsesside teoreetilist kirjeldamist. Leiti, et osakestevahelised pörkumised on nendes protsessides võtmeküsimuseks. Esitatud modelleerimises eeldati pörkumisi nii erineva suurusega osakeste kui ka erinevate tihedustega osakeste vahel. Seega on esitatud teoreetilise analüüsiga edukalt lahendatud keevkihis tahkete osakeste kahe fraktsiooni kohalolu efekt.
3. 3D RANS ja RTSM modelleerimise samaaegne kasutamine võimaldas hinnata vooluse turbulentsi anisotroopia mõju osakeste kontsentratsioonijaotuse formeerumisele keevkihtkatla kihipealses ruumis.
4. Nagu numbriline analüüs näitas on osakeste suurusel ja vooluse faaside masside suhtel võtmetähtsust massi- ja soojusvahetuse protsesside optimeerimisel, sest nendest sõltub tahkete osakeste kontsentratsiooni ühtlane jaotus keevkihis.

Käesolevas väitekirjas esitatud tulemused võivad osutada kasulikeks nii CFB katelde kui ka muu energeetilise seadmetiku konstruktsioonelementide projekteerimisel eesmärgiga parendada nende eksploateerimise karakteristikaid.

## **ABSTRACT**

### **RANS Numerical Modelling of Turbulent Polydispersed Flows in CFB Freeboard**

The main goal of the thesis is focused on the numerical analysis of the mass transfer in the freeboard of circulating fluidized bed (CFB) and determination of the optimal operating regimes of the CFB unit to increase its performance. The criterion of optimality is the uniform distribution of concentration of solid particles that occurs in the CFB freeboard.

In the scope of the present thesis the numerical simulation of the turbulent gas-solid particles flow has been performed within 2D and 3D Reynolds Averaged Navier-Stokes (RANS) Euler/Euler approach for the CFB freeboard, which has an advantage over of the Lagrange approach of modelling of the CFB freeboard due to its direct acquisition of distributions of particle mass concentration. The particulate phase, which is the heat carrier, was modelled both by the oil-shale ash and sand particles having their own size and material density distributions.

The scientific novelty of the thesis consists in the numerical analysis of mechanisms that occur in the CFB processes, mainly focusing on the particle-particle collisions and particle-turbulence interactions. The effect of variation of densities of contacting materials in the mixture of ash and sand particles along with effect of particle size distributions occurring for both materials have been analyzed for the first time.

The thesis consists of introduction, four chapters and conclusions.

The first chapter includes the review of the formerly published results of investigations which concern the topic of the given study, the analysis of the main factors that influence the heat and mass transfer processes in CFB, and the problem statement of the study.

The second chapter presents the results of the detailed 2D RANS numerical simulation of the isothermal upward pipe particulate flow. It is shown that the particle-turbulence and particle-particle interactions are the key factors for the mass and heat transfer processes at the moderate and high flow mass loadings. These results were used in the subsequent analysis of processes in the CFB freeboard.

The third chapter shows the results of 2D RANS numerical analysis of the mass and heat transfer processes taking places under the conditions of the non-isothermal particulate flow in the CFB freeboard. As a result, there have been revealed the main factors that influence the formation of the distribution of the particles mass concentration in the cross-section of the freeboard.

The fourth chapter presents the results of 3D RANS modelling of the square-section channel particulate flow, whose geometry is as close as possible to the flow pattern in the CFB freeboard. Analysis of the obtained results shows a significant influence of the flow turbulence anisotropy on formation of the particulate flow field, including the distribution of the particles mass concentration. The given analysis is a prerequisite for elaboration of the numerical model based on the Euler approach for the real 3D mass and heat transfer processes in the CFB freeboard.

The main conclusions of the thesis are as follows:

5. The direct and reasonable results concerning behaviour of the flow parameters (velocities, concentration, turbulence energy) were obtained by means of the Euler-Euler (two-fluid) model applied for the mathematical description of the confined turbulent particulate flows. The importance of the inherent effects, such as the particle-turbulence and particle-particle interactions, is shown with their significant role in exchange of the mass and heat transfer processes in turbulent particulate flows in pipes, channels as well as in the freeboard of CFB.
6. The four-way coupling approach is the most appropriate for modelling of transport of the particulate phase. This approach allows to capture and improve the theoretical description of the real processes in the CFB freeboard. It was obtained that the particle-particle collision is the key issue of the processes in the CFB freeboard. The presented simulation considers the collisions both between the particles of various size and material density. Thus, the effect of the presence of two fractions of solid particles in the CFB freeboard is successfully resolved by the presented theoretical analysis.
7. The joined 3D RANS and RSTM modelling approaches allowed to predict the effect of a flow turbulence anisotropy on a formation of distribution of particles concentration in the CFB freeboard.
8. As showed the numerical analysis, the particles size and the flow mass ratio are the key issues for optimization of the mass- and heat exchange processes in CFB, since they are responsible for the uniform distribution of concentration of solid particles that occurs in the CFB freeboard.

The results presented in this thesis can be useful for designing of structural elements of the CFB boilers and other power equipment, in order to improve their performance.

Keywords: Circulating fluidized bed, CFB, numerical simulation, gas-solid particles flow, two-fluid model, 2D RANS

## CURRICULUM VITAE

*Name* Alexander  
*Surname* Shablinsky  
*Date and place of birth* 02.08.1982, Estonia  
*Family status* Single  
*Contact* Pallasti 34-19, Tallinn, Estonia,  
Telephone: +372 58269408;  
E-mail: alexshablinsky@gmail.com  
*Workplace* VKG Soojus AS, Ritsika 1, 31027 Kohtla-Järve  
*Appointment* Member of the Board

### *Education:*

<i>Educational institution</i>	<i>Year of graduation</i>	<i>Education</i>
Tallinn University of Technology	2006	Master degree, thermal engineering
Tallinn University of Technology	2005	Bachelor degree, thermal engineering
Laagna Gymnasium	2001	Secondary Education

### *Work experience:*

2013- present	VKG Soojus AS	Member of the Board
2009-2013	AS Eesti Energia	Project Manager
2007-2009	OÜ Põhivõrk	Analyst
2006-2007	AS Eesti Gaas	Specialist

### *Language skills:*

<i>Language</i>	<i>Level</i>
Russian	native language
Estonian	higher level
English	average level
French	primary level

*Scientific degree* Master of Science in Engineering  
*Certificate of education* Tallinn Technical University, 2006  
*Scientific work* Development of Theory of the Dispersed Gas-Solid Particles Flows

## ELULOOKIRJELDUS

*Eesnimi* Aleksandr  
*Perekonnanimi* Šablinski  
*Sünniaeg ja -koht* 02.08.1982, Estonia  
*Perekonnaseis* Vallaline  
*Kontaktandmed* Pallasti 34-19, Tallinn, Eesti,  
Telefon: +372 58269408;  
E-mail: alexshablinsky@gmail.com  
*Töökoht* VKG Soojus AS, Ritsika 1, 31027 Kohtla-Järve  
*Ametikoht* Juhatuse liige

*Hariduskäik:*

<i>Õppeasutus</i>	<i>Lõpetamise aeg</i>	<i>Haridus</i>
Tallinna Tehnikaülikool	2006	Tehnikateaduste magister, soojustehnika
Tallinna Tehnikaülikool	2005	Tehnikateaduste bakalaureus, soojustehnika
Tallinna Laagna Gümnaasium	2001	Keskharidus

*Teenistuskäik:*

2013- praeguseni	VKG Soojus AS	juhatuse liige
2009-2013	AS Eesti Energia	projektijuht
2007-2009	OÜ Põhivõrk	analüütik
2006-2007	AS Eesti Gaas	spetsialist

*Keelteoskus:*

<i>Keel</i>	<i>Tase</i>
Vene	emakeel
Eesti	kõrgtase
Inglise	kesktase
Prantsuse	algtase

*Teaduskraad* Master of Science in Engineering  
*Teaduskraadi välja  
andnud asutus, aasta* Tallinna Tehnikaülikool, 2006  
*Teadustöö põhisuunad* Disperssete (gaas-tahked osakesed) vooluste  
teooria arendamine

**DISSERTATIONS DEFENDED AT  
TALLINN UNIVERSITY OF TECHNOLOGY ON MECHANICAL  
ENGINEERING**

1. **Jakob Kubarsepp**. Steel-Bonded Hardmetals. 1992.
2. **Jakub Koo**. Determination of Residual Stresses in Coatings & Coated Parts. 1994.
3. **Mart Tamre**. Tribocharacteristics of Journal Bearings Unlocated Axis. 1995.
4. **Paul Kallas**. Abrasive Erosion of Powder Materials. 1996.
5. **Juri Pirso**. Titanium and Chromium Carbide Based Cermets. 1996.
6. **Heinrich Reshetnyak**. Hard Metals Serviceability in Sheet Metal Forming Operations. 1996.
7. **Arvi Kruusing**. Magnetic Microdevices and Their Fabrication methods. 1997.
8. **Roberto Carmona Davila**. Some Contributions to the Quality Control in Motor Car Industry. 1999.
9. **Harri Annuka**. Characterization and Application of TiC-Based Iron Alloys Bonded Cermets. 1999.
10. **Irina Hussainova**. Investigation of Particle-Wall Collision and Erosion Prediction. 1999.
11. **Edi Kulderknup**. Reliability and Uncertainty of Quality Measurement. 2000.
12. **Vitali Podgurski**. Laser Ablation and Thermal Evaporation of Thin Films and Structures. 2001.
13. **Igor Penkov**. Strength Investigation of Threaded Joints Under Static and Dynamic Loading. 2001.
14. **Martin Eerme**. Structural Modelling of Engineering Products and Realisation of Computer-Based Environment for Product Development. 2001.
15. **Toivo Tahemaa**. Assurance of Synergy and Competitive Dependability at Non-Safety-Critical Mechatronics Systems design. 2002.
16. **Juri Resev**. Virtual Differential as Torque Distribution Control Unit in Automotive Propulsion Systems. 2002.
17. **Toomas Pihl**. Powder Coatings for Abrasive Wear. 2002.
18. **Sergei Letunovits**. Tribology of Fine-Grained Cermets. 2003.
19. **Tatyana Karaulova**. Development of the Modelling Tool for the Analysis of the Production Process and its Entities for the SME. 2004.
20. **Grigori Nekrassov**. Development of an Intelligent Integrated Environment for Computer. 2004.
21. **Sergei Zimakov**. Novel Wear Resistant WC-Based Thermal Sprayed Coatings. 2004.
22. **Irina Preis**. Fatigue Performance and Mechanical Reliability of Cemented Carbides. 2004.
23. **Medhat Hussainov**. Effect of Solid Particles on Turbulence of Gas in Two-

Phase Flows. 2005.

24. **Frid Kaljas**. Synergy-Based Approach to Design of the Interdisciplinary Systems. 2005.
25. **Dmitri Neshumayev**. Experimental and Numerical Investigation of Combined Heat Transfer Enhancement Technique in Gas-Heated Channels. 2005.
26. **Renno Veinthal**. Characterization and Modelling of Erosion Wear of Powder Composite Materials and Coatings. 2005.
27. **Sergei Tisler**. Deposition of Solid Particles from Aerosol Flow in Laminar Flat-Plate Boundary Layer. 2006.
28. **Tauno Otto**. Models for Monitoring of Technological Processes and Production Systems. 2006.
29. **Maksim Antonov**. Assessment of Cermets Performance in Aggressive Media. 2006.
30. **Tatjana Barashkova**. Research of the Effect of Correlation at the Measurement of Alternating Voltage. 2006.
31. **Jaan Kers**. Recycling of Composite Plastics. 2006.
32. **Raivo Sell**. Model Based Mechatronic Systems Modeling Methodology in Conceptual Design Stage. 2007.
33. **Hans Rammal**. Experimental Methods for Sound Propagation Studies in Automotive Duct Systems. 2007.
34. **Meelis Pohlak**. Rapid Prototyping of Sheet Metal Components with Incremental Sheet Forming Technology. 2007.
35. **Priidu Peetsalu**. Microstructural Aspects of Thermal Sprayed WC-Co Coatings and Ni-Cr Coated Steels. 2007.
36. **Lauri Kollo**. Sinter/HIP Technology of TiC-Based Cermets. 2007.
37. **Andrei Dedov**. Assessment of Metal Condition and Remaining Life of Inservice Power Plant Components Operating at High Temperature. 2007.
38. **Fjodor Sergejev**. Investigation of the Fatigue Mechanics Aspects of PM Hardmetals and Cermets. 2007.
39. **Eduard Sevtsenko**. Intelligent Decision Support System for the Network of Collaborative SME-s. 2007.
40. **Runno Lumiste**. Networks and Innovation in Machinery and Electronics Industry and Enterprises (Estonian Case Studies). 2008.
41. **Kristo Karjust**. Integrated Product Development and Production Technology of Large Composite Plastic Products. 2008.
42. **Mart Saarna**. Fatigue Characteristics of PM Steels. 2008.
43. **Eduard Kimmari**. Exothermically Synthesized B<sub>4</sub>C-Al Composites for Dry Sliding. 2008.
44. **Indrek Abiline**. Calibration Methods of Coating Thickness Gauges. 2008.
45. **Tiit Hindreus**. Synergy-Based Approach to Quality Assurance. 2009.
46. **Karl Raba**. Uncertainty Focused Product Improvement Models. 2009.

47. **Riho Tarbe**. Abrasive Impact Wear: Tester, Wear and Grindability Studies. 2009.
48. **Kristjan Juhani**. Reactive Sintered Chromium and Titanium Carbide-Based Cermets. 2009.
49. **Nadezda Dementjeva**. Energy Planning Model Analysis and Their Adaptability for Estonian Energy Sector. 2009.
50. **Igor Krupenski**. Numerical Simulation of Two-Phase Turbulent Flows in Ash Circulating Fluidized Bed. 2010.
51. **Aleksandr Hlebnikov**. The Analysis of Efficiency and Optimization of District Heating Networks in Estonia. 2010.
52. **Andres Petritsenko**. Vibration of Ladder Frames. 2010.
53. **Renee Joost**. Novel Methods for Hardmetal Production and Recycling. 2010.
54. **Andre Gregor**. Hard PVD Coatings for Tooling. 2010.
55. **Tonu Roosaar**. Wear Performance of WC- and TiC-Based Ceramic-Metallic Composites. 2010.
56. **Alina Sivitski**. Sliding Wear of PVD Hard Coatings: Fatigue and Measurement Aspects. 2010.
57. **Sergei Kramanenko**. Fractal Approach for Multiple Project Management in Manufacturing Enterprises. 2010.
58. **Eduard Latosov**. Model for the Analysis of Combined Heat and Power Production. 2011.
59. **Jurgen Riim**. Calibration Methods of Coating Thickness Standards. 2011.
60. **Andrei Surzhenkov**. Duplex Treatment of Steel Surface. 2011.
61. **Steffen Dahms**. Diffusion Welding of Different Materials. 2011.
62. **Birthe Matsi**. Research of Innovation Capacity Monitoring Methodology for Engineering Industry. 2011.
63. **Peeter Ross**. Data Sharing and Shared Workflow in Medical Imaging. 2011.
64. **Siim Link**. Reactivity of Woody and Herbaceous Biomass Chars. 2011.
65. **Kristjan Plamus**. The Impact of Oil Shale Calorific Value on CFB Boiler Thermal Efficiency and Environment. 2012.
66. **Aleksei Tsinjan**. Performance of Tool Materials in Blanking. 2012.
67. **Martins Sarkans**. Synergy Deployment at Early Evaluation of Modularity of the Multi-Agent Production Systems. 2012.
68. **Sven Seiler**. Laboratory as a Service - A Holistic Framework for Remote and Virtual Labs. 2012.
69. **Tarmo Velsker**. Design Optimization of Steel and Glass Structures. 2012.
70. **Madis Tiik**. Access Rights and Organizational Management in Implementation of Estonian Electronic Health Record System. 2012.
71. **Marina Kostina**. Reliability Management of Manufacturing Processes in Machinery Enterprises. 2012.
72. **Robert Hudjakov**. Long-Range Navigation for Unmanned Off-Road Ground Vehicle. 2012.

73. **Arkadi Zikin**. Advanced Multiphase Tribo-Functional PTA Hardfacings. 2013.
74. **Alar Konist**. Environmental Aspects of Oil Shale Power Production. 2013.
75. **Inge Roos**. Methodology for Calculating CO<sub>2</sub> Emissions from Estonian Shale Oil Industry. 2013.
76. **Dmitri Shvarts**. Global 3D Map Merging Methods for Robot Navigation. 2013.
77. **Kaia Loun**. Company's Strategy Based Formation of e-Workplace Performance in the Engineering Industry. 2013.
78. **Maido Hiimaa**. Motion Planner for Skid-Steer Unmanned Ground Vehicle. 2013.
79. **Dmitri Goljandin**. Disintegrator Milling System Development and Milling Technologies of Different Materials. 2013.
80. **Dmitri Aleksandrov**. Light-Weight Multicopter Structural Design for Energy Saving. 2013.
81. **Henrik Herranen**. Design Optimization of Smart Composite Structures with Embedded Devices. 2014.
82. **Heiki Tiikoja**. Experimental Acoustic Characterization of Automotive Inlet and Exhaust System. 2014.
83. **Jelena Priss**. High Temperature Corrosion and Abrasive Wear of Boiler Steels. 2014.
84. **Aare Aruniit**. Thermoreactive Polymer Composite with High Particulate Filler Content. 2014.
85. **Dmitri Gornostajev**. Development of the Calculation Method for Barge Hull. 2014.